JOHN YATES.

Ph. D. FEBRUARY 1973.

SECOND BREAKDOWN IN TRANSISTORS.

SUMMARY.

Second breakdown in transistors is described in terms of thermal, magnetic and ionisation processes. The effect of charge-carrier concentration upon the effective values of base width and collection area, together with the dependence of breakdown upon these values, is discussed for epitaxial-collector transistors.

Expressions are derived for :-

1. the critical collector current required to cause second breakdown for given values of supply voltage and ambient temperature;
2. temperature gradient at the instant of breakdown;
3. delay time;
4. temperature and charge-carrier distribution in the breakdown condition.

Attempts are made to substantiate the theoretical analysis by comparing calculated and experimental relations between :

1. critical current and ambient temperature for forward base-terminal current and open base operation;
2. temperature distribution in the breakdown condition;
3. delay time as a function of the energy input to cause second breakdown;
4. delay time as a function of ambient temperature for given values of collector current and supply voltage.

The theory presented here deals specifically with epitaxial-collector transistors. The major portion of the analysis is, however, applicable to most semiconductor junction devices which are susceptible to second breakdown.

ACKNOWLEDGMENTS.

The author is grateful for the support given by the Science Research Council and the University of Aston in Birmingham during this project. Thanks are due for the facilities provided by the University and for the assistance and encouragement received from the staff of the University. In particular, the guidance and counsel recieved from Drs. Nield and Cotterhill proved invaluable.

eliminated from semiconductor devices. A detailed knowledge of the factors causing breakdown is needed, however, to enable the operating range to be clearly predicted and extended to the limits of design capability.

1.1 Characteristics of Second Breakdown in Transistors.

Second breakdown in transistors is characterised by an abrupt change in the terminal operating conditions, from a high voltage low current mode, to a low voltage high current mode. Breakdown occurs at a finite time after the application of a suitably large pulse of power and can occur for all conditions of base-bias. The time taken to establish a breakdown is dependent upon the transistor base-bias mode and the magnitude of the power pulse and is referred to as the "delay time" (Refs. 6,7). In general the transfer from high to low voltage occurs as a single step but multiple breakdown levels and oscillatory conditions have been observed, see Fig. 1.1 (Refs. 7,8, 9,10). Only the final breakdown is thought to exhibit the sign reversal of the $V_{CE} - I_b$ relationship, considered by Schafft and French (Ref. 9) to be an essential characteristic of second breakdown.

The negative resistance region of the $I_c - V_{CE}$ characteristic encountered in breakdown decreases in value as the current rises. At very high current levels internal resistive potential differences mask this effect.

Typical collector-emitter voltages during second breakdown are of the order of ten volts. High values of voltage associated with a breakdown which appears to have the second breakdown form, are usually associated with devices and operating conditions at which multiple levles will exist.

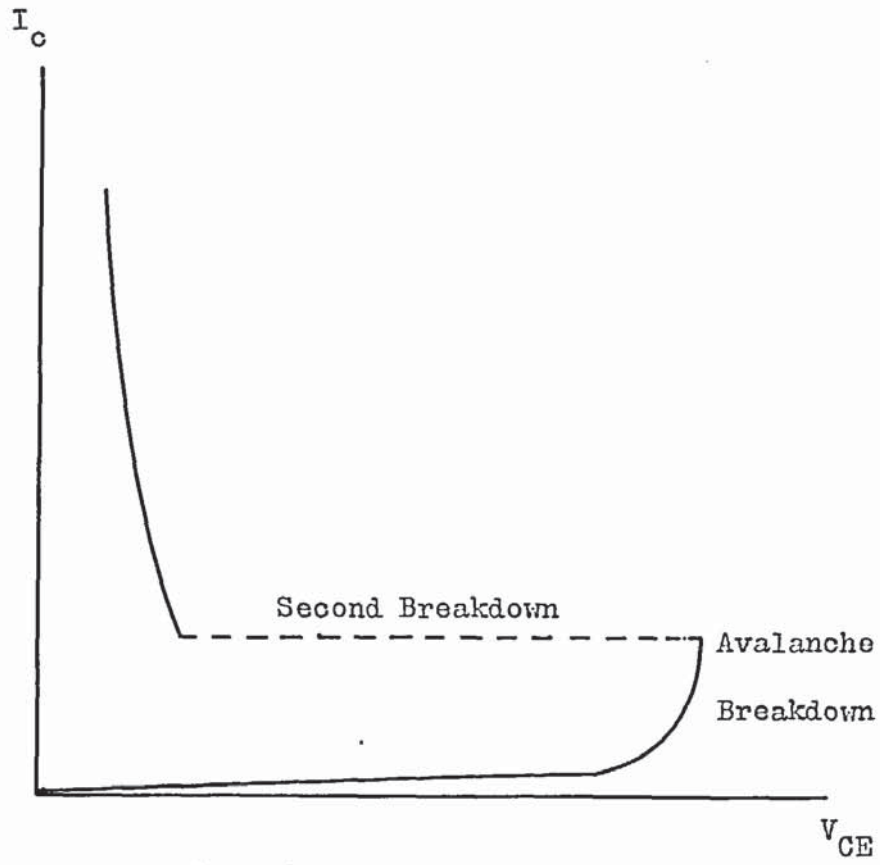

(a) Open Base $I_c - V_{CE}$ Breakdown Characteristic

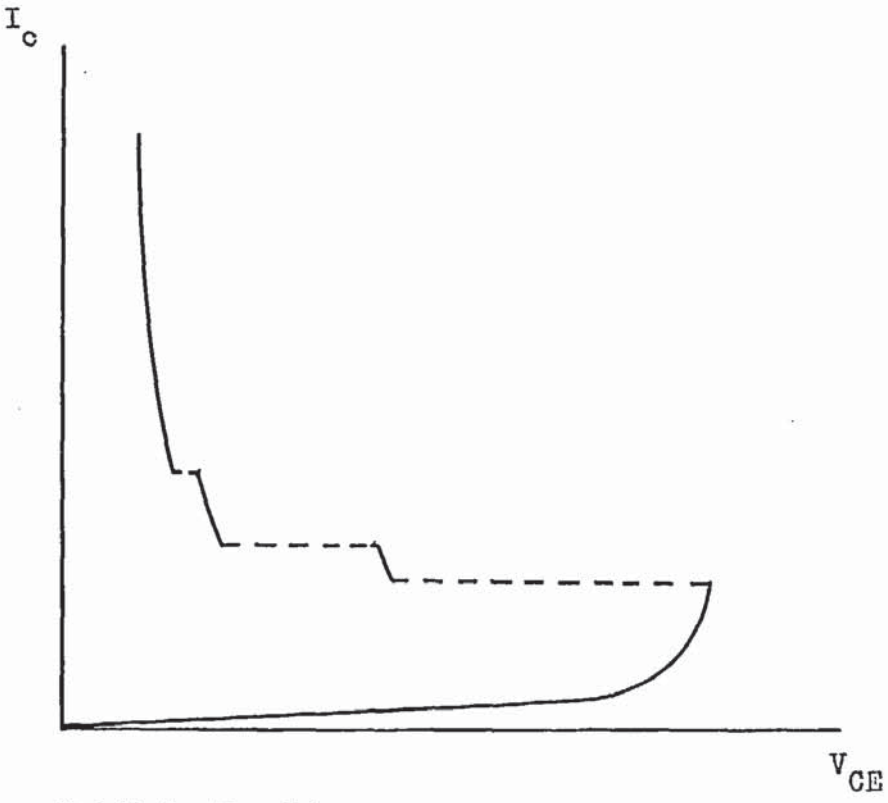

(b) Multiple Breakdown

Fig. 1.1 Open Base Breakdown $I_c - V_{CE}$ Characteristics.

Both the delay time and the energy required to cause breakdown can be considered as measures of the device resistance to second breakdown. The delay time has been shown to be dependent upon temperature, collector current, collector voltage, base-bias current and device structure. Delay times have been reported for various modes of operation ranging from a few nano-seconds to hundreds of milli-seconds. Attempts have been made to link the delay time to the applied power and the energy required to cause breakdown, but with limited success (Refs. 11,12).

Several characteristic changes in the terminal electrical characteristics have been reported as indications of the imminence of second breakdown (Refs. 13,14). These include oscillations, or voltage dips, appearing at the base and a change in the voltage level on the current decay portion of the switching cycle using an inductive load.

2. DEVELOPMENT OF SECOND BREAKDOWN THEORIES.

Second breakdown was first reported for transistors operating under conditions of reverse base-bias (Ref.1). The operating mode was taken to be of primary significance in the initiation of breakdown. It was suggested that the reverse base current generated a potential gradient along the emitter-base junction causing a local concentration of the current injected from the emitter into the base region. This was considered to lead to regenerative action culminating in breakdown for high current levels. Subsequent investigation revealed that second breakdown occurred in devices operating under conditions of forward and zero base-bias (Ref. 2). Processes other than resistive potential effects were therefore important in the formation of breakdown.

At this time an investigation of point-contact and junction diodes revealed a form of breakdown having characteristics which were very similar to those found in transistor second breakdown. English (Refs. 3,4) considered both types of device to exhibit second breakdown and described the formation of molten channels in junction devices. The extension of these molten regions between two areas of high conductivity was proposed as a means of reducing the terminal voltage of the devices. Similar effects were later observed in $n^+ - n - n^+$ and $p - n - p - n$ structures (Ref. 5) and in M.O.S. devices (Ref. 6). English calculated the temperature and voltage profiles in the diodes during breakdown as a function of distance from a spherical molten zone (Refs. 4,7). The breakdown characteristics appeared to be independent of current and English suggested changes in the size and boundary conditions of the molten

zone as a means of accommodating the observed breakdown characteristics. The primary component of the constricted current was assumed to be the reverse current of the collector base junction.

A more complex analysis using elliptical melt co-ordinates suggested that the meso-plasma, or melt, was unstable until it formed a channel between two regions of high electrical conductivity (Ref. 8). The formation of narrow channels was considered to produce negligible changes in the electrical characteristics of the device. Calculations of the maximum channel dimensions permissible without any observable external effect showed a considerable disagreement with experimental observations. It was found that channel widths calculated for a specific operating condition were too great to be ignored although no external electrical change was observed. The formation of a molten channel could, however, be applicable to operation with a very high current pulse which can initiate a breakdown culminating in total device destruction.

Scarlett et al., (Ref. 9) suggested that thermally generated base current maintained the emitter current at reduced collector voltages. The current constriction, or pinch, associated with second breakdown produced high local power dissipation. The resultant local temperature rise caused a reduction in the voltage needed to produce the thermal base current. Such a theory fails to explain the initiation of a significant current constriction and is in conflict with the observed increase in breakdown voltage with the application of forward base current. (See Fig. 2.1).

Thermal processes were considered to play an important part in the formation of a current constriction. The search for temperature

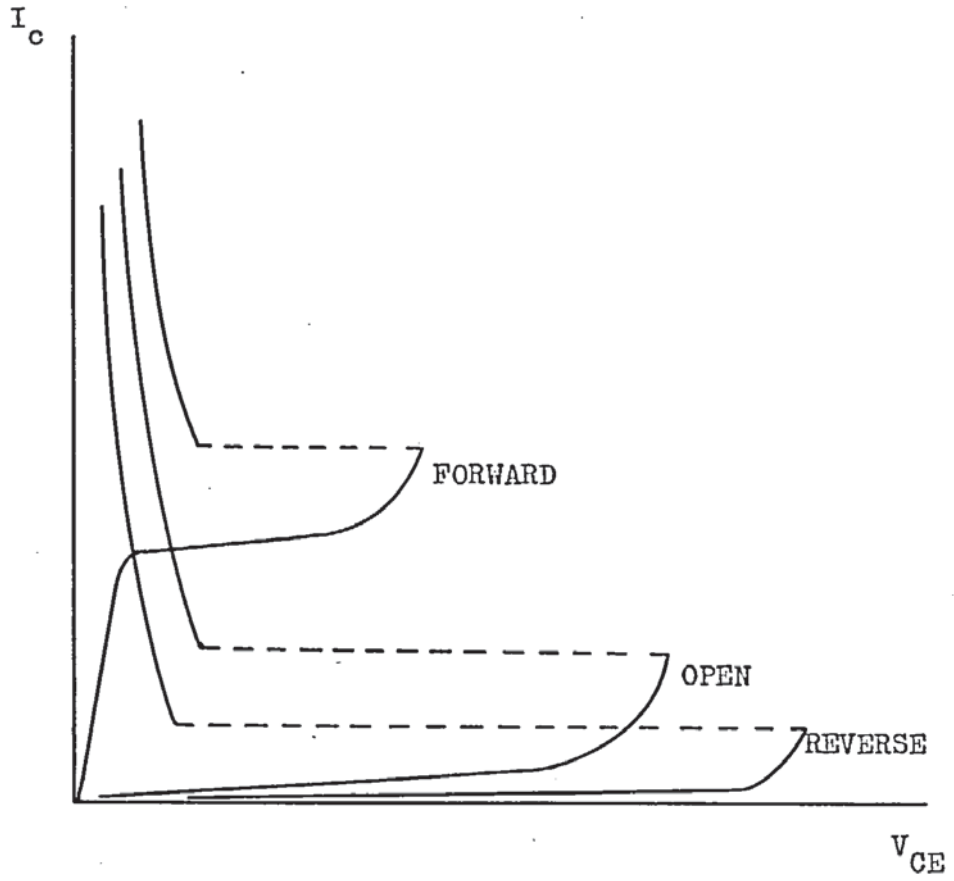

Fig. 2.1 The Effect of Base Terminal Current Upon the $I_c - V_{CE}$ Breakdown Characteristic.

dependent current and voltage relationships capable of developing a regenerative action led to the theory of lateral thermal instability. (Refs. 9,10).

2.1 Lateral Thermal Instability.

Transistors were considered to be operating with a constant total emitter current and constant emitter base-voltage. Avalanche effects were assumed to be negligible, collector voltages being restricted to values below the zero base-bias avalanche breakdown voltage. The current distribution before the onset of breakdown was assumed to be uniform over the whole of the emitter area.

The theory of lateral thermal instability was the first attempt to explain second breakdown for transistors operating in the forward and zero base-bias modes. It was proposed that breakdown resulted from an increase in emitter injection linked with a localised temperature perturbation. Operating conditions promoting this type of action are large power dissipation and poor thermal coupling to the heat sink and between different regions of the emitter. Resistive potential differences occurring in the emitter, base and collector regions act as stabilising influences by improving the uniformity of current distribution. Resistive stabilisation should produce a greater resistance to breakdown when operation is at low voltage and high current for a given power level.

The thermal instability theory was developed using linear approximations to the temperature relationships involved. These approximations limit the theory to the prediction of a critical condition for the onset of current constriction, which is

independent of any external stabilising circuits. It is not possible to relate the formation of the constriction to a delay time by this theory. This is a serious deficiency if the transistor is to be used to its fullest potential.

Lateral thermal instability results from a local temperature disturbance which is sufficiently large to generate enough local current to cause a further rise in temperature. Ford (Ref. 11) and later Melchior and Strutt (Ref. 12) suggested that a "triggering temperature" existed for a given operating condition, below which no breakdown could occur. This was related to the intrinsic temperature of the high resistivity side of the junction. At this temperature a low impedence path is formed across the physical junction, the junction becoming non-existent locally, and the voltage across the junction falls. It was assumed that the effective thermal resistances and capacitances of the device remained constant. The junction temperature at breakdown was calculated using these assumptions and information obtained from measurements of the power dissipation required to maintain a constant delay time for varying ambient temperature conditions. The results obtained are in fair agreement with the intrinsic temperatures involved.

A consideration of constant power dissipation in cylindrical device geometries led to an expression for the junction temperature of the form (Ref. 8),

$$T = \frac{CP}{A}(t)^{\frac{1}{2}} + T_A$$

where C = constant

A = area over which power is dissipated

P = power

T_A = ambient temperature

The time period was limited by the assumption of a constant temperature at the semiconductor-heatsink interface. The inclusion of a temperature dependent term in the power dissipation resulted in an unlimited rise in junction temperature in a finite time. The time for the temperature to approach infinity was taken as the delay time, t_d . It was found that the product $P\sqrt{t_d}$ was constant for a given ambient temperature.

With short delay times it has been reported that the product Pt_d is constant. This indicates an expression for the junction temperature of the form (Ref. 13)

$$T = C P t + T_A$$

An expression of this form may result from considering the temperature rise to be confined to the depletion region. Thermal runaway mechanisms have been associated with delay times as short as 100 ns., (Ref. 11).

Refinements in the theory are required since the large change in operating conditions encountered during the initiation of breakdown make the simplifying assumptions of constant thermal resistance and capacitance inaccurate. Expressions are also required for the temperature dependence of the power dissipation and the effective active area of the device.

Reich and Hakim (Refs. 14,15,16) have proposed a simple relationship between a variable thermal resistance factor and

second breakdown conditions. Two conclusions formed from the investigation of "hot spot" thermal resistance under pulse conditions are :

(i) The threshold voltage for the formation of hot spots is related to the device avalanche voltage.

(ii) There appears to be a large variation in the hot spot thermal impedence above this threshold voltage.

Two basic forms of second breakdown were proposed following these principles. A current controlled mode associated with the reduction of current gain as the current density rises. A voltage controlled mode related to the operation at voltages in the region of avalanche breakdown produces breakdown for high voltage operation.

2.2 Electrical Phenomena and Second Breakdown.

Thermal processes have generally been considered inadequate in describing second breakdown with short delay times ($<1\mu s$). One of the earliest attempts to account for rapid breakdown was by means of p - n - p - n action (Ref. 17) which formed a positive feedback pair within the device.

The effect of a large concentration of free charge carriers has been considered both as an initiating mechanism for breakdown and as a stabilising influence (Refs. 18,19). Avalanche breakdown and the formation of the associated micro-plasma have also been considered as initiating processes for second breakdown (Refs. 20, 21).

Egawa (Ref. 18) calculated the electric field in reverse biased p - ν - n diodes and showed regions of positive and

negative current dependence. A free charge density less than the impurity concentration gave rise to a positive resistance region. Greater free-charge concentrations than impurity concentrations resulted in a negative resistance. The negative resistance condition would be expected to lead to second breakdown, since a local perturbation would cause a current constriction. Experimental evidence gave breakdown current densities a factor of ten lower than the calculated values. This was attributed largely to non-uniform current distribution. Once the critical current density has been reached breakdown will occur with very short delay times, determined largely by the transport properties within the device regions. The delay times reported by Egawa were generally greater than 1μs. which is considered too great for electrical effects to be the only mechanism controlling breakdown.

Josephs (Ref. 19) considered the decrease in collector voltage induced by free charge-carriers in transistors having abrupt collector-base junctions and with a higher impurity concentration in the base than in the collector. A local collector-base voltage decrease could result in a current constiction to this site resulting in a further voltage reduction. Second breakdown would result with a very short delay time, the collector-emitter voltage being determined by the collector current. In transistors having a greater impurity concentration in the collector an increase in collector voltage is predicted for increasing current density. This can act as a stabilising mechanism until the free-charge density is greater than the collector impurity density.

Modulation of the base depletion region by large current pulses has been proposed as a breakdown mechanism in epitaxial transistors (Ref. 19). The depletion region can expand until it reaches the

low-resistivity collector contact, or the semiconductor substrate layer. The change in junction conditions initiates second breakdown by requiring a lower junction voltage to maintain a given current level. All processes considered by Josephs were restricted to conditions of low avalanche multiplication and the current gain at the constriction site was assumed to be constant throughout the transition into breakdown.

Following the theory of base width modulation at high current densities, proposed by Kirk (Ref. 22), breakdown was thought to occur when the effective base region penetrated to the substrate layer (Ref. 23). Triple-diffused epitaxial collector transistors operating at moderate collector current levels exhibited an oscillatory form of breakdown. Devices with narrow collector regions had a collector-emitter voltage characteristic which switched between a voltage in excess of the open-base breakdown voltage and approximately half that value. The oscillations were thought to be initiated by the collector space-charge region extending to the collector-substrate junction. Under these conditions the electric field in the space-charge region can produce significant avalanche multiplication at relatively low current levels. The transverse flow of avalanche current in the base region acts to create a high current density. This does not, however, lead to second breakdown, as proposed by Josephs, but to the collapse of the collector voltage to the base-substrate breakdown voltage. The lower voltage is maintained until the charge stored in the collector-base space-charge region is removed. The collector voltage then rises at a rate determined by the collector-base capacitance.

Roman (Ref. 24) also considered the effect of base-width

modulation which was considered to produce a negative resistance region in the collector junction. The charge stored in the collector space-charge region discharges through the localised negative impedence area. The radial electric field created develops a high concentration of energy dissipation at this site and initiates a thermal breakdown process. The thermal breakdown was considered to be dependent upon a critical temperature in the current density temperature relationship. Above this temperature the device enters a positive feedback regime and a continuing current constriction is produced.

Avalanche injection from the collector-substrate junction is proposed as a breakdown mechanism by Hower and Reddi (Ref. 25). Localised thermal gradients are considered to play a minor role in determining breakdown conditions. The neglect of heating effects and the temperature dependence of important device parameters limits the application of this theory to small area devices operating under very short pulse drives. The condition $M\alpha_{cc} \geq 1$ (where M is the avalanche multiplication factor and α_{ce} is the current amplification factor) is taken as a necessary condition for breakdown. This inequality corresponds to a negative resistance region in the open base characteristics. The presence of a mobile charge-carrier concentration in the collector region is thought to act as a stabilising influence by adding a positive resistance to the collector circuit. The magnitude of this resistance is proportional to the square of the depletion layer width.

Localised avalanche multiplication can occur at the edge of shallow diffused collector regions. This can become significant at

voltages much lower than the normal collector-base avalanche breakdown voltage because of the junction curvature (Refs. 26,27). Effects of this kind can lead to high local current densities and initiate a thermal breakdown process.

2.3 Experimental Techniques.

The initial experimental effort was directed towards an investigation of the electrical terminal characteristics of devices under varying ambient conditions. This was performed largely by use of a sinusoidally-swept oscillographic display of the common-emitter $I_c - V_{ce}$ characteristic. A system of this kind has the disadvantage of introducing distortion into the breakdown characteristic due to the slow sweep rate used. Practical conditions under which second breakdown is likely to occur are associated with rapid power increases. A slow rate of rise of the power dissipation produces more general device heating and leads to a false value of critical breakdown current for a given operating voltage. This form of test proceedure makes the transistor more susceptible to total destruction.

Improvements on this technique were made by reconstructing the most common practical situation in which second breakdown occurs. Transistors were driven from a square wave source and an inductive load adjusted to give the required peak power dissipation (Refs. 28, 29). This system is difficult to apply safely to untested transistors and provides poor control of the time spent in the breakdown condition.

The most useful system for breakdown-testing employs a rectangular power pulse drive. This can be used in common-base,

or common-emitter, modes with precise control of the current and voltage amplitudes (Refs. 15,16). This system can also be modified to provide control of the time period spent in breakdown (Ref. 30). An adequate description of the complex processes involved in second breakdown cannot be derived from terminal electrical characteristics alone. Attempts have been made to determine the thermal and potential distribution in the transistor under breakdown conditions. Early investigations into the junction temperature relied upon the temperature dependence of the collector leakage current and the base-emitter voltage. These methods do not allow measurements to be made during breakdown and provide an average value for the whole junction area. The use of the collector current is complicated by its dependence upon diffusion and recombination-generation currents in the space-charge region. These two currents have different dependencies upon the operating and ambient conditions. More detailed information has been obtained by the use of temperature sensitive phosphors and paints (Refs. 5, 31-33). This system depends upon a change of state in the detector occurring at a critical temperature. The information obtained is non-cyclic and involves a lengthy preparation of several identical specimens if any detail is required.

Probes have been used to determine the potential distribution across the device surface by direct measurement (Refs. 34,35). Although direct information concerning the device potential distribution and hence the charge-carrier concentration is obtained, the method is difficult to use. The probes must make contact with the device and so introduce a perturbation in the region where the measurement is performed. Improved techniques in electron microscopy have allowed the measurement to penetrate beneath the surface

of the device. Both pulsed and static responses can be determined. Unfortunately the measurement techniques introduce perturbations which are capable of triggering spurious second breakdown (Refs. 36-38).

The recent development of sensitive infra-red radiation detectors has provided a means of observing the surface temperature of a semiconductor device without actual contact (Refs. 16, 39-42). Coupled with a reflective microscope, a mean temperature for a small area of the device surface can be obtained for all operating conditions.

3. THEORY.

3.1 General Semiconductor Theory.

Consideration of the state distribution of charge carriers, in a semiconductor medium, when referred to a six co-ordinate system, should provide a means of describing the operation of a semiconductor device. The application of suitable boundary conditions would make a system of equations describing the state distribution applicable to a particular device region in all modes of operation. The solution of these equations would include static and dynamic characteristics and could be extended to cover normal transistor and breakdown operation.

The most widely accepted expression relating the rate of change of the state distribution to the processes affecting the semiconductor charge carriers is the Boltzman Transport Equation (Refs. 1,2). If the distribution function is represented as f, the equation can be expressed as

$$f' = f'_{drift} + f'_{diffusion} + f'_{scattering} \qquad (3.1.1)$$

This equation is applicable to gases, liquids, solids and in this instance, to charge carriers in a semiconducting material. The solution of the Boltzman equation can yield the distribution in position and velocity of all particles in the semiconductor region being considered. The statistical nature of the distribution must be accounted for in this solution.

The equation given above has the most general form. Consideration of the three right hand terms with specific reference to semiconductors will make this more useful for the present purpose.

Consider the distribution of charge carriers in a six-dimensional cartesian system (x,y,z,u_x,u_y,u_z) to be represented as a function of position, r, velocity, u and time, t. Let this be expressed as $f(\bar{r},\bar{u},t)$. The number of charge carriers having position within the limits $\bar{r} + \bar{dr}$ and velocity within the limits $\bar{u} + \bar{du}$ at a time t can be expressed as

$$dN = f(\bar{r},\bar{u},t)\bar{dr}.\bar{du} \qquad (3.1.2)$$

But $\bar{dr} = dx.dy.dz = d^3r$

$du = du_x.du_y.du_z = d^3u$

giving $$dN = f(r,u,t)d^3r.d^3u \qquad (3.1.3)$$

The effect of drift, diffusion and scattering processes, involving the charge carriers, is to make this quantity time dependent. The rate of change of dN can be obtained by a detailed examination of these processes.

3.1.1 Diffusion.

As a result of the spatial velocity of the charge carriers, the region $\bar{r} + \bar{dr}$ will receive carriers from adjacent regions. Similarly charge carriers will be lost to adjacent regions. If $f(\bar{r},\bar{u},t)$ is not constant for all phase-space (i.e., a concentration gradient exists, at least on a local scale) there will be a net rate of change of the distribution function, f, with time, due to diffusion. This can be represented by

$$\dot{f}_{\text{diffusion}} = -\bar{u}.\ \text{grad}_r f \qquad (3.1.4)$$

3.1.2 Drift.

Electric and magnetic fields exert forces upon the moving charge carriers. These forces will cause a change of points in the velocity co-ordinates by imparting an acceleration to the charge carriers. The change will be determined by the Newtonian inter-relationship of force, $\bar{F}$, mass, m, and rate of change of velocity, giving

$$f'_{drift} = \frac{\bar{F}}{m} . \text{grad}_u f \qquad (3.1.5)$$

The force exerted on a charged particle in combined electric and magnetic fields is described by the Lorentz relationship as

$$\bar{F} = q(\bar{E} + \bar{u}x\bar{B}) \qquad (3.1.6)$$

The rate of change of the charge carrier distribution with time due to drift processes can be expressed as a function of the field strength as

$$f'_{drift} = \frac{q}{m^*} (\bar{E} + \bar{u}x\bar{B}) . \text{grad}_u f \qquad (3.1.7)$$

where m^* is the effective mass of the charge carrier.

3.1.3 Scattering.

Charge carriers can undergo a change of state by their mutual interaction or, by interaction with the crystal lattice. Scattering attributable to lattice interactions is caused by impurities, inhomogeneties and stresses in the crystal lattice structure (Refs. 1,10,11). The processes can be separated into two basic groups, depending upon conservative, or non-conservative, scattering.

A conservative interaction can be considered as a spontaneous change in velocity, without a change in position and without an

increase in the number of charge carriers. This is in effect an elastic collision and is expressed as f'_{coll}.

The most straightforward and non-conservative process is the ionising collision. Impact ionisation causes a simultaneous change in the number and the velocity of charge carriers and can be represented as f'_{ion}.

Processes which do not involve ionisation occur in the presence of recombination-emission centres and trapping centres. This action depends upon the ability of a region in the crystal to absorb, or emit, charge carriers. It is generally supposed that a centre of this kind has a unique energy level to which an electron can be thermally excited. The hole left in the valence band can then be removed by drift, or diffusion, forces. In this way the centre has "produced" a hole. The electron can subsequently be excited into the conduction band, leaving the centre neutral. The centre now appears to have "produced" an electron.

A more stable form of centre can trap an electron for a much longer time than that considered above. The presence of a charge in the trapping centre can alter the shape of the potential energy band edges in the region of the trap. This can make it easier for an electron to escape and more difficult for a hole to escape from a local centre. In general these two effects will not cancel (Ref. 14).

The presence of an electric field can make these centres appear as a continuing source of charge carriers of a particular polarity by removing any local concentration rapidly. The trapping centre action modifies the source strength according to the polarity of the charge it contains. This term is generally expressed as f'_{gr}.

Scattering processes are extremely complex, the total rate of change of the distribution function due to scattering being the sum of the above processes,

$$f^{\bullet}_{scat} = f^{\bullet}_{coll} + f^{\bullet}_{ion} + f^{\bullet}_{gr} \qquad (3.1.8)$$

The complex dependence of these terms upon temperature, impurity concentration and physical stresses leads to a consideration of scattering as a transient process. This enables it to be expressed as a function of time for non-equilibrium conditions and to be neglected once equilibrium is established.

3.1.4 Relaxation Time.

In thermal equilibrium the number of charge carriers entering a given elemental volume is equal to the number leaving it. The distribution function, f_o, is therefore independent of time. An externally applied disturbance will upset this balance condition. The distribution now becomes time dependent through the scattering term.

In a silicon crystal lattice the surfaces generated by points of equal energy are ellipsoidal. Since scattering can take place within these surfaces and also between surfaces any time constant representing scattering processes should have components in the direction of the major axes (Refs. 10,11). These three relaxation times will be related to the processes which randomise velocity and conserve energy. In the simplest approximation the assumption is made that the energy surfaces can be represented by a spherical surface. This allows the rate of change of the distribution function to be expressed as

$$f^{\bullet}_{\text{scat}} = -(f - f_o)/\gamma \qquad (3.1.9)$$

where γ is the relaxation time and f_o is the equilibrium distribution function.

When this approximation is not valid each scattering process must be examined in detail to produce a complex differential equation expressing the whole scattering process.

3.1.5 Distribution Functions.

The general form of the Boltzman Transport Equation applicable to a semiconductor material is therefore

$$f^{\bullet}_{\text{scat}} = f^{\bullet} + \bar{u}\nabla_r f + \frac{q}{m^*}(\bar{E} + \bar{u}\times\bar{B}).\nabla_u f \qquad (3.1.10)$$

There will be an equation for charge carriers of both polarities.

The statistical nature of this equation arises from the probability, under thermal equilibrium, that a quantum state of energy, $\mathcal{E}$, is occupied by an electron. The equilibrium distribution function will be the average value of the fraction of all the states of energy occupied by an electron. The situation can be described by the Fermi-Dirac distribution function which is dependent upon temperature and energy.

$$f = f\left(\frac{\mathcal{E} - \mathcal{E}_F}{kT}\right) = 1/(1 + \exp(\mathcal{E} - \mathcal{E}_F)/kT) \qquad (3.1.11)$$

where $\mathcal{E}_F$ is the Fermi Energy Level, at which the distribution function is 0.5.

The value of the Fermi energy is an indication of the occupancy of a range of energy levels. In a semiconductor the valence and conduction bands are separated by an energy gap. Normally the Fermi energy lies within this energy gap. The position of the Fermi Level relative to the two band edges indicates the

degree of occupancy of the bands.

In a partially occupied band system the number of electrons per unit volume in the conduction band can be expressed as the integral

$$n = \int_0^\infty f(\mathcal{E})\,\Phi(\mathcal{E})\,d\mathcal{E} \qquad (3.1.12)$$

where $f(\mathcal{E})$ is the charge carrier distribution function

$\Phi(\mathcal{E})$ is the number of energy levels in the range $\mathcal{E}$ to $\mathcal{E} + d\mathcal{E}$

Expressing energy as 1/2 m*u allows this to be written as (Ref.1)

$$\Phi(\mathcal{E}) = \frac{4\pi(2m^*)^{3/2}\,\mathcal{E}^{1/2}}{h^3} \qquad (3.1.13)$$

When the energy level of interest is greater than the Fermi energy level by several times kT , the exponential term dominates the distribution function. This allows an approximation to give (Ref. 14)

$$f \triangleq \exp(-(\mathcal{E}-\mathcal{E}_F)/kT) \qquad (3.1.14)$$

which is the Maxwell-Boltzman distribution function.

A semiconductor region being heated by a non-uniform source is limited to thermal equilibrium on a local scale. The detailed distribution must be considered as a local shifted Maxwellian (Refs. 4,5) which may have the form

$$\int_{\text{all } r} f(\bar{r},\bar{u}) = n\left(\frac{m^*}{2\pi kT}\right) \exp\left(\frac{-m^*(\bar{u}-\bar{v})}{2kT}\right) \qquad (3.1.15)$$

where $\bar{u}$ is the charge carrier velocity.

$\bar{v}$ is the local mean velocity $= \langle \bar{u} \rangle$

T is the local temperature.

Reik and Risken (Refs. 6,7) found that when the charge carriers had a high kinetic energy, the distributions within the valleys formed by the constant energy surfaces were Maxwellian. This was found to depend upon the inter-valley scattering rate being small compared with the intra-valley scattering rate. It has been proposed (Ref.6) that the assumption of a local Maxwellian distribution is also valid for non-equilibrium conditions provided that, on a local scale, the excess charge carriers have time to distribute themselves to appear in local equilibrium. This was considered to require three to four mean collision times.

The local velocity distribution can therefore be approximated by a Maxwellian form under conditions of avalanche breakdown and for thermal equilibrium. The assumption of spherical energy surfaces is consistent with this approximation since inter-valley scattering is neglected. This reduces the effective mass, in the above equations, to a scalar quantity.

The use of a single local temperature, in the above equations, implies a high rate of exchange of energy between charge carriers (Ref.9). This is given by a high concentration of charge carriers, a higher charge carrier density improving the approximation. These conditions are best fulfilled in a constricted plasma flow.

Under normal conditions the electron, hole and lattice temperatures are not equal. Little information is available concerning these values in detail. It has been found necessary to assume equal values of hole and electron temperatures which are negligibly higher than the lattice temperature. High local temperatures, such as those encountered under breakdown conditions, improve this approximation.

3.1.6 Ambipolar Transport Equations.

Under conditions of very low charge carrier injection the minority carrier current in a transistor base region is much smaller than the majority carrier current. The majority charge carrier distribution determines the boundary conditions for the continuity, or diffusion, equations which express the movement of charge carriers in the base. Either of these equations can be solved for a known electric field and to obtain the minority carrier distribution and current. The relationship between the minority and majority carrier concentrations can now be used to determine the majority carrier distribution and current.

High current levels produce high levels of charge carrier injection. The charge carrier density can be much larger than the impurity density, so that the minority and majority carrier currents are comparable. Under these conditions

$$n \doteq p \gg N_D$$

Normally a large portion of the base region is space-charge neutral. The space charge associated with injected charge carriers is neutralised by an increase in the number of charge carriers of the opposite polarity. Any local space-charge will establish an electric field which will attempt to restore space-charge neutrality. The charge carriers having the highest local density are distributed and charge carriers of the opposite polarity are attracted. Although local differences in concentration can exist, within the limits of space-charge neutrality, these will establish local diffusion currents to remove the concentration gradient. The existence of space-charge neutrality ensures that, even under

conditions of high injection, the boundary conditions are determined substantially by the majority carriers (Ref.31). Since the charge carrier densities of both polarities are comparable there must now be two simultaneous equations to describe the diffusion process.

In the presence of an externally applied electric field (i.e., a collector-emitter voltage) the holes and electrons drift in opposite directions. In the bulk of the base region, however, space-charge neutrality will still be maintained. The space-charge established by the externally applied voltage will generally be a thin layer at the collector-base junction.

Consideration of both types of charge carrier leads to the ambipolar transport expression. The similarity of the electron-hole flow to the flow of negative and positive ions in gases has prompted the use of the term, "ambipolar", which has been extensively used in the study of gaseous plasma flow.

Ambipolar transport processes depend upon the corresponding microscopic processes for electrons and holes. These give rise to values of diffusivity, apparent mobility and decay time as discussed by Van Roosbroeck (Ref.31). Very low injection levels reduce these to the diffusion constant, carrier mobility and the mean minority-carrier lifetime. The derivation of the ambipolar equations presented by Van Roosbroeck was based upon the assumption of space charge neutrality, uniform impurity concentrations and equal recombination rates for electrons and holes. It was also assumed that the immobilisation of charge carriers in trapping centres for times greatly in excess of their lifetime, before their recombination, or release, could be neglected. This limits the recombination to mechanisms described by Shockley and Read (Ref.32).

The most general form of the continuity equation was derived from the Boltzman Transport Equation which took the form

$$\frac{\partial n}{\partial t} + \nabla_r .(n\bar{v}) = g - r + \iiint_{\text{all } r} f'_i \; d^3u \qquad (3.1.16)$$

where g and r represent the rates of generation and recombination.

Van Roosbroeck proceeded by neglecting the ionisation term and limiting the equation to low electric field conditions. The substitution,

$$n\bar{v} = \bar{J}/q \qquad (3.1.17)$$

where $\bar{J}$ is the current density and q the electron charge, was made to introduce the current density. The generation and recombination terms were replaced by an expression involving the mean carrier lifetime, τ, and the thermal generation rate per unit volume

$$g - r = n/\tau - g_o \qquad (3.1.18)$$

The thermal generation and recombination rates were assumed to be equal under equilibrium conditions. The continuity equation for electrons now takes the form

$$\frac{\partial n}{\partial t} = \frac{1}{q} .\bar{J}_n + \frac{n}{\tau_n} - g_o \qquad (3.1.19)$$

A similar equation exists to describe the hole continuity. The characteristic lifetime used is taken to be independent of the charge carrier concentration.

To improve the generality of the continuity equations the ionisation term must be retained and the approximation used for the generation and recombination rates must be replaced by their

detailed expressions. The diffusion coefficient and the mobility must be treated as functions of position and time. This arises from their temperature dependence, which is discussed in Appendix 4. The presence of a magnetic field will cause the currents to flow in directions which differ from the potential and concentration gradients. This indicates that the diffusion coefficient and conductivity should be treated as tensors of rank 2 (Refs.14,33).

3.2 The Continuity Equations.

The continuity equations, in their most general form, can be derived from the Boltzman Transport Equation. Substitution of the appropriate function for f, (i.e., charge carrier density, momentum and energy) and integration over all velocity gives a mathematically rigorous result (Refs.34,35). Although this form is the most mathematically exact derivation, it is more informative to consider the processes affecting these functions in an elemental semiconductor volume. Mathematical expressions can be fitted to these processes giving a result which is identical to the mathematical one.

3.2.1 Continuity of Charge.

Consider a volume, V, enclosed by a surface, S, in a semiconductor material. The rate of change of charge density in V will be given by the rate of charge flow through S and the rates of recombination and generation in V. The rate of increase of charge density in V can therefore be expressed in the integral equation,

$$\int_V \frac{\partial \rho}{\partial t}\, dV = \int_S \rho \bar{u}.n\, da + \int_V (G - R)\, dV \qquad (3.2.1)$$

where ρ is the charge density

n is a unit vector perpendicular to the elemental area da

G is the rate of charge generation

R is the rate of charge recombination.

The divergence theorum relates surface and volume integrals so that

$$\int_S \bar{u}.n \, da = \int_V \nabla.(\rho\bar{u}) \, dV \qquad (3.2.2)$$

The integral equation can therefore be rearranged to give

$$\int_V (R - G + \nabla.(\rho\bar{u}) + \frac{\partial \rho}{\partial t}) \, dV = 0 \qquad (3.2.3)$$

To maintain this identity the terms in parenthesis must sum to zero. This yields the differential equation

$$\frac{\partial \rho}{\partial t} = G - R - \nabla.(\bar{u}) = G - R - \nabla.\bar{J} \qquad (3.2.4)$$

The rate of change of charge carrier density is therefore given by

$$\frac{\partial n}{\partial t} = \frac{1}{q}(G - R - \nabla.\bar{J}) \qquad (3.2.5)$$

Following the theory of Misawa (Ref.12) the generation and recombination rates can be divided into two parts. One part will depend upon ionisation. The impact ionisation processes can be expressed in terms of electric field, E, carrier mobility, μ, and ionisation coefficients, α_i, and β_i (for electrons and holes respectively). The generation and recombination terms thus become

$$G - R = (g - r) + (\alpha_i \mu_n n + \beta_i \mu_p p)Eq \qquad (3.2.6)$$

where g and r are the thermal generation and recombination rates respectively.

Substitution into the differential equation yields the rate of increase of charge carrier density for electrons as

$$\frac{\partial n}{\partial t} + \frac{1}{q}\nabla.\,\bar{J}_n = g - r + (\alpha_i \mu_n n + \beta_i \mu_p p)E \qquad (3.2.7)$$

Similarly the rate of increase of charge carrier density will be

$$\frac{\partial p}{\partial t} + \frac{1}{q}\nabla.\bar{J}_p = g - r + (\alpha_i \mu_n n + \beta_i \mu_p p)E \qquad (3.2.8)$$

The total current density $\bar{J}$ is given by the sum of the electron and hole currents

$$\bar{J} = \bar{J}_n + \bar{J}_p \qquad (3.2.9)$$

$$\nabla.\bar{J} = \nabla.(n\bar{v}_n + p\bar{v}_p)q \qquad (3.2.10)$$

where $\bar{v}$ is the average velocity of charge carriers over the volume V.

The ambipolar charge continuity equation is obtained by adding the equations for the individual charge carriers to give

$$\frac{\partial(n+p)}{\partial t} + \frac{1}{q}\nabla.\bar{J} = 2(g - r + (\alpha_i \mu_n n + \beta_i \mu_p p)E) \qquad (3.2.11)$$

substitution for the current density yields

$$\frac{\partial(n+p)}{\partial t} + \nabla.(n\bar{v}_n + p\bar{v}_p) = 2(g - r + (\alpha_i \mu_n n + \beta_i \mu_p p)E) \qquad (3.2.12)$$

3.2.2 Continuity of Momentum.

The momentum equation can be derived by considering the forces associated with the charge carriers in an elemental volume, dV, in a

semiconducting material. These forces are related to the momentum of the charge carriers by Newton's Second Law.

Forces exerted by electric and magnetic fields are expressed in the Lorentz equation. For an electron the field forces will be

$$\bar{F}_f = q(\bar{E} + \bar{u}x\bar{B}) \qquad (3.2.13)$$

The force exerted over the elemental volume with an electron density, n, will be

$$d\bar{F}_f = qn(\bar{E} + \bar{v}x\bar{B})\ dV \qquad (3.2.14)$$

where $\bar{v}$ is the average electron velocity over the volume considered.

The requirement of space charge neutrality does not preclude the existence of a temperature gradient. The random motion of the charge carriers will create a pressure tensor, $\bar{\bar{P}}$, on dV (Ref.34), (See Appendix 2). The force on the elemental volume due to electrons will be

$$d\bar{F}_{pr} = -\nabla.\bar{\bar{P}}_n\ dV \qquad (3.2.15)$$

There will be a similar force for holes.

The forces on the electrons arising from the electric and magnetic fields and from concentration gradients will cause them to move in concert. The interaction of electrons will therefore sum to zero, with the exception of the random motion discussed above. Similarly the interaction of holes will be zero except for the random motion term. The electrons will appear to be moving, under the influence of drift forces, in a medium of holes. Similarly, the holes will appear to drift in an electron medium. There will be forces generated by the interaction of holes and electrons. These

will be predominantly the forces exerted by charges of opposite polarity moving in opposition. The force on an electron due to the holes will be denoted by $\bar{f}_p$ and the force on a hole due to the electrons will be $\bar{f}_n$.

There will also be interaction between the charge carriers and the lattice. This can be considered as a factor affecting the mobility and the effective mass (Ref.14). The total force acting on the elemental volume will therefore be

$$d\bar{F} = d\bar{F}_f + d\bar{F}_{pr} + \bar{f}_p \, dV$$

$$= - qn \, dV \, (\bar{E} + \bar{v} \times \bar{B}) - \nabla.\bar{\bar{P}} \, dV + f_p \, dV \qquad (3.2.16)$$

Using Newton's Second Law the total force can be expressed as

$$d\bar{F} = \frac{\partial}{\partial t} \, (m^* \bar{v} n \, dV) \qquad (3.2.17)$$

A similar relationship will exist for holes, leading to the simultaneous equations

$$\text{Electrons :} \quad \bar{F}_n = m^*_n \frac{\partial}{\partial t}(n\bar{v}_n) = - \nabla.\bar{\bar{P}}_n - qn(\bar{E} + \bar{v}_n \times \bar{B}) + f_p \qquad (a)$$

(3.2.18)

$$\text{Holes :} \quad \bar{F}_p = m^*_p \frac{\partial}{\partial t}(p\bar{v}_p) = - \nabla.\bar{\bar{P}}_p - qp(\bar{E} + \bar{v}_p \times \bar{B}) + f_n \qquad (b)$$

Combining the two equations yields the ambipolar momentum equation. Over the volume considered the interaction of holes on electrons and electrons on holes sums to zero. The ambipolar

equation can be written as

$$\bar{F} = \bar{F}_n + \bar{F}_p$$

$$= \operatorname{div}(\bar{\bar{P}}_n + \bar{\bar{P}}_p) + q(p\bar{E}_p - n\bar{E}_n + p\bar{v}_p x\bar{B} - n\bar{v}_n x\bar{B}) \qquad (3.2.19)$$

3.2.3 Continuity of Energy.

The energy continuity equation can be deduced from a consideration of the energy in an arbitary volume, V, in a semi-conducting material. The rate of energy accumulation in V is given by the rate of flow of energy across the surface, S, of the volume and the rate of increase of energy due to generation within V. If this is considered to be heat energy this gives the heat flow equation (Ref.13)

$$\int_V p_v \, dV = \int_S (-K \nabla T).\hat{n} \, da + \int_V \frac{\partial (CT)}{\partial t} \, dV \qquad (3.2.20)$$

where P_v is the power density of the energy generation in V

K is the thermal conductivity

C is the specific heat per unit volume.

The divergence theorum gives

$$\int_S (-K \nabla T).n \, da = \int_V \nabla.(-K \nabla T) \, dV \qquad (3.2.21)$$

Substitution into the heat flow equation yields

$$\int_V (p_v + \nabla.(K \nabla T) - \frac{\partial CT}{\partial t}) \, dV = 0 \qquad (3.2.22)$$

To maintain this relationship the terms in parenthesis must sum to zero. The resulting differential equation is therefore

$$\frac{\partial CT}{\partial t} = p_v + \nabla.(K \nabla T) \qquad (3.2.23)$$

The energy source within V will be derived from the increase in kinetic energy of the charge carriers moving in an electric field. The magnetic field will not affect the kinetic energy of the charge carriers. The power in V will be given in terms of the forces acting on the charge carriers as

$$P = p_v V = \bar{F}.\bar{u} \qquad (3.2.24)$$

where $\bar{u}$ is the charge carrier velocity and $\bar{F}$ is the force acting on the charge carrier.

The Lorentz relationship gives the force on the volume as

$$\bar{F} = \rho V \bar{E} \qquad (3.2.25)$$

where ρ is the charge density.

The power density will therefore be

$$p_v = \rho \bar{E}.\bar{u} \qquad (3.2.26)$$

but $$\bar{u} = \bar{J} = \bar{E} \sigma \qquad (3.2.27)$$

where σ is the conductivity

which gives the power density in terms of the electric field as

$$p_v = \sigma E^2 \qquad (3.2.28)$$

The energy continuity equation becomes on substitution

$$C \frac{\partial T}{\partial t} = \sigma E^2 + \nabla.(K \nabla T) \qquad (3.2.29)$$

3.2.4 Simplifying Assumptions.

The system of three simultaneous continuity equations derived above describes the behaviour of charge carriers in a semiconducting material. The application of suitable boundary conditions can extend their application to any region in a semi-conductor device where space charge neutrality is maintained. In the forms given above the equations are difficult to manipulate and are consequently of little practical use. It is therefore necessary to make some simplifying assumptions without drastically reducing their generality. In this way it is hoped that the equations can be made tractable under conditions of practical interest.

The following assumptions are proposed for this purpose :

1. The constant energy surfaces are spherical. The effective mass of the charge carriers thus becomes a scalar quantity.
2. Two dimensional effects are considered to arise from the bulk behaviour of charge carriers and not from contact or junction regions. This neglects the non-uniform and multi-dimensional effects of the charge carrier source at the emitter, the charge carrier sink at the collector, the heat source at the collector junction and the heat sinks at the contact areas.
3. Potential gradients generated by the base terminal current are negligible.
4. The impurity concentration in the base region is uniform.
5. Local electron and hole temperatures are equal and negligibly higher than the local lattice temperature. This assumption is made necessary by the lack of detailed information concerning these temperatures.
6. The charge carriers have a Maxwell-Boltzman distribution.

7. The pressure tensors, $\bar{P}$, can be reduced to scalar quantities. This leads to the identities

$$P_n = nkT_n \qquad (3.2.30)$$

$$P_p = pkT_p$$

The set of three simultaneous continuity equations can therefore be written as

Charge $$\frac{\partial (n + p)}{\partial t} + \nabla.(n\bar{v}_n + p\bar{v}_p) = 2(g - r + E(\alpha_i \mu_n n + \beta_i \mu_p p)) \qquad (3.2.31)$$

Momentum $$\bar{F} = -k\nabla(n + p)T + q(p\bar{E}_p - n\bar{E}_n) + q(p\bar{v}_p - n\bar{v}_n)x\bar{B} \qquad (3.2.32)$$

Energy $$C\frac{\partial T}{\partial t} = \sigma E^2 + \nabla.(K\nabla T) \qquad (3.2.33)$$

These equations are applicable to normal current flow across the base region and also to the current flow in a radial direction during a current constriction. The continuity equations can therefore be considered, in conjunction with the radial forces causing current constriction, to describe the behaviour of charge carriers during the pinch associated with second breakdown.

3.3 Pinching Forces.

A constriction in the current flowing across the base region of a transistor is caused by an imbalance in the radial forces acting on the body of charge carriers. The radial distribution of the charge carriers will change, until a localised increase in

concentration establishes a balance of radial forces.

There are three basic conditions under which the constriction, or pinch, must be considered : (i) A region which has a minority carrier concentration very much smaller than the majority carrier concentration.

(ii) A region in which the charge carrier concentrations are comparable, but where the radial forces cause a separation of the electrons and holes.

(iii) A region as in (ii) but where the radial forces cause the holes and electrons to move in the same radial direction.

In conditions (i) and (ii) a space-charge will be established by the radial movement of the charge carriers. The electric field generated by this space-charge will oppose the initial radial forces and limit the change in carrier concentration.

In condition (iii) space-charge neutrality is maintained and there is no electric field to limit the pinching process. The forces opposing constriction are now only those derived from the concentration gradient.

The conditions of current and voltage required to drive a transistor into second breakdown indicate that it is operating at a high injection level. The concentrations of holes and electrons in the base are therefore approximately equal and conditions (ii) and (iii) are applicable. It can be seen from the absence of the electric field generated in (ii) that the pinch associated with (iii) will be much greater. The degree of constriction observed in the transistors tested indicated that the electric fields under conditions described in (i) and (ii) would be very high.

The most significant processes leading to the current constriction associated with second breakdown will therefore be those which enable space-charge neutrality to be maintained. A significant pinch will therefore be restricted to one containing an equal number of holes and electrons.

Consider the instantaneous application of radial forces acting on the charge carriers and causing holes and electrons to move in the same direction. The greater mobility of the electrons will cause them to move at a greater initial rate than the holes. This will cause a radial charge separation. The electric field generated by this local space-charge will act to reduce the apparent mobility of the electrons and increase the apparent mobility of the holes until an equilibrium state is reached. During the current constriction the apparent mobilities of the holes and electrons, in the radial direction, will be equal.

The radial forces acting on the charge carriers are considered to originate from two sources. One of these is thermal and depends upon a local thermal non-uniformity to initiate the pinching process. The other is the radial magnetic field associated with the flow of charge carriers.

3.3.1 Thermally Generated Radial Forces.

Local temperature differences occuring in the base region, in a plane parallel to the junctions, will give rise to radial forces acting on the charge carriers. The current flow will be constricted to hot regions at the expense of the colder regions. As the temperature rises the energy of the system is increased and the n - p product increases. The energy band edges move towards the

intrinsic energy as the temperature rises. (See Fig. 3.3.1). This movement of the band edges is considered to be a combination of (a) Conductivity Modulation and (b) Energy Gap Modulation. (See Fig.3.3.1) (Ref.14).

The base region is considered to be in thermal equilibrium to facilitate the evaluation of the radial forces. The Fermi Level is therefore constant.

Energy Gap Modulation is sufficiently small in silicon to be approximated by a linear temperature dependence (Refs.3,14). This allows the energy gap to be expressed as

$$\mathcal{E}_g = \mathcal{E}_g(0) - \gamma T \qquad (3.3.1)$$

where $\mathcal{E}_g(0)$ is the energy gap at $0^{\circ}K$

γ is the rate of change of energy gap with temperature and is assumed to be constant.

The values of $\mathcal{E}_g(0)$ and γ for silicon have been variously reported as

$\mathcal{E}_g(0)$ (eV)	γ (eV./ K)	Reference.
1.205	$2.8.10^{-4}$	3
1.21	$4.1.10^{-4}$	17
1.21	$3.6.10^{-4}$	18

The product of the charge carrier densities can now be written as

$$np = N_c N_v \exp\left(-\frac{\mathcal{E}_g(0)}{kT} - \frac{\gamma}{k}\right) \qquad (3.3.2)$$

where N_c and N_v are the effective densities of states in the conduction and valence bands respectively.

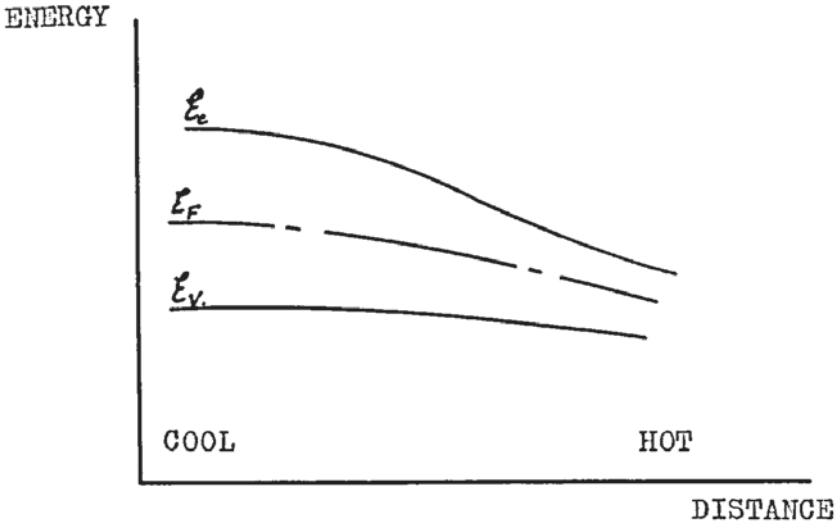

(a) Total

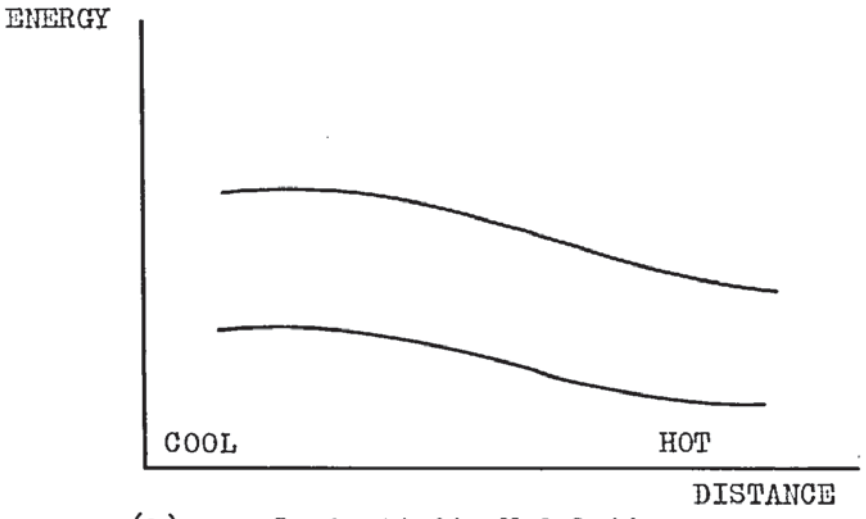

(b) Conductivity Modulation

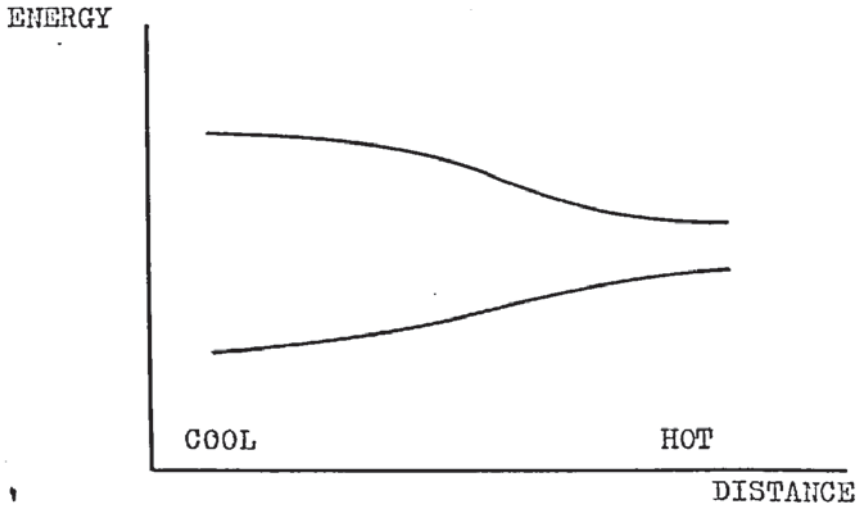

(c) Energy-Gap Modulation

Fig. 3,3,1 Temperature Dependence of the Energy Band Gap.

Assuming that the change in energy gap can be shared equally between the changes at both band edges enables the carrier densities to be expressed as

$$n = N_c \exp\left(\left(\mathcal{E}_F - \mathcal{E}_c + \frac{\gamma T}{2}\right)/kT\right) \quad \text{(a)}$$

$$p = N_v \exp\left(\left(\mathcal{E}_v - \mathcal{E}_F + \frac{\gamma T}{2}\right)/kT\right) \quad \text{(b)} \qquad (3.3.4)$$

It is now convenient to define two electric potentials related to the Fermi, $\mathcal{E}_F$, and the Intrinsic, $\mathcal{E}_i$, Energies.

$$\mathcal{E}_F = -q\Phi$$

$$\mathcal{E}_i = -q\Psi$$

$$= \frac{1}{2}\left(\mathcal{E}_c - \mathcal{E}_v + kT \ln\left(N_v/N_c\right)\right) \qquad (3.3.5)$$

The charge carrier concentrations can be expressed in terms of these potentials as (Ref.14).

$$n = n_i \exp\left(\frac{q(\Psi_n - \Phi)}{kT} + \frac{\gamma}{2k}\right) \quad \text{(a)}$$

$$p = n_i \exp\left(\frac{q(\Psi_p - \Phi)}{kT} + \frac{\gamma}{2k}\right) \quad \text{(b)} \qquad (3.3.6)$$

where n_i is the intrinsic concentration and $np = n_i^2$

These equations can be rearranged to give

$$\Psi_n = \Phi + \frac{kT}{q}\left(\ln\left(n/n_i\right) - \frac{\gamma}{2k}\right) \quad \text{(a)}$$

$$\Psi_p = \Phi - \frac{kT}{q}\left(\ln\left(p/n_i\right) - \frac{\gamma}{2k}\right) \quad \text{(b)} \qquad (3.3.7)$$

The electric field acting on each charge carrier will be given by $\nabla\psi$. This will give rise to a force on the charge carrier of $q\nabla\psi$. The total force, acting in a radial direction on the column of charge carriers, will be the sum of the forces acting on the holes and electrons.

$$\bar{F}_r = nq(\nabla\psi_p - \nabla\psi_n) \qquad (3.3.8)$$

where $n = p$ is the density of holes and electrons taking part in the pinch. Substitution for ψ_n and ψ_p from Equation 3.3.7 gives

$$\bar{F}_r = -k\nabla Tn(\ln(p/n_i) + \ln(n/n_i)) + n\gamma\nabla T \qquad (3.3.9)$$

The first term on the right hand side of this equation represents the Conductivity Modulation and the second term represents Energy Gap Modulation. Since the number of holes and electrons is equal, the conductivity term reduces to zero. The radial pinching force acting on the column of charge carriers due to temperature non-uniformities is therefore

$$\bar{F}_{rT} = n\gamma\nabla T \qquad (3.3.10)$$

This is a force which will cause both holes and electrons to move with a common direction. The conductivity term produces no pinching effect, the action of the forces on the holes and electrons causing a charge separation. Since the hole and electron currents are approximately equal in the breakdown condition, this would not lead to a constriction for a low radial force. Charge movement would result in two concentric current columns in an extreme case.

3.3.2 Magnetic Pinching Forces.

The magnetic field generated by the flow of charge across the base will cause a radial force to act on the charge carriers, concentrating them towards a central point. The size of the force can be obtained from a consideration of the forces acting on a cylindrical shell, radius r and thickness dr, enclosing a current I. Ampere's Law expresses this current in terms of a line integral of the magnetic field as

$$I = \int \bar{J}.\hat{n}\, da = \oint \bar{H}.\, d\bar{s} \qquad (3.3.11)$$

where $\bar{s}$ is in the direction of the current flow and $\hat{n}$ is a unit vector in the $\bar{s}$ direction.

Considering the current flow to be in a cylindrical column and applying the identity $\bar{J} = \sigma \bar{E}$ gives the current as

$$I = 2\pi E \sigma \int_o^r r\, dr \qquad (3.3.12)$$

The magnetic field generated by this current is therefore

$$B = \mu_o \frac{E\sigma}{r} \int_o^r r\, dr \qquad (3.3.13)$$

where μ_o is the permeability.

An equal number of holes and electrons will be involved in the pinch so that the radial forces causing the pinch can be expressed as (Ref.19),

$$\bar{F}_{rB} = \bar{J} \times \bar{B} = \mu_o \frac{\sigma^2 E^2}{r} \int_o^r r\, dr.\, \hat{r} \qquad (3.3.14)$$

The total pinching force will be the sum of the thermal and magnetic forces

$$\bar{F}_r = \bar{F}_{rT} + \bar{F}_{rB} \qquad (3.3.15)$$

Applying the continuity equations to the pinching charge carrier flow and substituting the radial forces derived above into the momentum equation, gives the continuity of radial momentum as

$$\bar{F}_r = -2k\nabla(nT) + \frac{\mu_o \sigma^2 E^2}{r} \int_o^r r\, dr.\hat{r} + n\gamma\nabla T \qquad (3.3.16)$$

Assuming cylindrical symmetry for the pinching current column, allows the energy continuity equation to be written as

$$C \frac{\partial T}{\partial t} = \sigma E^2 + \frac{1}{r}\frac{\partial}{\partial r}\left(Kr\left(\frac{\partial T}{\partial r}\right)\right) \qquad (3.3.17)$$

The radial force will be opposed by the development of a concentration gradient. The radial force generated by the concentration gradient will be

$$\bar{F}_{rc} = \frac{\alpha n}{\mu_a}(\bar{v}_n + \bar{v}_p) \qquad (3.3.18)$$

where μ_a is the common apparent mobility of the charge carriers. Under equilibrium conditions this will be equal to the pinching force. This allows the equality

$$n(\bar{v}_n + \bar{v}_p) = \frac{\mu_a \bar{F}_r}{q} \qquad (3.3.19)$$

where $\bar{F}_r$ has the value assigned above in the momentum continuity equation 3.3.16.

Substituting this relationship into the charge continuity equation reduces the system to two simultaneous equations describing the equilibrium current constriction

Charge

$$2\frac{\partial n}{\partial t} = \nabla.\frac{\mu_a}{q}\left(2k\nabla(nT) - \mu_o\frac{\sigma^2E^2}{}\int_o^r r\,dr.\hat{r} - n\gamma\nabla T\right)$$

$$+ 2(g - r + (\alpha_i\mu_n n + \beta_i\mu_p p)E) \qquad (a)$$

Energy (3.3.20)

$$C\frac{\partial T}{\partial t} = \sigma E^2 + \frac{1}{r}\frac{\partial}{\partial r}\left(Kr\frac{\partial T}{\partial r}\right) \qquad (b)$$

3.3.3 Steady State Breakdown Conditions.

Consideration of the steady state conditions of the pinched current flow greatly reduces the complexity of the above equations. It allows the time derivative, the net radial force and the generation-recombination terms to be discarded. Although this does not give any information about the dynamics of the pinching process, it does allow the charge-carrier distribution in the pinch, to be evaluated. The steady state conditions can be described by the equations

Charge

$$\frac{2kq}{\mu_a}\frac{d(nT)}{dr} - \mu_o\frac{\sigma^2E^2q}{r}\int_o^r r\,dr - qn\gamma\frac{dT}{dr} = 0 \qquad (a)$$

(3.3.21)

Energy

$$E^2 = -\frac{1}{r}\frac{d}{dr}\left(K\frac{dT}{dr}\right) \qquad (b)$$

Rearrangement of the energy equation yields the relationship

$$\sigma E^2\int_o^r r\,dr = -Kr\frac{dT}{dr} \qquad (3.3.22)$$

Substitution into the charge equation results in

$$\frac{2kq}{\mu_a}\frac{d(nT)}{dr} + q\mu_o\sigma K\frac{dT}{dr} - nq\gamma\frac{dT}{dr} = 0 \qquad (3.3.23)$$

where μ_a is the composite hole and electron apparent mobility

μ_o is the permeability of the pinched region.

The mobility and the thermal conductivity are both functions of temperature (Refs.3,14,15,16,17). These can be approximated by the simple relationships (See Appendix 4)

$$\mu_a = A_T T^{-a_T} \qquad (a)$$

$$K = B_T T^{-b_T} \qquad (b) \qquad (3.3.24)$$

where A_T, a_T, B_T, b_T are constants.

Substituting into the above differential equation gives

$$\frac{d(nT)}{dr} - \frac{n\gamma A_T T^{-a_T}}{2k}\frac{dT}{dr} = -\frac{\mu_o A_T B_T T^{-(a_T+b_T)}}{2k}\frac{dT}{dr} \qquad (3.3.25)$$

This differential equation in n has an approximate solution of the form

$$\ln(n) + \ln(T).\left(1 - \frac{\gamma A_T T^{-a_T}}{2\,k}\right) + \frac{\mu_o \sigma A_T B_T T^{-(a_T+b_T)}}{2k(a_T + b_T)} = \ln(n_o) \qquad (3.3.26)$$

where n_o represents the value of n at a convenient reference temperature, T_o, and is considered to be constant.

Rearrangement gives the charge carrier concentration as a function of temperature

$$n = n_o T^{\left(\frac{\gamma A_T T^{-a_T}}{2\,k} - 1\right)} \exp\left(\frac{\mu_o \sigma A_T B_T T^{-(a_T+b_T)}}{2k(a_T + b_T)}\right) \qquad (3.3.27)$$

The spatial temperature distribution is required to complete the equation. This can be obtained experimentally, by infra-red microscope measurements, or derived from consideration of the thermal dissipation arising from the power in the pinched current column.

The theoretical separation of the magnetic and thermal effects can be achieved by assuming either $\gamma = 0$ to give the magnetic effect, or $B = 0$ for the thermal relationship. This is not possible in practical device operation, but is useful as an indication of the importance of each process under different operating conditions.

3.4 Power in the Pinched Plasma.

The energy transported across unit area in unit time, in the presence of electric and magnetic fields is given by the Poynting

vector S (Ref.21).

$$\bar{S} = \bar{E} \times \bar{H} \qquad (3.4.1)$$

Neglecting thermo-electric effects allows the power in the plasma to be expressed in terms of the fields as

$$P = \bar{E} \times \bar{H} \cdot \hat{n}\, da$$

where $\hat{n}$ is a unit vector normal to the elemental cross-sectional area da.

Integration over the plasma cylinder yields the total power as

$$P = E H 2\pi r_m w \qquad (3.4.3)$$

where r_m is the maximum pinch radius

w is the cylinder length.

Ampere's Law gives the magnetic field relationship

$$H = \sigma E \int_0^{r_m} r\, dr = qE \int_0^{r_m} \mu_a n r\, dr \qquad (3.4.4)$$

The power in the pinched plasma is therefore

$$P = 2\pi q \varepsilon w E^2 \int_0^{r_m} \mu_a n r\, dr \qquad (3.4.5)$$

The expressions for mobility and charge carrier density as functions of temperature can be substituted into this equation to give the power dissipation in the pinch as a function of temperature. This will take the form

$$P = A \int_0^{r_m} r T^B \exp(-CT^{-D})\, dr \qquad (3.4.6)$$

where A, B, C and D are constants.

An incremental technique can be used to derive the temperature, power and charge concentration distribution as a function of the plasma radius. An initial estimate of the maximum temperature is used, in conjunction with the temperature gradient, to calculate the temperature at the plasma edge. This is compared with a known ambient temperature and the initial estimate corrected. The temperature gradient can be obtained from the energy equation

$$Kr \frac{dT}{dr} = -qE^2 \sigma \int_0^r r\, dr \qquad (3.4.7)$$

Substitution for the temperature dependent terms and rearranging gives the form of equation as

$$\frac{dT}{dr} = \frac{FT^G}{r} \int_0^r r T^B \exp(-CT^{-D})\, dr \qquad (3.4.8)$$

where B, C, D, F and G are constants.

3.5 Conditions for Current Constriction.

The energy densities of the charge carriers and of the fields causing constriction can be used to define the critical conditions for pinching to occur. The limiting condition for pinching is given by the equality of the energy density of the charge carriers

and the energy densities of the radial electric field and the circumferential magnetic field (Refs.20,22). The charge carrier concentration involved in the pinch will be that which is in excess of the impurity concentration, since only an equal number of holes and electrons can participate.

The total energy density of the charge carriers is k (nT + pT). Conditions in the pinched plasma allow the approximation $T_n = T_p$ and n = p. The energy densities of holes and electrons are therefore equal and the approximation

$$\psi_c = nkT \qquad (3.5.1)$$

can be used.

The energy density of the fields is given by (Ref.21)

$$\psi_F = \frac{1}{2}(K_p \varepsilon_o \langle E^2 \rangle + \mu_o \langle H^2 \rangle) \qquad (3.5.2)$$

where ε_o is the permittivity of free space and K_p is the relative permittivity.

μ_o is the permeability.

The circumferential field is obtained by applying Ampere's Law to the current in the plasma column. This results in the relationship

$$B = \mu_o I/2\,r \qquad (3.5.3)$$

The radial electric field will be generated by the Energy Gap Modulation as discussed above. The radial electric field will therefore be

$$E_r = \frac{\chi}{q} \nabla T \qquad (3.5.4)$$

At the limit of pinching steady state conditions still apply, allowing the energy continuity equation to be written as

$$\sigma E^2 = -\frac{1}{r}\frac{d}{dr}\left(Kr\,\frac{dT}{dr}\right) \qquad (3.5.5)$$

The temperature gradient for the constricting column is therefore

$$\nabla T = -\frac{1}{Kr}\int_o^r \mu_a\, qnE^2\, r\, dr$$

$$\nabla T = -\frac{1}{Kr}\int_o^r v_d\, qnE\, r\, dr \qquad (3.5.6)$$

where v_d is the drift velocity of the charge carriers.

The current enclosed in the cylinder can be expressed in terms of the rate of charge transport over the plasma area as

$$I = \int_o^r 2\pi\, qnv_d r\, dr \qquad (3.5.7)$$

Substituting for the integral in the temperature gradient relationship gives the gradient as a function of current in the plasma column as

$$\nabla T = -\frac{E\,I}{2\pi Kr} \qquad (3.5.8)$$

The radial electric field can therefore be expressed as a function of the plasma current and the lateral electric field, by substitution for ∇T , namely

$$E_r = -\frac{E\,I}{2\pi Kr} \qquad (3.5.9)$$

The critical equality defining the limit of current constriction is

$$\psi_c = \psi_F$$

which can be expressed more fully as

$$K_p \left(\frac{\gamma EI}{2\pi qKr} \right)^2 + \mu_o \left(\frac{I}{2\pi r} \right)^2 = 2nkT_m \qquad (3.5.10)$$

The current in this equality will be that current involved in the pinch. Rearrangement of the equation gives the pinched current as

$$I_p = \left(\frac{nkT_m 8\pi^2 q^2 r^2 K^2}{K_p \varepsilon_o \gamma^2 E^2 + \mu_o K^2 q^2} \right)^{\frac{1}{2}} \qquad (3.5.11)$$

Assuming a uniform current distribution at the onset of pinching allows the current integral to be simplified to

$$I_q = \pi qvnr^2 \qquad (3.5.12)$$

This will be the current flowing across the base region over an area defined by the radius r. At the critical point the current flowing over the pinched plasma area will be defined by both expressions and the critical current, I_{cr}, will be

$$I_p = I_q = I_{cr}$$

The critical current for pinching is therefore

$$I_{crit} = I_p^2 / I_q$$

$$= \frac{8 k T q K^2 \pi}{v(K_p \varepsilon_o \gamma^2 E^2 + \mu_o K^2 q^2)} \qquad (3.5.13)$$

This expression has a similar form to that derived for the constriction in an ionised gas stream (Ref.20). An additional

term appears here derived from the temperature dependent radial electric field. This term will be of greatest importance in a transistor having a high level of avalanche multiplication. Operating conditions under which avalanche multiplication is negligible gives a value of critical current which is closely approximated by the value required for ionised gas constriction.

The expression given in Equation 3.5.13, represents a critical condition of equilibrium between the three parameters determining the transistor operating conditions, temperature, current and electric field. It would be equally valid to describe a critical value of temperature, or electric field, having the other two parameters independently defined.

The electric field generated by the base resistance has been neglected in the above analysis. The effect on the critical current is dependent upon the base bias condition. Under forward base-bias the base terminal current acts to oppose pinching. Under reverse base-bias the pinch is assisted by the resistive field and the effective value of critical current is reduced. The expression given above is for the base open condition only.

The critical current has a temperature dependence which is largely determined by the charge carrier temperature, T_m . Under conditions of short duration current pulses having a low repetition rate it can be assumed that the charge carrier temperature is closely coupled to the ambient temperature. Although this will be far from true during breakdown, it is assumed that the device temperature has sufficient time between pulses to decay to the ambient temperature.

The expression is also temperature dependent through the

thermal conductivity. This will become more important under high electric field and high temperature conditions. The electric field has a temperature dependence but this is relatively small (Ref. 36).

The charge carrier drift velocity is also a function of temperature. Drift velocity saturation is encountered at an electric field strength considerably lower than the avalanche breakdown field strength (Refs.24-26). Under conditions of operation which produce second breakdown, the field strength will be of sufficient magnitude to cause velocity saturation. The saturation drift velocity has a temperature dependence which can be represented by the empirical form (Ref.26)

$$v(T) = v_o(1 - GT) \qquad (3.5.14)$$

where $v_o = 1.37\ 10^7$ cm./s. and $G = 6.7\ 10^{-4}\ /^oK.$

The temperature dependence of the critical current can therefore be demonstrated by substituting these relationships into the critical current equation given above to yield

$$I_{crit} = \frac{8 \pi k T_m}{q v_o (1 - GT)} \left(1 + \frac{K_p \varepsilon_o^2 E^2 q^2}{B_T^2 T^{-2b_T}} \right)^{-1} \qquad (3.5.15)$$

This relation will be maintained up to the intrinsic temperature. At that temperature the conditions of charge carrier distribution within the device change. Although the operation of the device, as a transistor, is modified the dependence of the Energy Gap upon temperature is maintained and hence the effect of Energy-Gap Modulation upon the charge carrier concentration is

unaltered. Some change may be observed in the terminal conditions of the transistor as the intrinsic temperature is reached but, current constriction will continue to depend upon the above mechanism, provided that ambipolar conduction is maintained.

3.6 Time Dependent Thermal Dissipation.

The system of continuity equations derived above can give a detailed analysis of the dynamics of second breakdown, with the aid of appropriate boundary conditions. The solution of these equations in their time dependent form is, however, extremely complex. It is proposed therefore to derive an expression for the delay time by treating the thermal breakdown processes in isolation. In this way the time dependent relationship can be simplified, although a complete description of the whole range of breakdown conditions is not possible.

Thermal processes are considered to control breakdown when the delay time is long. The limit to this approximation is not clearly defined, but is dependent upon the size and structure of the device and the ambient temperature. For the medium power devices used in this project the controlling breakdown process can be considered to be thermal for delay times as short as 10μs.

An investigation of the time dependent temperature distribution, resulting from a step input of power, is proposed. The resultant expression can be used in conjunction with the temperature dependent properties controlling conduction and constriction in the transistor, to provide a value of the delay time.

The assumptions made to simplify the thermal analysis are as follows :-

1. The region of the transistor of interest can be considered to be infinite in two directions and to be bounded by an adiabatic surface in the other. The heat conduction at the surface is assumed to have a zero normal component.
2. Thermal conduction through the metal contacts and leads is negligible during the delay time.
3. Convection at the surface is negligible.
4. The medium of heat conduction is homogeneous.
5. Power is dissipated in one region only.
6. Radiation from the surface is considered to be negligible during the delay time.

These approximations are usually considered acceptable for high-speed medium-power transistors. (Refs.50,51). Most of the thermal spreading occurs in the base region, in which the width is small compared with the other device dimensions. The region of greatest interest thus has a low impurity concentration and the assumption of constant thermal properties is a good approximation.

Power dissipation occurs mainly in the collector-base space-charge region carrying the bulk of the current. Charge carriers in this region attain a high velocity and transfer energy to the crystal by interactions with the lattice. The geometry of the high power dissipation region is determined by the emitter and the mode of operation, coupled with the injection level. The onset of second breakdown ends normal device operation. Power dissipation during breakdown occurs in a cylindrical column, formed by the pinching process.

The time dependent equation for the conduction of heat in a solid is given by (Refs.21,52,53),

$$\nabla^2 T = \frac{\rho_m C}{K} \frac{\partial T}{\partial t}$$

$$= \frac{1}{k_T} \frac{\partial T}{\partial t} \qquad (3.6.1)$$

where ρ_m is the density of the medium

C is the specific heat

K is the thermal conductivity

k_T is the thermal diffusivity

In rectangular co-ordinates this becomes

$$\frac{\partial^2 T}{\partial x^2} + \frac{\partial^2 T}{\partial y^2} + \frac{\partial^2 T}{\partial z^2} = \frac{1}{k_T} \frac{\partial T}{\partial t} \qquad (3.6.2)$$

To determine the temperature distribution resulting from a source of finite dimensions, it is convenient to consider the effect of a point source and extend this to cover the practical source dimensions. An expression can be derived for the temperature distribution in terms of the power density, by means of the point-source relationship. Integration over the source co-ordinates yields the complete temperature distribution (Ref.53).

The temperature in an infinite solid due to a quantity of heat, $Q\rho c$, generated at time $t = t_o$ and position (x_o, y_o, z_o), is given by (Refs.53,54)

$$T = \frac{Q}{8(k_T(t - t_o))^{1.5}} \exp\left\{ \frac{-m^2}{4k_T(t - t_o)} \right\} \qquad (3.6.3)$$

where $m^2 = (x - x_o)^2 + (y - y_o)^2 + (z - z_o)^2$

Continuous liberation of heat from this source allows the heat generation to be expressed in terms of the power density per unit volume, $P(t)/V$, over the elemental volume dx,dy,dz. This leads to the expression of the temperature distribution as

$$T(x,y,z,t) = \frac{1}{8\rho_o cV(\pi k_T)^{1.5}} \cdot \int_{-\frac{W}{2}}^{\frac{W}{2}} \int_{-\frac{L}{2}}^{\frac{L}{2}} \int_{-\frac{H}{2}}^{\frac{H}{2}} \int_{t_o}^{t} \frac{P(t)}{(t - t_o)^{1.5}} \exp\left(\frac{-m^2}{4k_T(t - t_o)} \right) dx.dy.dz.dt \qquad (3.6.4)$$

The method of images (see Fig. 3.6.1) is used to obtain a solution for a medium bounded by an adiabatic surface. The boundary conditions are in this case

$$\begin{aligned} &\text{Limit } (x,y \to \infty) \qquad T \to 0 && \text{(a)} \\ &T = p(t)/K \qquad \text{for} \quad \left(\begin{matrix} -W/2 < x < W/2 \\ -L/2 < y < L/2 \end{matrix} \right) && \text{(b)} \\ &T = 0 \quad \text{for all other regions.} \end{aligned} \qquad (3.6.5)$$

This results in a temperature distribution which can be expressed as

$$T(x,y,z,t) = \frac{1}{8\rho cV(\pi k_T)^{1.5}} \int_{t_o}^{t} \frac{P(t)}{(t - t_o)^{1.5}}\, dt \cdot \left(\int_{-W/2}^{W/2} \exp\left(\frac{-(x - x_o)^2}{4k_T(t - t_o)} \right) dx. \int_{-L/2}^{L/2} \exp\left(\frac{-(y - y_o)^2}{4k_T(t - t_o)} \right) dy. \left[\int_{-(W_b+H)}^{-W_b} \exp\left(\frac{-(z - z_o)^2}{4k_T(t - t_o)} \right) dz + \int_{W_b}^{(W_b+H)} \exp\left(\frac{-(z - z_o)^2}{4k_T(t - t_o)} \right) dz \right] \right)$$

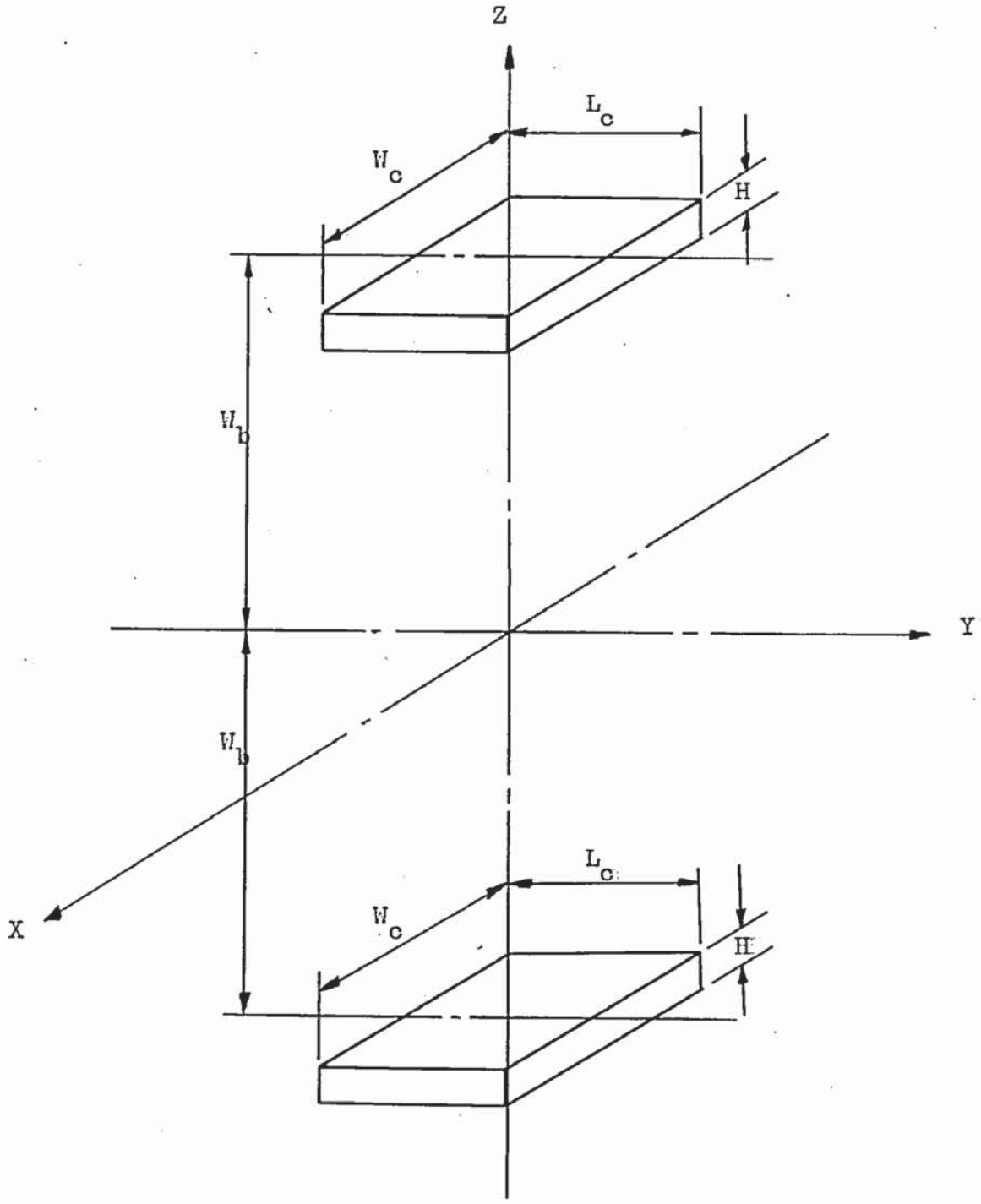

Fig. 3.6.1 Spatial Arrangement of Power Source and Im age.

The assumption of a step function of input power applied at $t = 0$ of amplitude, P, simplifies the relationship to

$$T(x,y,z,t) = \frac{P}{8\rho CV}\int_{t_o}^{t} \left\{\operatorname{erf}\left(\frac{W_c/2 + x}{\delta}\right) + \operatorname{erf}\left(\frac{W_c/2 - x}{\delta}\right)\right\} \cdot$$

$$\left\{\operatorname{erf}\left(\frac{L_c/2 + y}{\delta}\right) + \operatorname{erf}\left(\frac{L_c/2 - y}{\delta}\right)\right\} \cdot \left\{\operatorname{erf}\left(\frac{W_b + H + z}{\delta}\right) +\right.$$

$$\left.\operatorname{erf}\left(\frac{-W_b - z}{\delta}\right) + \operatorname{erf}\left(\frac{z - W_b}{\delta}\right) + \operatorname{erf}\left(\frac{W_b + H - z}{\delta}\right)\right\} dt \qquad (3.6.6)$$

where $\delta^2 = 4k_T(t - t_o)$

The complete solution for a multiple emitter device can be obtained by super-position, contributions from the sources associated with each emitter being added linearly at all points in space and time. The expression will be made considerably more complex by the inclusion of the spatial distribution of the power density. This distribution will depend upon the base bias mode and the injection level.

A similar expression is derived for the temperature distribution in devices having a circular emitter configuration (See Appendix 6)

$$T(r,z,t) = \frac{P}{4\rho CV\pi^{\frac{1}{2}}}\int_{t_o}^{t} \frac{1}{\delta^3}\left(\left(2r\operatorname{erf}\left(\frac{r}{\delta}\right) + \frac{1}{\frac{1}{2}}\left(\exp\left(-\frac{r^2}{\delta^2}\right) - 1\right)\right) \cdot\right.$$

$$\left.\left(\operatorname{erf}\left(\frac{W_b + H - z}{\delta}\right) + \operatorname{erf}\left(\frac{-W_b - z}{\delta}\right) + \operatorname{erf}\left(\frac{W_b + H - z}{\delta}\right) + \operatorname{erf}\left(\frac{z - W_b}{\delta}\right)\right)\right) dt \qquad (3.6.7)$$

These expressions for the transient thermal response can be used in conjunction with the temperature dependence of the electrical characteristics, involved in the normal and breakdown conduction processes, to determine the delay time. An analysis of the thermal breakdown time dependence can be obtained in two ways :

(i) Examination of the critical conditions for current constriction to occur. The temperature dependence of the radial forces causing constriction of the current is used in conjunction with the transient thermal response.

(ii) The derivation of a temperature dependent expression for the collector current-voltage relationship. A negative resistance region will occur when conditions favourable to breakdown are established. At this point the maximum current density can be supported by a voltage which is lower than the applied voltage. The temperature required for this leads to a value of delay time. Electrical effects can be assumed to follow the temperature variations instantaneously.

3.6.1 Critical Temperature Gradient.

The critical conditions defining the onset of current constriction were introduced in Section 3.5, where they were used to provide a value of critical collector current. The same energy balance equation can be used to provide critical values of electric field and temperature gradient. An expression for the temperature gradient can be derived from the energy balance equation when presented in the form

$$K_p \, \mathcal{E}_o \left(\nabla T \, \frac{\gamma}{q} \right)^2 + \mu_o \left(\frac{I_c}{2\pi r} \right)^2 = 2 n k T_n \quad (3.6.8)$$

A critical condition is reached at a temperature gradient given by

$$\nabla T = \frac{q}{\gamma}\left(\frac{2nkT_m}{K_p \varepsilon_o} - \frac{\mu_o}{K_p \varepsilon_o}\left(\frac{I_c}{2\pi r}\right)^2 \right)^{\frac{1}{2}} \qquad (3.6.9)$$

There will be a similar expression for a system defined by rectangular co-ordinates. The critical gradient will occur in a plane perpendicular to the current flow.

The examination of the relative magnitude of the two terms in parenthesis in Equation 3.6.9, shows that at room temperature the expression can be simplified to

$$\nabla T = \frac{q}{\gamma}\left(\frac{2nkT_m}{K_p \varepsilon_o} \right)^{\frac{1}{2}} \qquad (3.6.10)$$

This derivation has taken no specific account of the spatial distribution of the charge carriers. Non-uniformities of the charge carrier concentration due to base bias and injection level effects will not change the essential character of the relationship, although the complexity will be greatly increased.

The radial temperature gradient can be derived from the transient response given in Section 3.6. The critical gradient then yields the delay time for the onset of current constriction after the application of the power pulse, and hence the delay time for Second Breakdown.

3.7 Operation at High Collector Current.

Under conditions leading to second breakdown the transistor is operating with a high level of charge-carrier injection from the

emitter into the base region. As the injection level rises factors generally neglected, when normal transistor operation is analysed, must be taken into account. Four factors become increasingly important as the collector current rises, namely :

(i) Ohmic potential gradients in the base and epitaxial regions. (It is assumed that the devices under consideration are of the planar epitaxial structure and that the emitter and substrate have a high impurity concentration).

(ii) Lateral current injection.

(iii) Base width modulation.

(iv) Avalanche injection.

The last three factors demonstrate the dependence of the charge carrier density upon both the space variable, x, and the current density, J, at high injection levels.

3.7.1 Ohmic Potential Gradients.

In a planar diffused transistor the base terminal current is caused primarily by recombination in the active base area under the emitter (Ref.27). A potential gradient is formed by the flow of recombination current from the base contact through the high resistivity base to the region under the emitter. When the transistor is operating under conditions of forward base-bias, the potential gradient causes an increase of current density in areas of the emitter closest to the base contact. A charge carrier density gradient is formed to produce an equilibrium condition, the maximum charge concentration being near the emitter extremities. The high impurity density in the emitter produces a negligible stabilising

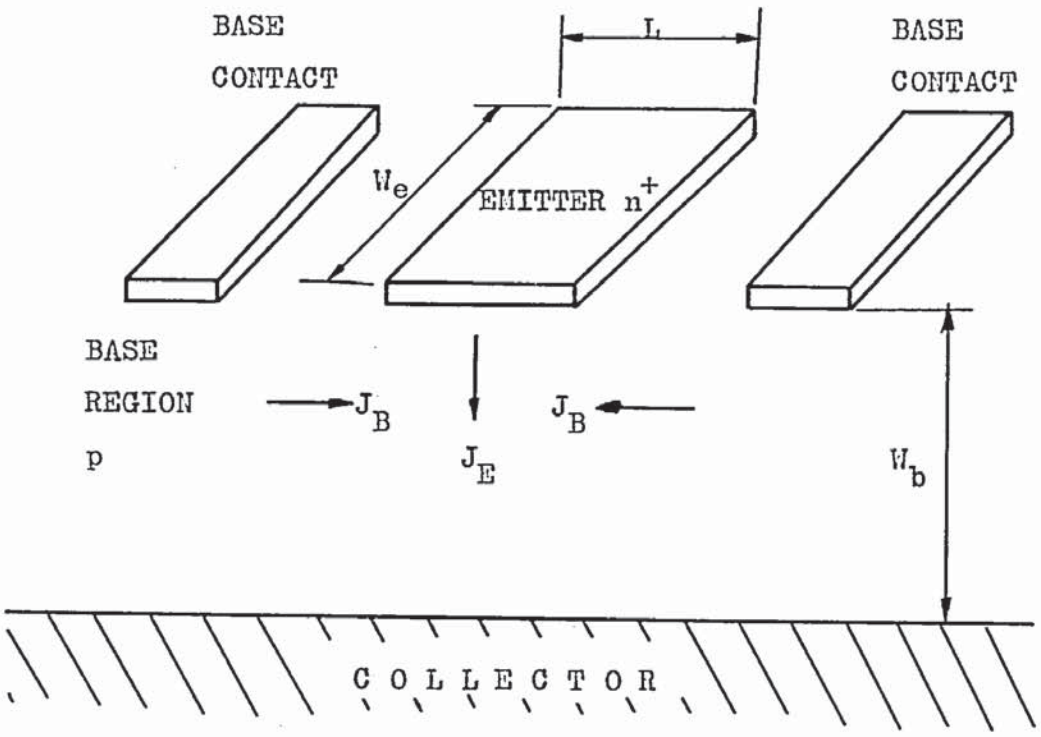

Fig. 3.7.1 Current Flow in the Base Region.
(Forward Base-Bias)

influence over this non-uniformity of current distribution.

This form of non-uniformity in charge carrier distribution will be enhanced by rapid emitter profile changes. Star and comb shaped emitters will have localised high field regions near the emitter extremities. These will act to increase the local power dissipation, since the current profile at the collector closely follows that at the emitter, particularly for narrow base widths. Non-uniformities in power dissipation lead to the early onset of second breakdown by the production of thermal gradients in the space-charge region.

Current crowding due to the transverse base current becomes significant when the potential difference across the emitter stripe is in the region of kT/q (Refs.37,38). This arises from the exponential potential relation of the emitter current density and emitter-base voltage

$$J_e(x) = J_o \exp\left(\frac{V}{V_o} - 1\right) \qquad (3.7.1)$$

where J_o is the reverse bias saturation current density

and $V_o = kT/q$

Assuming that the current distribution is uniform before the injected current density reaches a critical value, the value of collector current above which resistive currents cause significant crowding can be expressed as

$$I_c = \frac{hJ_b\alpha}{(1-\alpha)} = \frac{kT}{q}\sigma_b \frac{h\alpha}{(1-\alpha)} \qquad (3.7.2)$$

where W is the base width
h is the emitter length
α is the current amplification factor

} See Fig. 3.7.1

Ohmic potential gradients in the collector region help to prevent second breakdown by reducing the non-uniformity of the power distribution. Potential differences outside the space-charge region reduce the voltage drop across that region to a minimum at points of highest current density. The dependence of the carrier density within the space charge region upon the current density masks the stabilising effect of potential gradients in the space-charge, (Refs.41,42).

The deliberate addition of high resistivity regions in the emitter can be used to improve the uniformity of the current distribution for forward base-bias operation, but the effect upon open base performance is negligible.

3.7.2 Mobile Charge-Carrier Effects.

In an n - p - n transistor operating at low current levels the collector current is carried almost entirely by electrons. The limit for this to be an accurate representation of the operation is defined by the impurity concentration in the collector region (epitaxial). Increasing the current density above a value given by

$$J_o = q\mu N_{DC} \frac{V_{CB}}{W_{epi}}$$

changes the operation of the device. As the current density increases conduction becomes ambipolar and the electric field distribution becomes dependent upon mobile charge carriers.

Assuming that charge-carrier transport in the collector space-charge region is due entirely to drift, gives the charge-carrier concentration as

$$\rho_c = q\left(\frac{J}{qv} - N_{DC}\right) \qquad (3.7.3)$$

The one-dimensional Poisson Equation can be expressed as

$$\frac{dE}{dz} = \frac{q}{K_p \varepsilon_o}\left(\frac{J}{qv_1} - N_{DC}\right) \qquad (3.7.4)$$

Assuming that J and v are independent of z allows the integration of Equation 3.7.4 to be simplified, so that

$$E(z) = E(0) + \frac{qz}{K_p \varepsilon_o}\left(\frac{J}{qv_1} - N_{DC}\right) \qquad (3.7.5)$$

In this case v_1 is the saturated drift velocity.

The effect of increasing current density upon the electric field distribution is shown in Fig. 3.7.2.

A considerable change in operating conditions must occur if the collector current is to exceed a value given by

$$I_{cT} = J_T A_e = qv_1 A_e\left(\frac{2K_p \varepsilon_o V_{CB}}{q W_{epi}^2} + N_{DC}\right) \qquad (3.7.6)$$

where A_e is the emitter area and diffusion effects have been neglected.

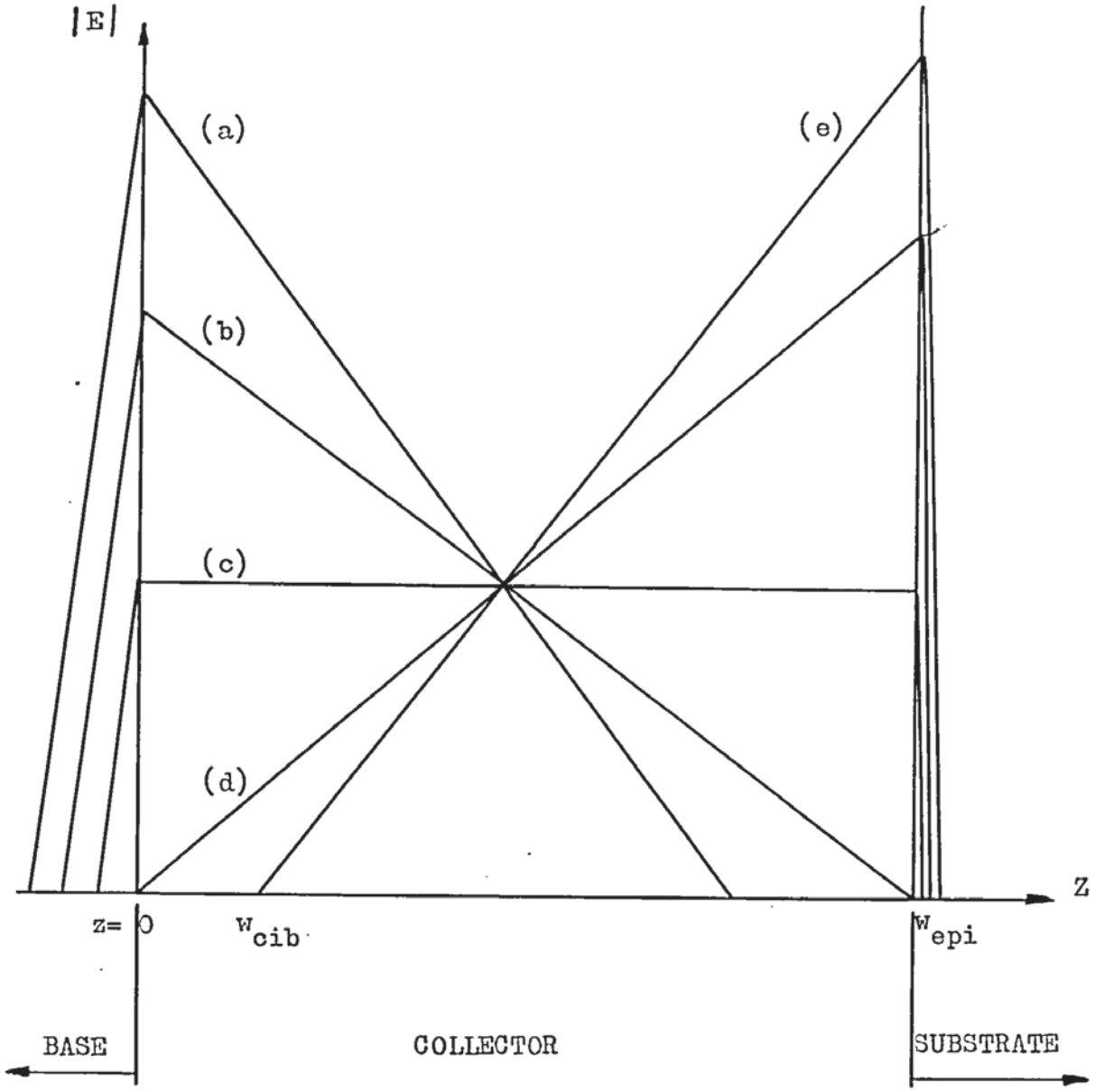

Fig. 3.7.2 Electric Field Distribution .

Current increses (a) to (e)

The collector current can exceed this value by means of two changes :

(i) The current density is limited to J_T and the effective collection area increases (Lateral Current Injection).

(ii) The collection area remains constant and the current density increases above J_T , causing a change in the effective collector and base dimensions (Base Width Modulation).

3.7.2 (a) Lateral Current Injection.

The emitter area is defined clearly by device construction, but the collection area can vary from the low current case, in which it is equal to the emitter area, up to a maximum defined by the epitaxial layer area. The current flow across the base is no longer unilateral, but has longitudinal and transverse components (See Fig. 3.7.3).

If the current density is constant the collection area is related to the collector current by (Ref.39), $A = A_e(I_c/I_T)$

3.7.2 (b) Base Width Modulation.

Assuming the collection area to be constant results in a large number of minority carriers entering the collector region at current densities in excess of J_T. Charge storage occurs in the vicinity of the collector-base junction, positive charge-carriers being accumulated to neutralise the injected negative carriers. The electric field distribution in the collector is modified, as shown in Fig.3.7.2. The substrate must now be considered as an integral part of the device, giving an $n^+ - p - n - n^+$ structure.

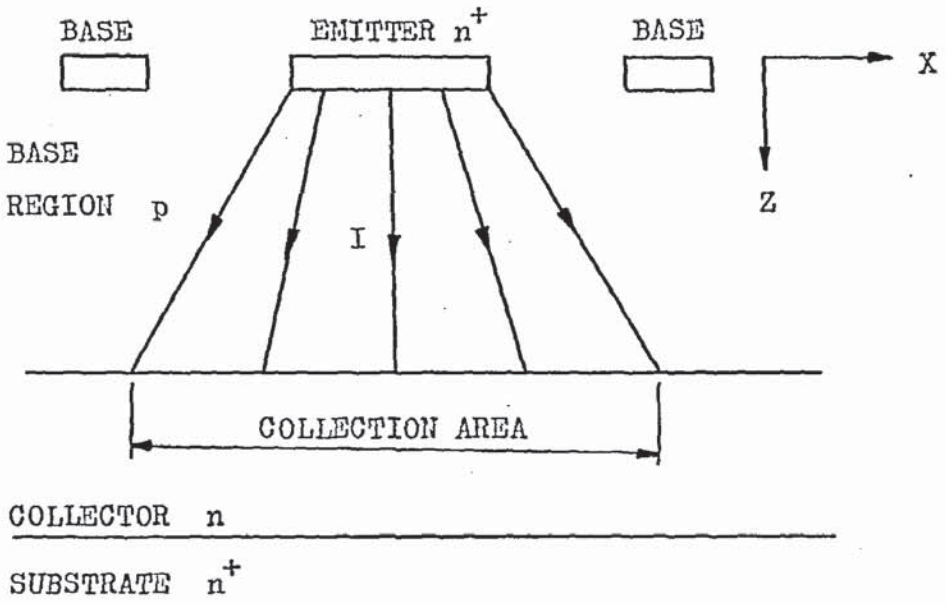

Fig. 3.7.3 Lateral Current Injection.

As the collector current density increases above J_o, the maximum electric field is transferred from the collector-base junction to the collector-substrate junction. The high impurity concentration in the substrate region makes this junction more sensitive to avalanche multiplication.

As the electric field at the substrate junction increases avalanche multiplication produces an increasing number of electron-hole pairs near this junction. The holes drift towards the base junction, where they are neutralised by electrons injected from the base. At the epitaxial substrate junction the hole concentration must be zero, the n^+ region being incapable of injecting holes into the n region. The current at the substrate is composed entirely of electrons, while in other regions the current is a combination of electron and hole movement.

The operation of the collector-base junction will be modified by the injection of holes from the vicinity of the substrate junction. As the ionisation rate increases the base becomes incapable of providing sufficient electrons to neutralise the holes in the collector. The hole concentration in the vicinity of the base junction increases until it reaches the level of the impurity concentration in the base region. The collector region adjacent to the junction is now electrically identical to the base region. The effective base-collector junction is no longer located at the metallurgical junction. The effective base width has been increased and the effective collector width reduced. The region of the collector which resembles the base region is referred to as the "current induced base". The length of the drift path in the collector region has been reduced, increasing the rate of charge

carrier transport across the region.

The width of the current induced base region, W_{cib}, can be approximated by (Refs.30,40),

$$W_{cib} = W_{epi}\left\{ 1 - \frac{I_{CT} - qN_{DC}v_1A_e}{I_c - qN_{DC}v_1A_e} \right\} \qquad (3.7.8)$$

3.7.3 Second Breakdown at High Collector Current.

High levels of charge-carrier injection will significantly affect the breakdown characteristics of a transistor. The change in characteristics will depend upon the charge-carrier distribution, the electric field distribution and the effective dimensions of the transistor regions. At high collector currents a triple-diffused epitaxial collector transistor can behave in a manner similar to that seen in p - i - n diodes (Refs.43,44).

When the breakdown mechanism is predominantly thermal, non-uniformities in the charge-carrier distribution, in the space-charge region, will cause high local power dissipation. Changes in the electric field distribution and in the effective regional dimensions can alter the position of this maximum power dissipation. Base width modulation increases the depth of the heat source below the surface and lateral injection reduces the power density. Both of these processes act to increase the delay time by their effect upon the transient thermal response.

3.7.4 Current Distribution at High Injection Levels.

The simplest operating condition is given by the open base mode. The effect of base terminal current upon the current distribution in the base region can be neglected. This allows the current density immediately under the emitter area to be approximated by the uniform distribution given by

$$J = I / A_e$$

where A_e is the emitter area.

At low injection levels the current distribution at the collector closely resembles the distribution at the emitter. As the current increases lateral current flow occurs in the base region, the diffusion of charge carriers in the base region becoming increasingly important as the current increases. The effective collection area increases as the charge-carrier density under the emitter rises.

Space-charge neutrality is maintained in the bulk of the base region, conduction being ambipolar. Charge-carrier movement in the base is controlled predominantly by diffusion processes. Ambipolar diffusion can be treated in exactly the same way as single carrier diffusion provided that the mobility and diffusion coefficients are replaced by common values (Refs.14,47). These modified values are related to the individual charge-carrier values by

$$\mu_a = \frac{\mu_e \mu_h}{\mu_e + \mu_h} \qquad (3.7.10)$$

$$D_a = (D_e \mu_h + D_h \mu_e)/(\mu_e + \mu_h) \qquad (3.7.11)$$

The charge continuity equation for the base region is

$$\frac{\partial n}{\partial t} = \nabla.(\Delta n\bar{v}) - (n - N_{AB})/\tau \qquad (3.7.12)$$

where Δn is the injected carrier concentration, N_{AB} is the impurity concentration and τ is the carrier lifetime.

This can be rearranged in terms of the injected carrier to give

$$\frac{\partial n}{\partial t} = D_a \nabla^2(\Delta n) - \Delta n/\tau \qquad (3.7.13)$$

This differential equation has a solution of the general form (Refs.45,47),

$$n = \sum_{m=0}^{\infty} b_m \exp(\frac{-t}{\tau_m}) \cdot J_o(\frac{a_m r}{R}) \qquad (3.7.14)$$

where $\tau_m = D_a(a_m/R)^2$

J_o is a zero'th order Bessel Function.

b_m is determined by the distribution of the charge carriers at time $t = 0$

a_m is a constant evaluated at each m

τ_m decreases rapidly as m increases, allowing Equation 3.7.14 to be simplified to

$$n = b_o \exp(-t/\tau_o) \cdot J_o(4r/R) \qquad (3.7.15)$$

The approximation improves as t increases.

The action of the transistor can be analysed by applying a step function injection of charge-carriers of density N, at time $t = 0$, in a plane $x = 0$. The complexity of the result can be reduced by limiting the system to one-dimension. This assumes a symmetrical distribution of charge carriers and that local effects at the boundaries can be neglected. The collector junction provides a bounding surface, for the charge-carrier diffusion, which exhibits an almost infinite recombination velocity. The excess carrier concentration at this surface is therefore considered to be zero (Ref.47). This results in a charge-carrier distribution expressed as

$$n(r,t) = N\left\{\exp\left(\frac{-r}{L_a}\right)\operatorname{erfc}\left(\frac{r}{(4Dt)^{\frac{1}{2}}} - \left(\frac{t}{\tau}\right)^{\frac{1}{2}}\right) + \exp\left(\frac{z}{L_a}\right)\operatorname{erfc}\left(\frac{z}{(4Dt)^{\frac{1}{2}}} + \left(\frac{t}{\tau}\right)^{\frac{1}{2}}\right)\right\} \tag{3.7.16}$$

where L_a is the effective ambipolar diffusion length.

The mean square distance travelled by the charge-carrier is given by (Refs.14,45,47),

$$\langle r^2 \rangle = \frac{1}{N}\int_0^{r_m} r^2 n(r,t)\, dr \tag{3.7.17}$$

which for the one-dimensional case becomes

$$\langle r^2 \rangle = 2Dt \tag{3.7.18}$$

The average displacement of the charge-carriers is related to this by (Ref.46),

$$\bar{r} = \left(\frac{2\langle r^2 \rangle}{\pi}\right)^{\frac{1}{2}} \tag{3.7.19}$$

In general the base width is small in comparison with the unrestricted mean diffusion length. The transit time across the base region is therefore smaller than the recombination time constant. Recombination in the base region therefore plays a minor part in determining the charge carrier distribution. Neglecting the effects of recombination and generation, in the space-charge-neutral base region, allows the charge-carrier distribution to be simply expressed as

$$n(r,t) = N \operatorname{erfc}\left(\frac{r}{(4Dt)^{\frac{1}{2}}}\right) \qquad (3.7.20)$$

The limit to the value of t, in this equation, is obtained by the consideration of the transit time for charge-carriers in the base region. For diffused transistor structures this is usually given as (Refs.30,39,47),

$$t_{tr} = W_b^2 / aD \qquad (3.7.21)$$

where a is a constant dependent upon the "built in" base electric field, usually between 2 and 10 ($a = 2$ for uniform base impurity density).

Increasing the injected concentration of charge-carriers in the base makes the diffusion coefficient more dependent upon the mobile charge carrier distribution, reducing the dependence upon the impurity concentration. At high injection levels the transit time approaches the value (Ref.30),

$$t_{tr} = \frac{W_b^2}{4D_{ba}} + \frac{W_{cib}^2}{4D_{ca}} \qquad (3.7.22)$$

where D_{ba} and D_{ca} are the ambipolar diffusion coefficients for the base and current-induced base regions respectively.

At the base edge of the collector-base junction space-charge region the charge-carrier distribution is given by

$$n(r) = N \operatorname{erfc}\left(\frac{r}{w_{be}}\right) \qquad (3.7.23)$$

where w_{be} is the effective base width ($= w_b + w_{cib}$) and it is assumed that $D_{ba} = D_{ca}$.

3.7.5 Power Distribution in the Collector Space-Charge Region.

In an epitaxial collector transistor the impurity concentration in the collector is low. Most of the power dissipation takes place in the collector region. At high collector current levels, when conduction approaches space-charge-limited conditions, power dissipation can be assumed to occur exclusively in the collector region. Under conditions leading to second breakdown, the current density can be expressed as

$$\bar{J} = q N \bar{v}_1 \qquad (3.7.25)$$

where N is the total charge-carrier concentration.

The electric field in the collector region will be given by the system of equations

$$\nabla.\bar{E} = \frac{q \Delta n}{K_p \varepsilon_o} \qquad (3.7.26)$$

$$\frac{\partial N}{\partial t} = \mu E(\nabla(\Delta n) - \alpha_i N) \qquad (3.7.27)$$

$$\alpha_i = \alpha_e = \alpha_h = \alpha_\infty \exp(-\frac{b}{E}) \qquad (3.7.28)$$

(Refs.36,48,57)

where Δn is the excess charge carrier concentration $(n - p - N_D)$

α is the ionisation coefficient

α_∞ is the asymptotic value of α as E approaches infinity.

The application of equilibrium conditions to this system results in the differential equation

$$\nabla^2 E - \frac{q\alpha_\infty N}{K_p \varepsilon_o} \exp(-\frac{b}{E}) = 0 \qquad (3.7.29)$$

In the regions remote from the high current density areas the maximum electric field will be located at the collector-base junction and have the low current value (Refs.30,47),

$$E_m = \left(\frac{2qN_i V_{CB}}{K_p \varepsilon_o} \right)^{\frac{1}{2}} \qquad (3.7.30)$$

In regions of high current density the maximum electric field will be located at the collector-substrate junction and will have the approximate value

$$E_m = \frac{2 V_s}{W_{epi} - W_{cib}} \qquad (3.7.31)$$

Equation 3.7.29 has no analytical solution. Values of electric field strength can be obtained for selected points in the collector region by means of numerical techniques. To obtain an expression for the power density in the collector-region it is therefore necessary to make further simplifying assumptions. The assumptions appropriate to the problem under consideration are

(i) $E(z).J(z) \gg E(r).J(r)$

(ii) High level injection such that the electric field at the metallurgical collector-base junction is zero for all regions to be considered.

(iii) The region of highest power dissipation is the only region of interest, allowing the electric field distribution to be approximated by (Ref.30),

$$E(z) = \frac{qnz}{K_p \varepsilon_o} \qquad (3.7.32)$$

For zero base-terminal current the power density can therefore be approximated by

$$p_w = \frac{vz}{K_p \varepsilon_o} \left(qN \operatorname{erfc}\left(\frac{r}{w}\right) \right)^2 \qquad (3.7.33)$$

The approximations made above will be most accurate at high charge-carrier concentrations. The power density derived here can be used in conjunction with the manipulations of Section 3.6 to give a more accurate time dependent temperature distribution.

A similar expression can be obtained for forward base-terminal current operation using the expression for charge-carrier distribution to be derived in Section 3.9 and given by Equation 3.9.14.

3.8 Avalanche Injection and Second Breakdown.

The impact ionisation coefficient, α_i, is a function of the electric field strength, E, given approximately by (Refs.36,48 57),

$$\alpha_i = \alpha_\infty \exp(-\frac{b}{E}) \qquad (3.8.1)$$

where α_∞ is the asymptotic value of α_i for E approaching infinity.

b is a constant determined by the material and the type of charge carrier.

At high collector currents the electric field is an approximately linear function of position, as shown in Equation 3.7.5

$$E(z) = E(0) + \frac{qz}{K_p \varepsilon_o} \left(\frac{J}{qv} - N_i \right)$$

The current multiplication factor, M is related to the ionisation coefficient by (Refs.47,49,57),

$$M = 1/(1 - \int \alpha_i(E)\, dz) \qquad (3.8.2)$$

Current multiplication is therefore dependent upon position in the collector space-charge region. Regions of highest current density will have the highest value of M. Current flows preferentially to regions of high multiplication. Positive feedback can therefore be established, regions with initially high current density gaining current at the expense of regions with a lower current density, due to the difference in multiplication. It can

be shown that, in epitaxial collector transistors, the critical condition for which ionisation controls second breakdown is given by $M = 2$ (See Appendix 7). The ionisation integral at the threshold of second breakdown is therefore

$$\int_0^h \alpha_\infty \exp\left(-\frac{b}{E}\right) dz = 0.5 \qquad (3.8.3)$$

The ionisation coefficients associated with both electrons and holes have the form given by Equation 3.8.1. Ambipolar conduction will therefore produce an ionisation coefficient of the same form. An approximate evaluation of the ionisation integral has been proposed by Hall (Ref.36),

$$\int_0^h \alpha_\infty \exp\left(-\frac{b}{E}\right) dz = \alpha_i(E_m)\, W_{eff} \qquad (3.8.4)$$

where W_{eff} is a function of the space-charge-layer width and the maximum electric field strength, E_m.

$$W_{eff} = hQ \left(\frac{b}{E_m}\right)^{-u} \qquad (3.8.5)$$

where Q and u are constants determined by the material and the junction profile.

The breakdown condition expressed in Equation 3.8.3 and the relations given in Equations 3.7.5 and 3.8.1 to 3.8.5, lead to a value of critical collector current defining the threshold at which second breakdown becomes dependent upon avalanche injection from the collector-substrate junction into the region of the base junction.

$$I_{crit} = qvA_c \left(\frac{bK_p \mathcal{E}_o}{q \ln(0.5/\alpha_\infty W_{eff})} + N_i \right) \qquad (3.8.6)$$

where v is the drift velocity

A_c is the collection area

Penetration of the space-charge region into the substrate has been neglected and the current flow is assumed to be space-charge-limited.

The rate of current constriction is related to the charge-carrier mobility in the collector region for avalanche controlled breakdown. The delay time associated with this form of second breakdown will therefore be very short. For initial current densities giving $M \geqslant 2$ a delay time in the order of tens of nano-seconds is anticipated for medium power devices. Lower initial current densities will depend upon thermal and magnetic constricting forces to create a condition for which $M = 2$.

Avalanche injection modifies the expression given for the critical temperature gradient in Equation 3.6.10 to

$$\nabla T_{crit} = \frac{q}{\gamma} \left(\frac{2kT_A \Delta n(2 - M)}{K_p \mathcal{E}_o} \right)^{\frac{1}{2}} \qquad (3.8.7)$$

where Δn is the injected charge-carrier density.

3.9 Critical Current with Forward Base Terminal Current.

Base terminal current is determined predominantly by recombination in the base region, immediately below the emitter. The potential gradient created by this current flow causes an

increase of current density at the emitter extremities.

The dependence of the electric field strength upon the current density, expressed in Equation 3.7.5, indicates that high electric field strength will be associated with high current density. Non-uniform current distribution therefore leads to high local power densities, reducing the total power input needed to cause second breakdown. Local concentrations of current are reduced by diffusion in the base region and by resistive potential gradients in the collector space-charge region. A detailed analysis of the current distribution at the point of maximum power dissipation is complex, usually requiring numerical techniques to match practical conditions. The present requirement is for an algebraic solution and approximation to actual conditions must therefore be accepted.

Assume that the base width is small, so that the distribution at the collector-base junction is a strong function of the distribution immediately under the emitter. Consider the level of charge-carrier injection to be high, so that

$$n(r,z) = p(r,z) \qquad (3.9.1)$$

The impurity density in the emitter region is assumed to be sufficiently high to allow the boundary condition

$$\frac{\partial J_p(z)}{\partial z} = 0 \quad \text{and} \quad \frac{\partial^2 p}{\partial z^2} = 0 \qquad (3.9.2)$$

to be used.

The distribution of charge carriers is assumed to be symmetrical about the point $r = 0$ at the centre of the emitter. The charge-carrier concentration at $z = 0$, under the emitter is given by

$$n(r,0) = n_o \exp\left(\frac{qV_{be}(r)}{kT}\right) \qquad (3.9.3)$$

where the base-emitter voltage is

$$V_{be}(r) = V_{be}(0) + \int_o^r \frac{J_b(r)}{\sigma_b}\, dr \qquad (3.9.4)$$

The high impurity density in the emitter ensures that the emitter edge of the emitter-base junction will be an equi-potential surface.

$$\left.\frac{dV}{dr}\right|_{z=0} = 0$$

The equilibrium radial diffusion current of electrons will be equal to the drift current caused by the resistive potential gradient, so that

$$\mu kT \frac{\partial n(r,0)}{\partial r} = 2q\mu E_r n(r,0) \qquad (3.9.5)$$

Space-charge neutrality is maintained in the base region by the hole concentration matching the electron concentration. Diffusion of holes into the emitter region is negligibly small. Holes must therefore recombine under the emitter-base junction according to

$$\nabla . J_p(r) = qp(r)/\tau \qquad (3.9.6)$$

where τ is the mean charge-carrier lifetime.

The radial hole current under the emitter will be the sum of the equal drift and diffusion current components. The total

recombination current is therefore given by

$$J_p(r,0) = n\mu kT \frac{\partial p(r,0)}{\partial r} + 2q\mu E_r p(r,0)$$

$$= -2\mu kT \frac{\partial p(r,0)}{\partial r}$$

$$= 2q\mu E_r p(r,0) \qquad (3.9.7)$$

Differentiating Equation 3.9.6 and substituting for the charge-carrier concentration gradient from Equation 3.9.7 yields the differential equation

$$\nabla^2 J(r) + \frac{J(r)\, q}{2\mu kT\tau} = 0 \qquad (3.9.8)$$

The equality of Equation 3.9.1 indicates that this equation is applicable to both hole and electron current densities immediately beneath the emitter-base junction. Equation 3.9.8 has the general solution in terms of Bessel Functions as

$$J(r) = AI_o(\lambda r) + BK_o(\lambda r) \qquad (3.9.9)$$

where A and B are constants.

A similar derivation can be used to obtain the solution for a rectangular co-ordinate system

$$J(x) = A\exp(\lambda x) + B\exp(-\lambda x) \qquad (3.9.10)$$

where $\lambda^2 = 2\mu kT\tau/q$

Emitter structures having a high horizontal aspect ratio allow the problem to be approximated by a two-dimensional system. Applying the boundary conditions to Equation 3.9.10, under these

circumstances, results in a current distribution of the form

$$J(x) = J(L_e) \frac{\cosh(\lambda x)}{\cosh(\lambda L_e)} \qquad (3.9.11)$$

where $2L_e$ is the emitter length in the x direction.
The reduction to two dimensions assumes that the distribution is independent of the emitter width, h_e

Transistors having a large horizontal aspect ratio have been found to operate with zero base-emitter voltage at the centre of the emitter, when large values of collector current are used (Ref.59).

The total collector current is given by

$$I_c = \int_0^{L_e} 2\nu h_e J(L_e) \frac{\cosh(\lambda x)}{\cosh(\lambda L_e)} \, dx \qquad (3.9.12)$$

where ν is the number of emitter elements.
The current density at the edge of the emitter can therefore be expressed, in terms of the collector current, as

$$J(L_e) = \frac{I_c}{2\nu h_e \tanh(\lambda L_e)} \qquad (3.9.13)$$

The charge carrier distribution is therefore

$$n(x) = \frac{I_c}{2\nu h_e q v} \frac{\cosh(\lambda x)}{\sinh(\lambda L_e)} \qquad (3.9.14)$$

Consider a single emitter segment and transfer the co-ordinate origin to the emitter edge (i.e., the point of maximum concentration of charge carriers). The mean charge-carrier concentration will be

given by

$$\langle n \rangle = \frac{1}{2L_e} \int_0^{L_e} n(x)\, dx$$

$$= \frac{I_c \lambda}{4 \mathcal{V} L_e h_e qv \sinh(\lambda L_e)} \int_0^{L_e} \cosh \lambda (L_e - x)\, dx$$

$$= I_c (2\cosh(\lambda L_e) - 1)/4 \mathcal{V} L_e h_e qv \qquad (3.9.15)$$

Neglecting the magnetic term in the energy balance equation and using Equation 3.9.15 results in the equality

$$K_p \mathcal{E}_o \left(\frac{\gamma E I}{2 h_e K} \right)^2 = \frac{I_c (2 \cosh(\lambda L_e) - 1) kT}{2 \mathcal{V} L_e h_e qv} \qquad (3.9.16)$$

The collector current obtained from this equality will be the critical current defining the onset of current constriction. The critical current for forward base-terminal-current operation is therefore

$$I_{crit} = \frac{2kT h_e K^2 (2 \cosh(\lambda L_e) - 1)}{\mathcal{V} L_e qv \gamma^2 E^2 K_p \mathcal{E}_o} \qquad (3.9.17)$$

The thermal conductivity, K, and the drift velocity, v, are temperature dependent (See Appendix 4). λ is also temperature dependent through the mobility, μ.

Applying the temperature dependent forms

$$K = A_T T^{-a_T}$$

$$v = v_o (1 - 6.7\ 10^{-4}\ T)$$

$$\lambda = \lambda_o T^{(1-b)}$$

to Equation 3.9.17 results in an expression for the critical current in terms of ambient temperature as

$$I_{crit} = \frac{2kh_e A^2 T^{(1-2a)}(2\cosh(\lambda_o T^{(1-b)} L_e) - 1)}{\nu L_e q v_o \gamma^2 E^2 K_p \mathcal{E}_o (1 - 6.7\,10^{-4} T)} \qquad (3.9.18)$$

The interaction of the temperature dependent terms, for practical device dimensions, is such that the critical current increases as the ambient temperature falls.

3.10 An Approximate Evaluation of Breakdown Delay Time.

The temperature rise of the transistor can be expressed in terms of a thermal resistance, θ , and the input power, P. The steady state equation will be

$$T(x,y,z,\infty) = P\theta(x,y,z) \qquad (3.10.1)$$

The dimensions of the heat source and its position with respect to the adiabatic surface affects the value of θ . The thermal resistance of an arbitrarily selected heat source can be related to the resistance, θ_o , for a heat source of defined shape and size, located at the surface, by a set of correction factors. The required correction factors will be :

(i) F_w expressing the change in θ caused by moving the heat source away from the adiabatic surface.

(ii) F_h expressing the change in θ caused by changing the thickness of the source.

(iii) F_A expressing the change in θ produced by varying the horizontal aspect ratio of the source. (The temperature on the centre-line of a heat source changes less for long thin sources.)

The correction factors can be presented in a general form by normalising all dimensions to the source upper surface area

$$F_w = f(w_s / (A_c)^{\frac{1}{2}}) \qquad (a)$$

$$F_h = f(h / (A_c)^{\frac{1}{2}}) \qquad (b)$$

$$F_A = f(L_c / w_c) \qquad (c) \qquad (3.10.2)$$

where w_s is the depth of the source below the adiabatic surface, h is the source thickness and $L_c W_c = A_c$

The thermal resistance on the centre line of the source is given by

$$\theta(0,0,w) = \frac{1}{2K A_c^{\frac{1}{2}}} .F_w.F_h.F_A \qquad (3.10.3)$$

The correction factors can be evaluated by comparison of Equation 3.10.3 with the full thermal response equation 3.6.6 or 3.6.7, allowing the time to approach infinity. The results shown graphically in Figs. 3.10.1 to 3.10.3 were obtained by starting with a symmetrical source at $z = 0$ and varying w_s, h and L_c / W_c in turn.

The transient thermal response can be considered to be a combination of bulk and local effects. Each of these is assumed to follow an exponential form, giving the temperature change, ΔT,

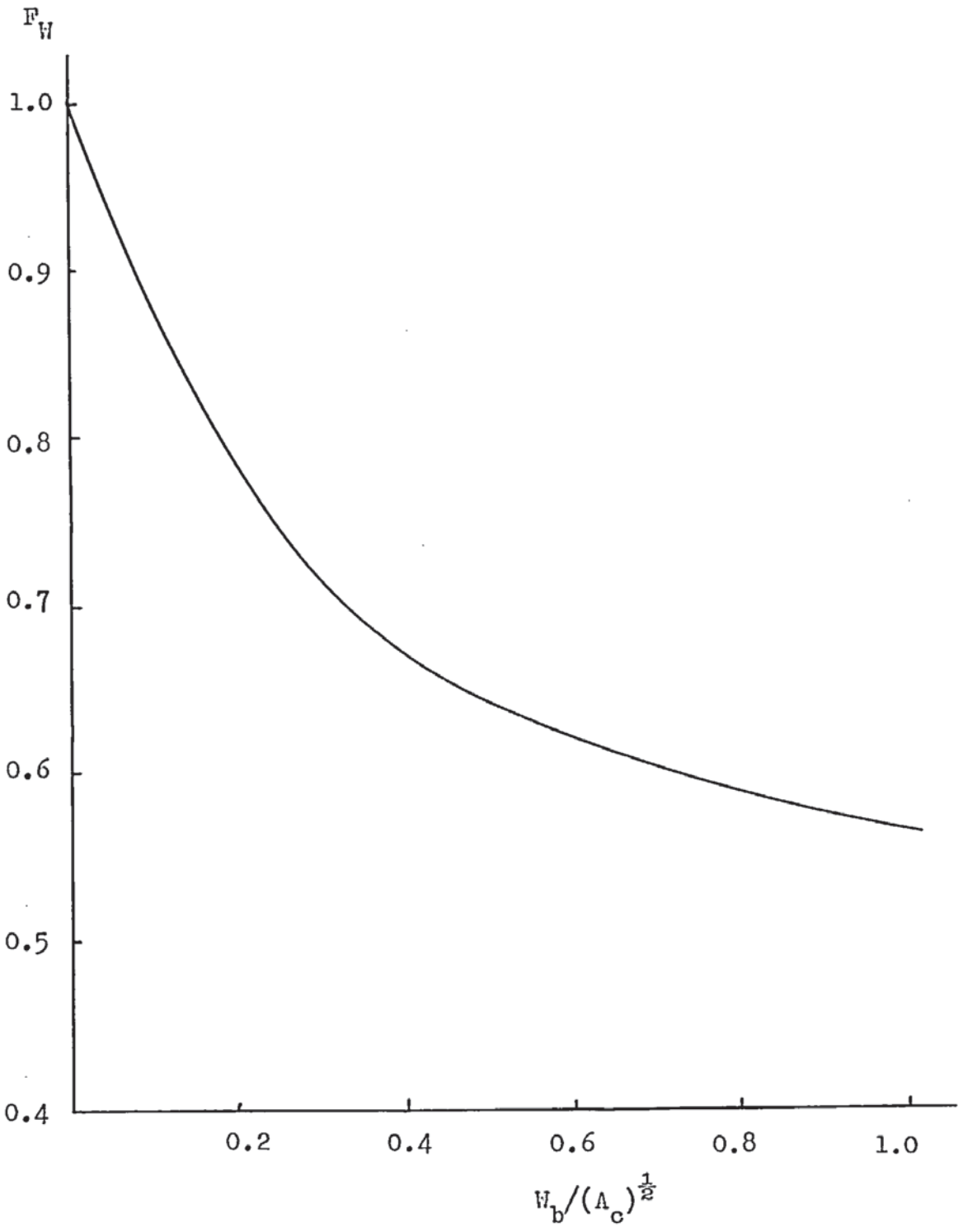

Fig. 3.10.1 Correction Factor F_W

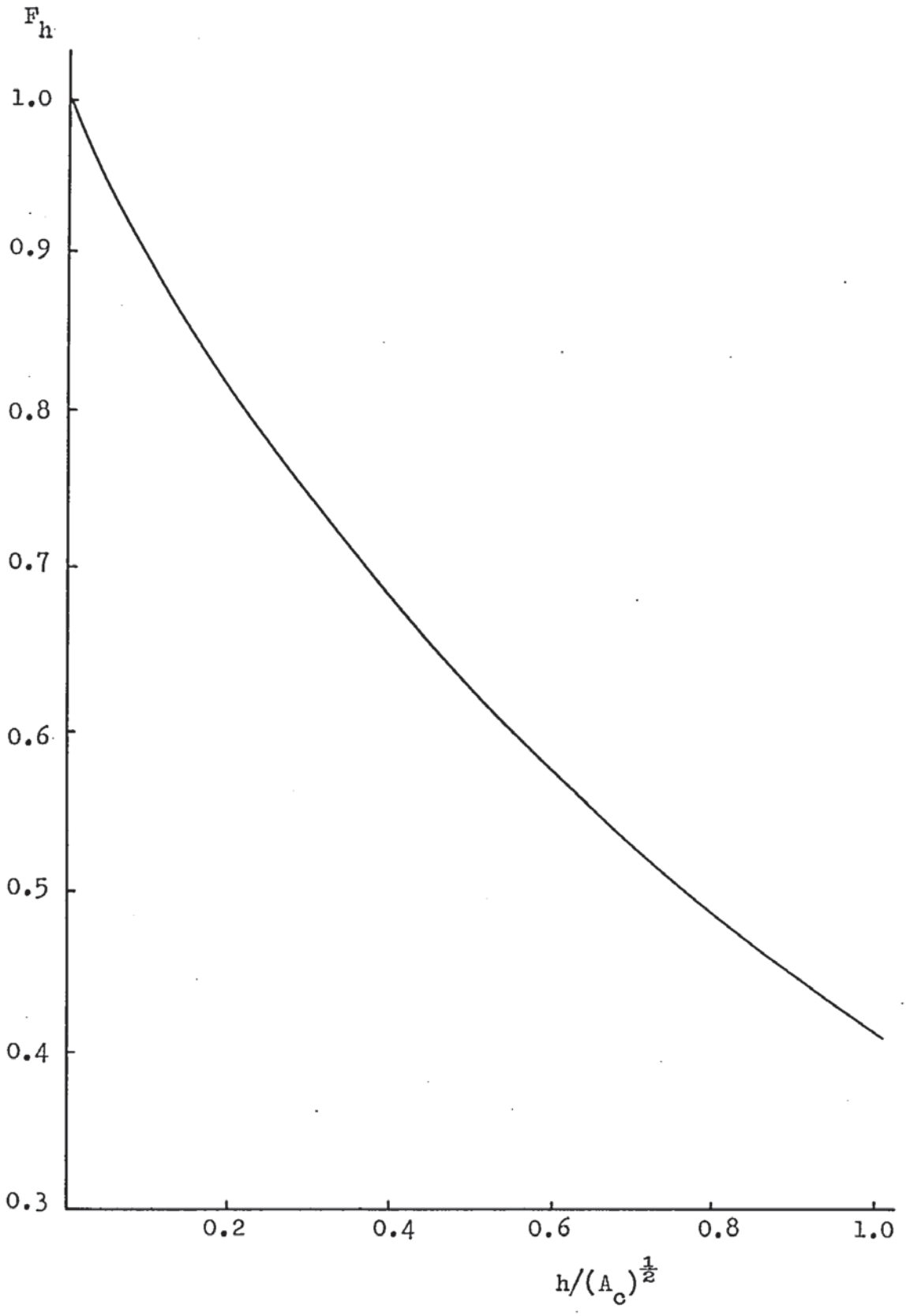

Fig. 3.10.2 Correction Factor F_h

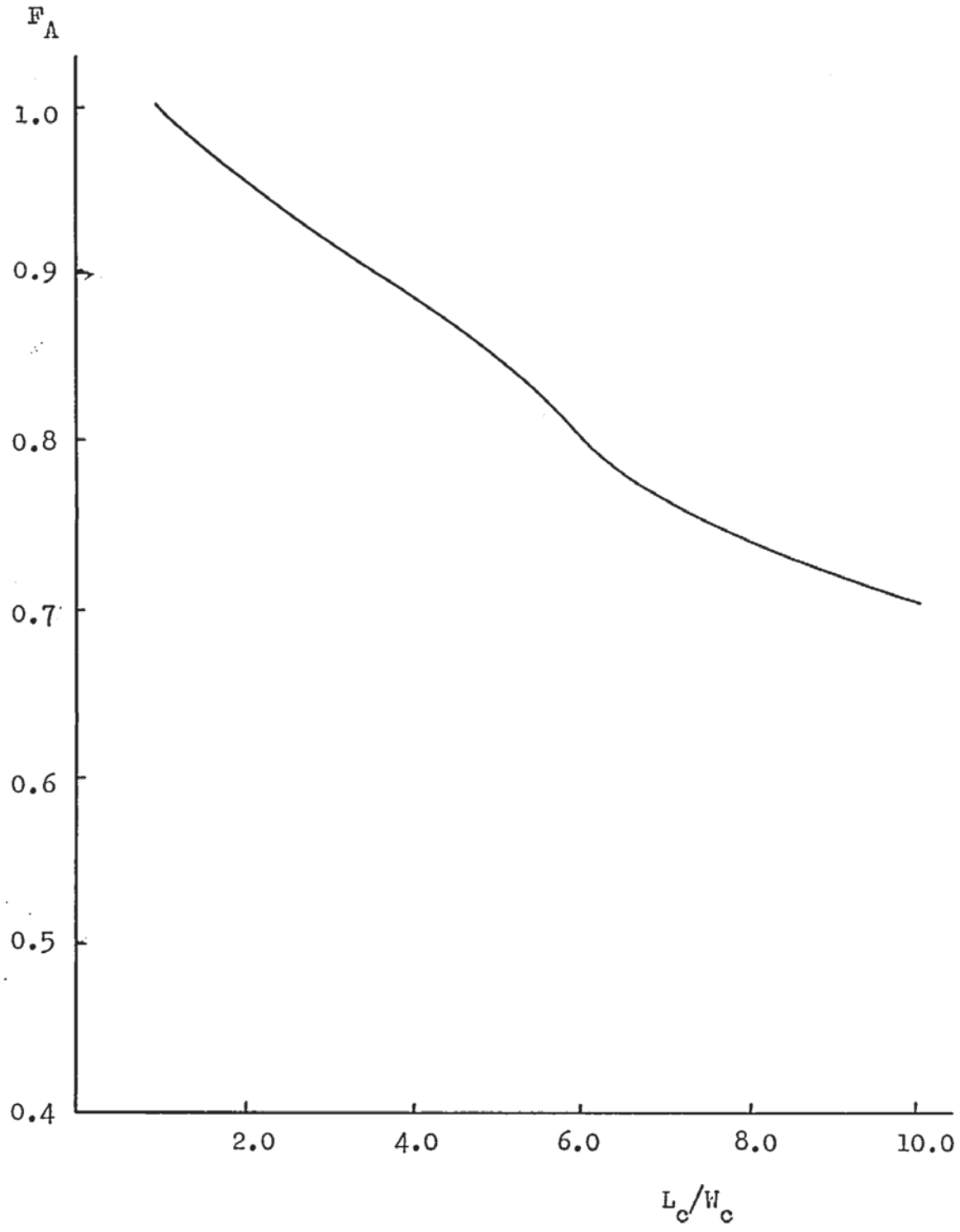

Fig. 3.10.3 Aspect Ratio Correction Factor F_A

for a uniform power distribution within the source as

$$T(t) = T(t) - T(0) = P\theta_s\left(1 - \exp\left(\frac{-t}{\tau_s}\right)\right) + P\theta_b\left(1 - \exp\left(\frac{-t}{\tau_b}\right)\right) \qquad (3.10.4)$$

where the subscripts s and b refer to local and bulk values respectively.

τ is the natural thermal time constant evaluated at $t = 0$.

Most operating conditions produce delay times which are sufficiently small to allow Equation 3.10.4 to be simplified to

$$T(t) = P\theta_s\left(1 - \exp\left(\frac{-t}{\tau_s}\right)\right) + \frac{Pt}{C_b} \qquad (3.10.5)$$

where C_b is the bulk capacity.

The temperature change can be expressed entirely in terms of local values when the time interval to be examined is very short (Refs.59,60). The natural time constant is given by (Ref.51),

$$\tau = R^2 / k_T \qquad (3.10.6)$$

where $R^2 = (x - x')^2 + (y - y')^2 + (z - z')^2$

k_T is the thermal diffusion coefficient

This is related to the thermal capacity by

$$\tau = \theta C \qquad (3.10.7)$$

Typical values for the transistors investigated in the experimental work are

τ_b = 7.04 ms.

τ_s = 146.9 μs.

$$\theta_s = 68.7\ ^{\circ}K/W.$$

$$C_b = 7.1\ 10^{-4}\ J/^{\circ}K.$$

$$C_s = 2.14\ 10^{-4}\ J/^{\circ}K.$$

obtained using $k_T = 0.511\ cm^2/s.$ and $K = 0.84\ J/cm.s.^{\circ}K$ (Ref.61).

An approximate value of delay time can be obtained by consideration of the critical temperature gradient introduced in Section 3.6. The current distribution is assumed to be uniform over an effective collection area, located under the emitter extremities for forward base bias, and under the emitter centre for open base operations. The effective area can be obtained by consideration of Equation 3.10.11, or a similar expression for circular structures. The area is taken to be that containing 80% of the current. The assumption of a linear temperature gradient leads to the temperature difference across the heat source, at breakdown, as

$$\Delta T_{crit} = \nabla T_{crit} \cdot \frac{1}{2} (A_c/\nu)^{\frac{1}{2}} \qquad (3.10.8)$$

where ν is the number of emitter segments.
The approximation improves as the source area decreases. A more accurate expression can be found from the transient thermal equation, 3.6.6, but this results in a complex expression, which is unnecessary for the present purpose. Immediately preceeding breakdown the heat source will have a small area and an aspect ratio approaching unity. The approximation is most accurate for high forward, or reverse, base terminal current.

The delay time is obtained by using Equations 3.10.5, 3.10.8 and the expression for the critical temperature gradient, 3.8.8, to give

$$\Delta T_{crit} = \frac{1}{4\gamma}\left(\frac{\Delta nkT_A(2 - M)A_c}{K_p \varepsilon_o}\right)^{\frac{1}{2}}$$

$$= P\theta_o F_w F_h F_A \left(1 - \exp\left(\frac{-t}{\gamma_s}\right)\right) + \frac{Pt}{C_b} \qquad (3.10.9)$$

The electric field distribution and the effective regional dimensions are required to enable values of M, F_w, F_h, and F_A to be obtained. Following the results obtained by Whittier and Tremere (Ref.30), it is assumed that base-width modulation and lateral injection have equal effects upon conduction, for currents exceeding the space-charge-limited threshold. The effective collection area is therefore given by

$$A_{eff} = A_c(I_c/I_T)^{\frac{1}{2}} \qquad \text{for } I_c > I_T \qquad (3.10.10)$$

where I_T is the threshold current for space-charge-limited operation.

The current-induced base width is therefore related to the collector region width by

$$W_{cib} = W_{epi}\left(1 - \frac{I_T - qvA_{eff}N_{DC}}{I_c - qvA_{eff}N_{DC}}\right) \qquad \text{for } I_c > I_T \qquad (3.10.11)$$

The width of the heat source is therefore

$$h = W_{epi} - W_{cib} \qquad \text{for } I_c > I_T \qquad (3.10.12)$$

The effective base width is

$$W_{bef} = W_b + W_{cib} \qquad \text{for } I_c > I_T \qquad (3.10.13)$$

These values of A_{eff}, h and W_{bef} are used in Equation 3.10.2 to give values of F_W and F_h.

The electric field used in the evaluation of the avalanche multiplication factor, M, is assumed to have the linear form given in Equation 3.7.5. This is related to the supply voltage by

$$V_s \triangleq E(0)h + |E(0) - E(h)| \frac{h}{2} \qquad (3.10.14)$$

The avalanche multiplication factor is obtained by combining Equations 3.7.5, 3.8.5, 3.8.6 and 3.10.14.

The assumption implicit in the simple form of Equation 3.10.9 is that the charge-carrier concentration, collection area, and avalanche multiplication remain constant up to the threshold of breakdown. These factors are all temperature dependent and the simple form of the equation therefore leads to values of temperature difference, and hence delay time, which differ widely from the experimental values.

3.10.1 Collection Area and Charge-Carrier Concentration as Functions of Temperature.

The charge-carrier concentration and the saturated drift velocity are functions of temperature. The charge-carrier density

exhibits a temperature dependence of the form (Refs.2,3,14)

$$n(T) = n(T_o) \left(\frac{T}{T_o}\right)^{1.5} \exp\left(-\frac{\mathcal{E}_g(T - T_o)}{2\,k\,T\,T_o}\right) \qquad (3.10.15)$$

The temperature dependence of the saturated drift velocity, discussed in Section 3.5, is given by

$$v(T) = v(T_o) \frac{(1 - 6.7\ 10^{-4}\ T)}{(1 - 6.7\ 10^{-4}\ T_o)} \qquad (3.10.16)$$

In a transistor supplied from a current source the total collector current remains constant, so that the collection area has a temperature dependence determined by Equations 3.10.15, 3.10.16 and

$$A_c(T) = I_c / qv(T)n(T) \qquad (3.10.17)$$

This is applicable for conditions below space-charge-limited conduction. In space-charge-limited conduction the area of collection becomes carrier-concentration dependent according to

$$A_c(T) = A_{cc}\left(\frac{J(T)}{J(T_{cc})}\right)^{\frac{1}{2}} \frac{(1 - 6.7\ 10^{-4}\ T)}{(1 - 6.7\ 10^{-4}\ T_{cc})} \qquad (3.10.18)$$

where subscipt cc refers to values at the threshold of space-charge-limited conduction.

The temperature dependent form of Equation 3.10.9 must be considered for two conditions:

(i) Space - charge - neutral up to breakdown

$$T_{crit} =$$

$$\frac{1}{2\gamma}\left(\left(n(T_o)\left(\frac{T}{T_o}\right)^{1.5}\exp\left(\frac{-\mathcal{E}_g(T-T_o)}{2kTT_o}\right)-N_{DC}\right)\frac{kT(2-M)}{K_p\mathcal{E}_o}\right)^{\frac{1}{2}} \qquad (3.10.19)$$

(ii) Space - charge - limited at breakdown, space - charge - neutral at $T = T_o$

$$T_{crit} =$$

$$\frac{1}{2\gamma}\left(\left(n(T_o)\left(\frac{TT_{cc}}{T_o 2}\right)^{\frac{3}{4}}\exp\left(\frac{-\mathcal{E}_g(T_{cc}(2T-T_o)-TT_o)}{4kT_oT_{cc}T}\right)-N_{DC}\right).\right.$$

$$\left.\frac{kT(2-M)}{K_p\mathcal{E}_o}\right)^{\frac{1}{2}} \qquad (3.10.20)$$

3.10.2 Avalanche Multiplication as a Function of Temperature.

The avalanche multiplication factor, M, is defined in terms of the ionisation coefficient, α, as

$$M = 1/(1-\int \alpha(E)\,dz) \qquad (3.10.21)$$

The approximate solution to the ionisation integral has the form

$$\int \alpha(E)\,dz = hQ\left(\frac{b}{E_m}\right)^{-u}\alpha_\infty \exp\left(-\frac{b}{E_m}\right) \qquad (3.10.22)$$

where Q and u are determined by the junction structure, (Ref.36)

E_m is the maximum electric field

α_∞ is the asymptotic value of α as E_m approaches infinity.

b is a constant dependent upon the type of charge carrier.

h is the space-charge-layer width.

Consider the current flow to be space-charge-limited. The space-charge region has a width

$$h = w_{epi}(n - N_{DC})/(n_{cc} - N_{DC}) \qquad (3.10.23)$$

where n_{cc} is the charge carrier concentration at the threshold of space-charge-limited current flow.

This can be expressed in its temperature dependent form as

$$h(T) = w_{epi} \frac{(n_{cc}(T/T_{cc})^{\frac{3}{4}}\exp(-\mathcal{E}_g(T - T_{cc})/(4kTT_{cc})) - N_{DC})}{n_{cc} - N_{DC}} \qquad (3.10.24)$$

The maximum electric field is therefore temperature dependent and is given approximately by

$$E_m = 2V_s/h$$

$$= \frac{V_s\ 2\ (n_{cc} - N_{DC})}{w_{epi}(n_{cc}(T/T_{cc})^{\frac{3}{4}}\exp(-\mathcal{E}_g(T - T_{cc})/4kTT_{cc}) - N_{DC})} \qquad (3.10.25)$$

The ionisation integral is therefore temperature dependent

$$\int \alpha(E)\ dz = Q\ \alpha_\infty (b/2V_s)^{-u} \cdot \left(w_{epi} \frac{(n_{cc}(T/T_{cc})^{\frac{3}{4}}\exp(-\mathcal{E}_g(T - T_{cc})/4kTT_{cc}) - N_{DC})}{n_{cc} - N_{DC}} \right)^{(1-u)}$$

$$\exp\left(\frac{-bw_{epi}(n_{cc}(T/T_{cc})^{\frac{3}{4}}\exp(-\mathcal{E}_g(T - T_{cc})/4kTT_{cc}) - N_{DC})}{2V_s\ (n_{cc} - N_{DC})} \right) \qquad (3.10.26)$$

This can be substituted into Equation 3.10.21 to give the temperature dependent value of M.

Considering an initial charge-carrier concentration less than n_{cc} introduces more complex terms containing T_o, T_{cc} and T, similar to those shown in Equation 3.10.20.

The simple form of the temperature, avalanche multiplication, delay time relation, given in Equation 3.10.9, must be used in conjunction with Equations 3.10.18, 3.10.20 and 3.10.26.

$$P\theta_o F_w F_h F_A (1 - \exp(-t/\gamma_s)) + Pt/C_b =$$

$$\frac{1}{4\gamma}\left\{(n(T_o).f(T,T_{cc},T_o) - N_{DC})\frac{kT_A A_c(1 - GT)(n_{cc}f(T,T_{cc}) - N_{DC})}{K_p \varepsilon_o (1 - GT_o)(n_{cc} - N_{DC})}\right\}^{\frac{1}{2}}$$

$$\left[\frac{1 - 2Q\alpha_\infty\left(\frac{b}{2V_s}\right)^{-u}\left(\frac{W_{epi}(n_{cc}f(T,T_{cc})-N_{DC})}{n_{cc} - N_{DC}}\right)^{(1-u)}\exp\left(\frac{-bW_{epi}(n_{cc}f(T,T_{cc})-N_{DC})}{2V_s(n_{cc} - N_{DC})}\right)}{1 - Q\alpha_\infty\left(\frac{b}{2V_s}\right)^{-u}\left(\frac{W_{epi}(n_{cc}f(T,T_{cc})-N_{DC})}{n_{cc} - N_{DC}}\right)^{(1-u)}\exp\left(\frac{-bW_{epi}(n_{cc}f(T,T_{cc})-N_{DC})}{2V_s(n_{cc} - N_{DC})}\right)}\right]^{\frac{1}{2}}$$

(3.10.27)

where $f(T,T_{cc}) = \left(\frac{T}{T_{cc}}\right)^{\frac{3}{4}}\exp\left(\frac{-\mathcal{E}_g(T - T_{cc})}{4kTT_{cc}}\right) = f_1$

and $f(T,T_{cc},T_o) = \left(\frac{TT_{cc}}{T_o^2}\right)^{\frac{3}{4}}\exp\left(\frac{-\mathcal{E}_g(T_{cc}(2T - T_o) - TT_o)}{4kTT_{cc}T_o}\right)$

$= f_2$

For $n_{cc} \gg N_{DC}$ this simplifies to

$$P\,\theta_o\,F_W\,F_h\,F_A\,(1 - \exp(-t/\gamma_s)) + Pt/C_b =$$

$$\frac{1}{4\gamma}\Bigg\{ n(T_o) f_1 f_2 \frac{kT_A A_c (1 - 6.7\ 10^{-4}\ T)}{K_{p\ o}(1 - 6.7\ 10^{-4}\ T_o)} \cdot$$

$$\frac{1 - 2Q\,\alpha_\infty (b/2V_s)^{-u}\,(w_{epi} f_1)^{(1-u)} \exp(-bw_{epi} f_1/2V_s)}{1 - Q\,\alpha_\infty (b/2V_s)^{-u}\,(w_{epi} f_1)^{(1-u)} \exp(-bw_{epi} f_1/2V_s)} \Bigg)^{\frac{1}{2}} \Bigg) \tag{3.10.28}$$

At collector currents for which $n(T_o) \geqslant n_{cc}$ the above equations are simplified by replacing $f(T,T_{cc},T_o)$ and $f(T,T_{cc})$ by the single expression $f(T,T_o)$ where

$$f(T,T_o) = \left(\frac{T}{T_o}\right)^{\frac{3}{4}} \exp\left(\frac{-\mathcal{E}_g(T - T_o)}{4kTT_o}\right) \tag{3.10.29}$$

Equations 3.10.27 and 3.10.28 express the dependence of delay time upon temperature and avalanche multiplication. This is a description of second breakdown in terms of energy gap modulation and avalanche multiplication. The effects of base width modulation and lateral injection are considered for charge-carrier concentrations of appropriate magnitude. These equations can be used with successive approximation techniques to provide values of the maximum temperature, the maximum charge-carrier concentration and the delay time. These values are given as functions of supply voltage and collector current, which determines $n(T_o)$. The values obtained will be those existing at the onset of second

breakdown current constriction.

The magnetic pinching forces have been neglected in the above analysis. This approximation has been found adequate for ambient temperatures as low as 195°K. Operation at lower temperatures, however, makes the magnetic pinching force significant in comparison with the thermal pinching force.

CALCULATIONS.

The critical collector currents for open-base and forward base-bias were calculated for a temperature range 400°K. to 77°K. using Equations 3.5.14 and 3.10.19 respectively. The values of the constants used were

$$A = 3.5.10^{5}$$

$$a = 1.33$$

$$B = 5.5.10^{6}$$

$$b = 1.5$$

$$\gamma = 3.6.10^{-4} \text{ eV/°K.}$$

$$v_o = 7.3.10^{7} \text{ cm/s}$$

The dependence of the characteristic upon the electric field strength was examined and a set of curves obtained for field strengths up to 5.10^{7} V/m. These results are shown in Figs. 4.1 and 4.2 where the collector currents are normalised to the value at 300°K. for zero electric field. This allows a comparison with the experimental curve which gives a mean value of electric field strength at the threshold of breakdown.

The open-base mode of operation produces a set of curves indicating an electric field strength greater than 10^{6} V/m. For the devices tested the field is in the region of 5.10^{6} V/m.

Forward base-bias operation produces a set of identical curves displaced from the curve for $E = 10^{6}$ V/m., used as a reference, according to E^{-2}.

The temperature distribution in the hot spot formed by the current constriction was calculated using Equations 3.4.5 and 3.4.8.

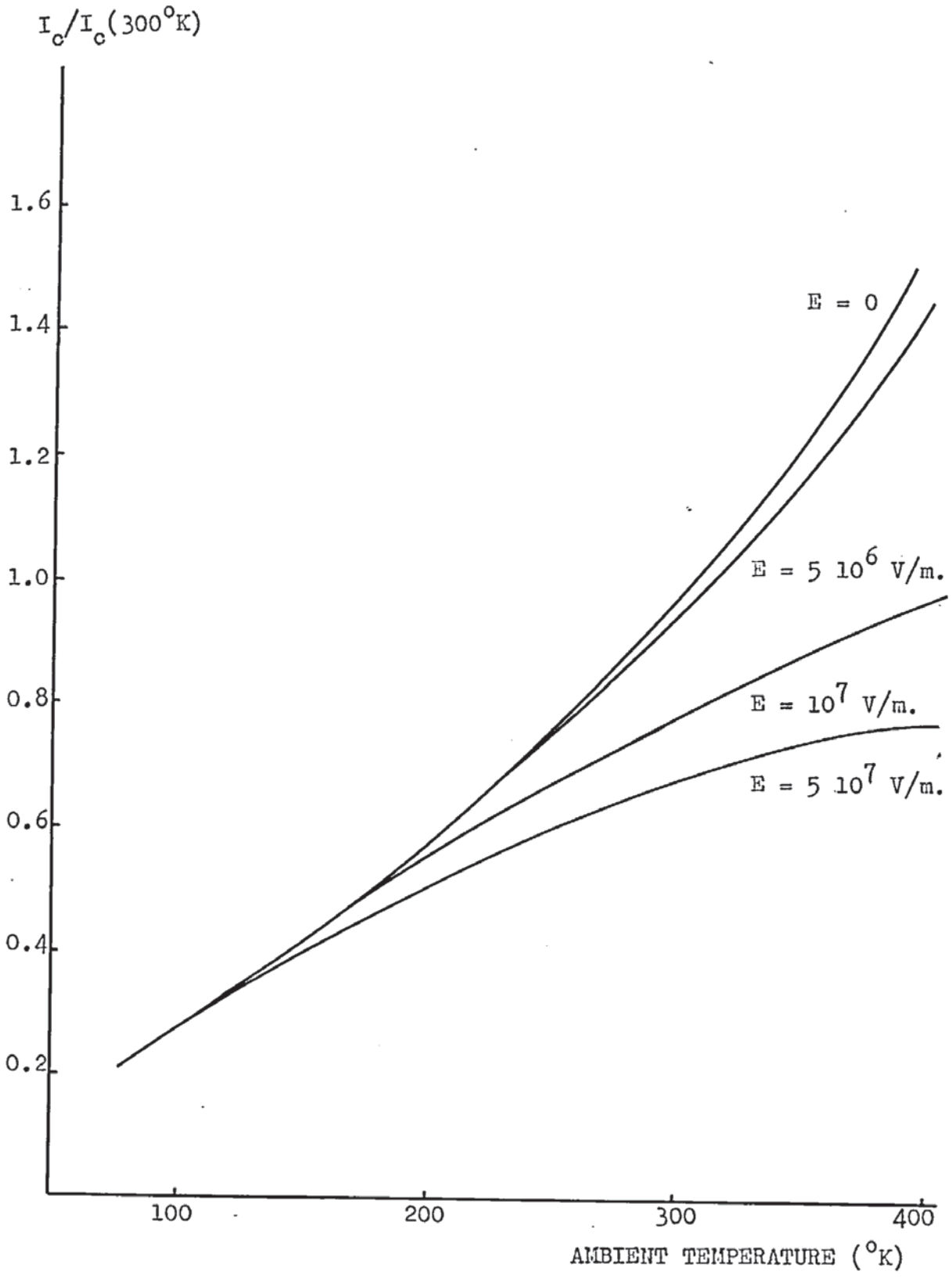

Fig. 4.1 (a) Theoretical Critical Collector Current - Ambient Temperature Characteristic, Normalised to I_c at 300°K. and E = 0 (Open Base Operation)

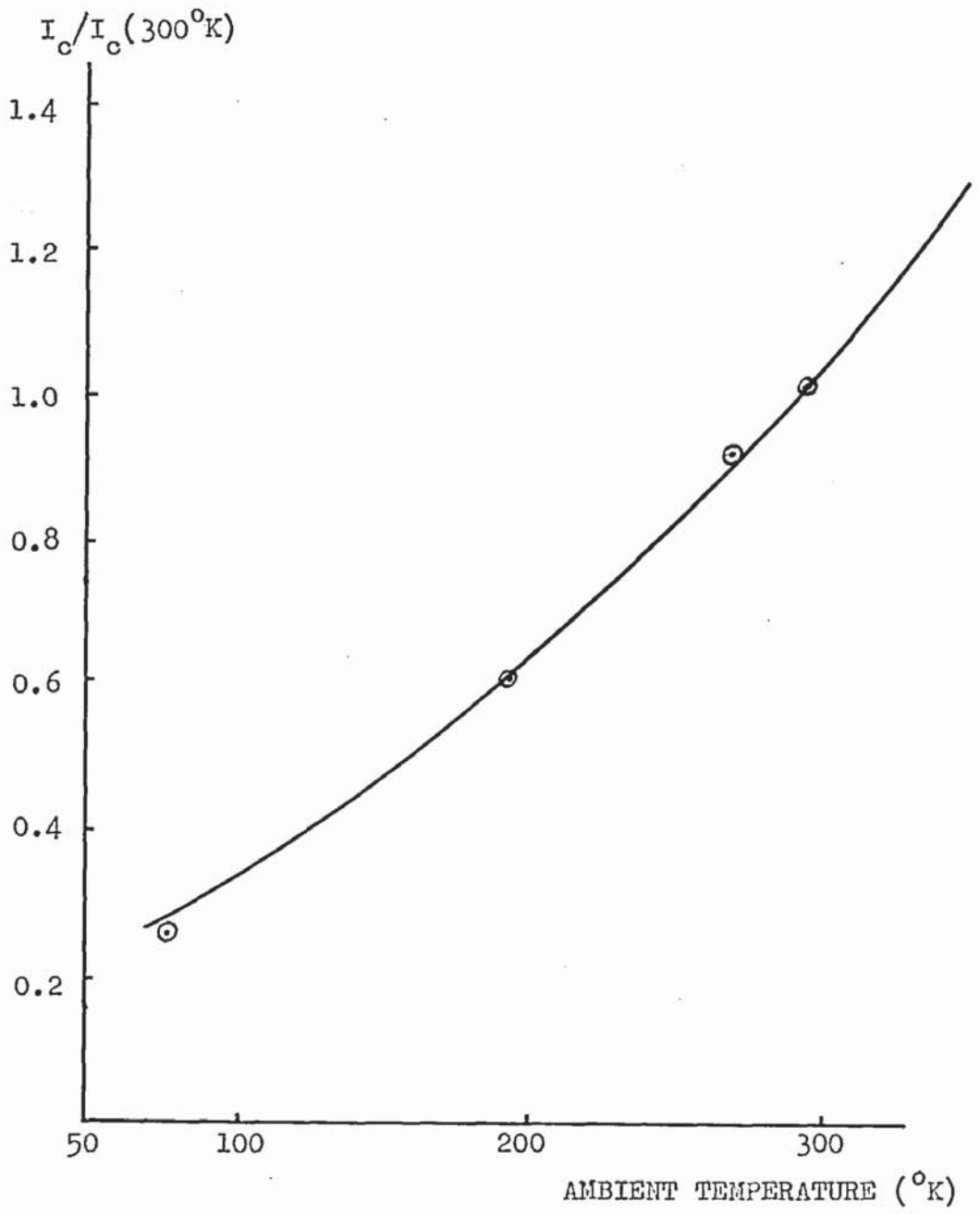

Fig. 4.1 (b) Critical Collector Current as a Function of Ambient Temperature (Open Base Operation)
(Line represents theoretical relation for an electric field E = 6 10^4 V/cm., points are experimental results averaged from 5 transistors)

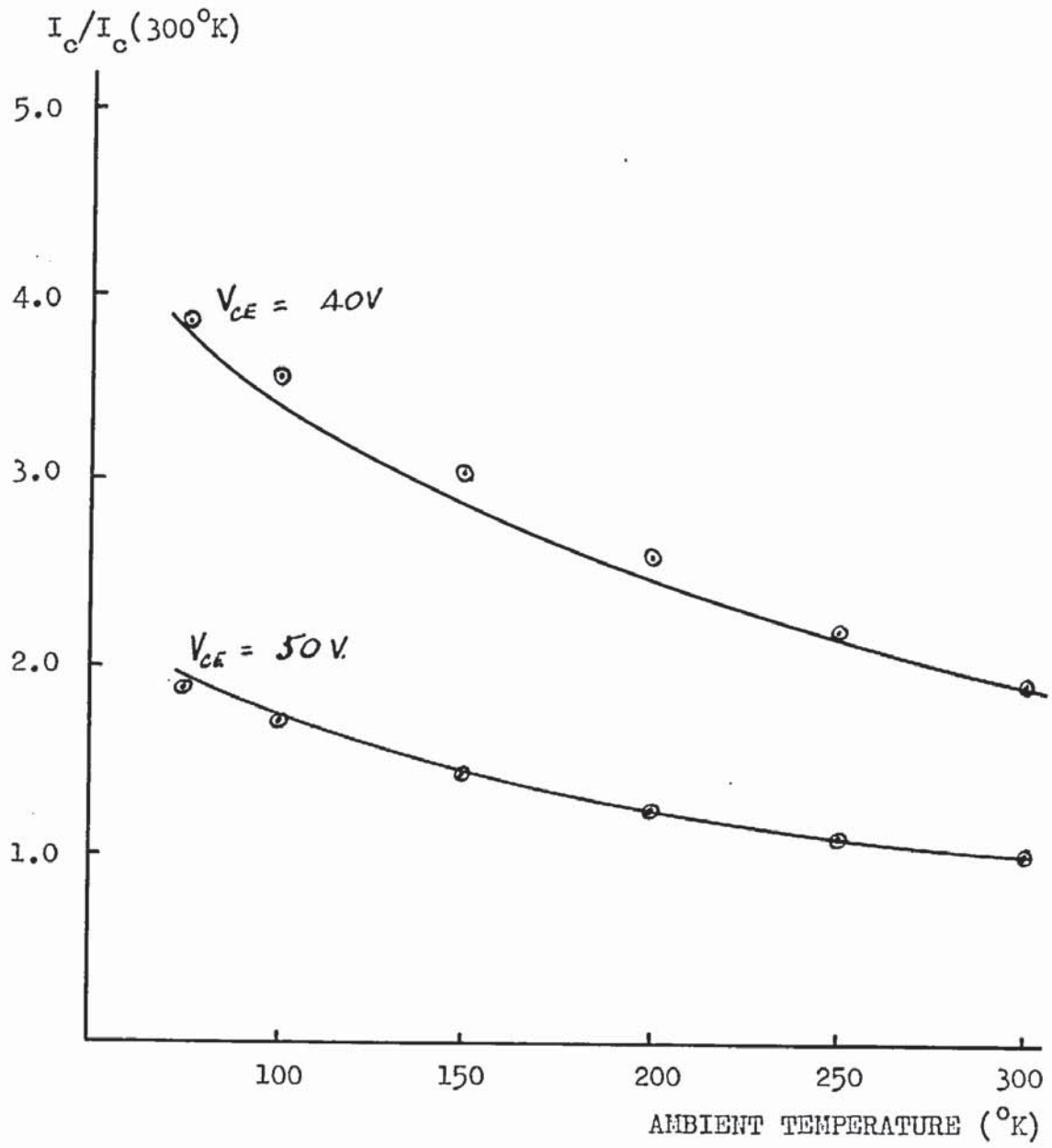

Fig. 4.2 Critical Collector Current as a Function of Ambient Temperature for Forward Base Bias Operation. (Lines represent theoretical values obtained from Equation 3.9.18, assuming the drift velocity to be independent of electric field strength. Points represent normalised average experimental results for BFY 72 transistors)

The constants used in these equations are derived from Equations 3.4.5 and 3.4.7 respectively in conjunction with the temperature dependent expressions for the charge-carrier density and mobility

$$n = n_i T^{1.5} \exp(-\mathcal{E}_g / 2kT)$$

$$\mu = 5.5\ 10^6\ T^{-1.5}$$

The temperature distribution was obtained by taking an initial estimate of the maximum temperature and using the temperature gradient, in an incremental process, to obtain the temperature at the edge of the hot spot. This value was compared with the ambient temperature and the maximum temperature adjusted until the re-calculated temperature at the edge of the hot spot was within $1^{\circ}K.$, of the ambient temperature. The hot spot radius was assumed to be determined by the emitter width at the breakdown site.

The effect of each breakdown mechanism was demonstrated by reducing the magnetic effect to zero. These calculations were restricted to zero recombination current conditions. The results are shown in Figs. 4.3 and 4.4 for two values of ambient temperature.

The charge-carrier distribution in the hot spot was obtained using these temperature distributions and Equation 3.3.27, the result being shown in Fig. 4.5.

The approximate delay time-breakdown energy characteristic was obtained using the system of equations given in Section 3.10.2 to give a value of delay time related to collector current, supply

voltage and ambient temperature. An iterative technique was employed to give a delay time with less than 1 μs deviation between consecutive values. The results are shown in Figs. 4.6 and 4.7 for forward base-bias operation.

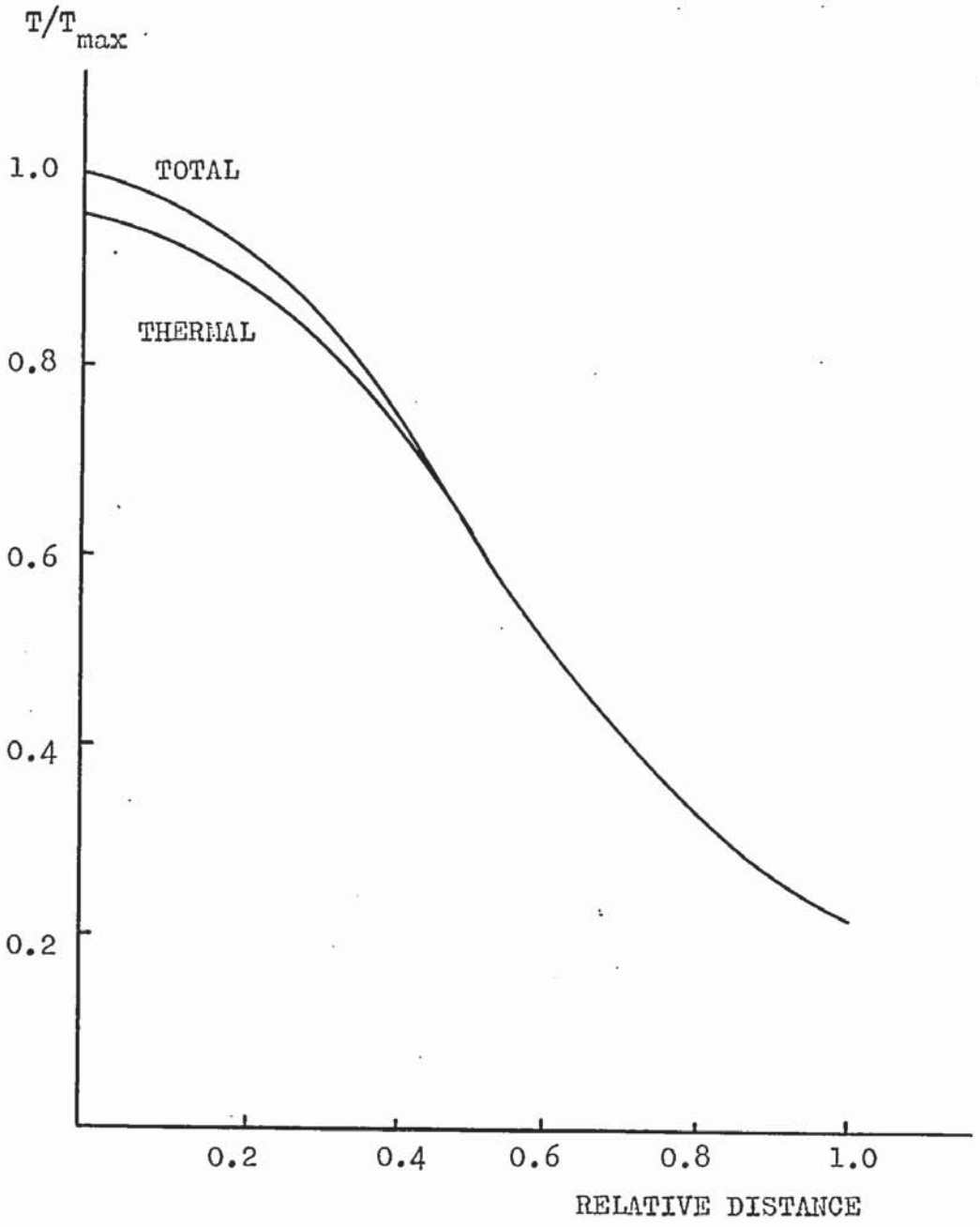

Fig. 4.3 · Plot of Relative Temperature Against Distance From The Hot-Spot Centre, (obtained from Equations 3.4.6 and 3.4.8 at an Ambient Temperature of 297°K)

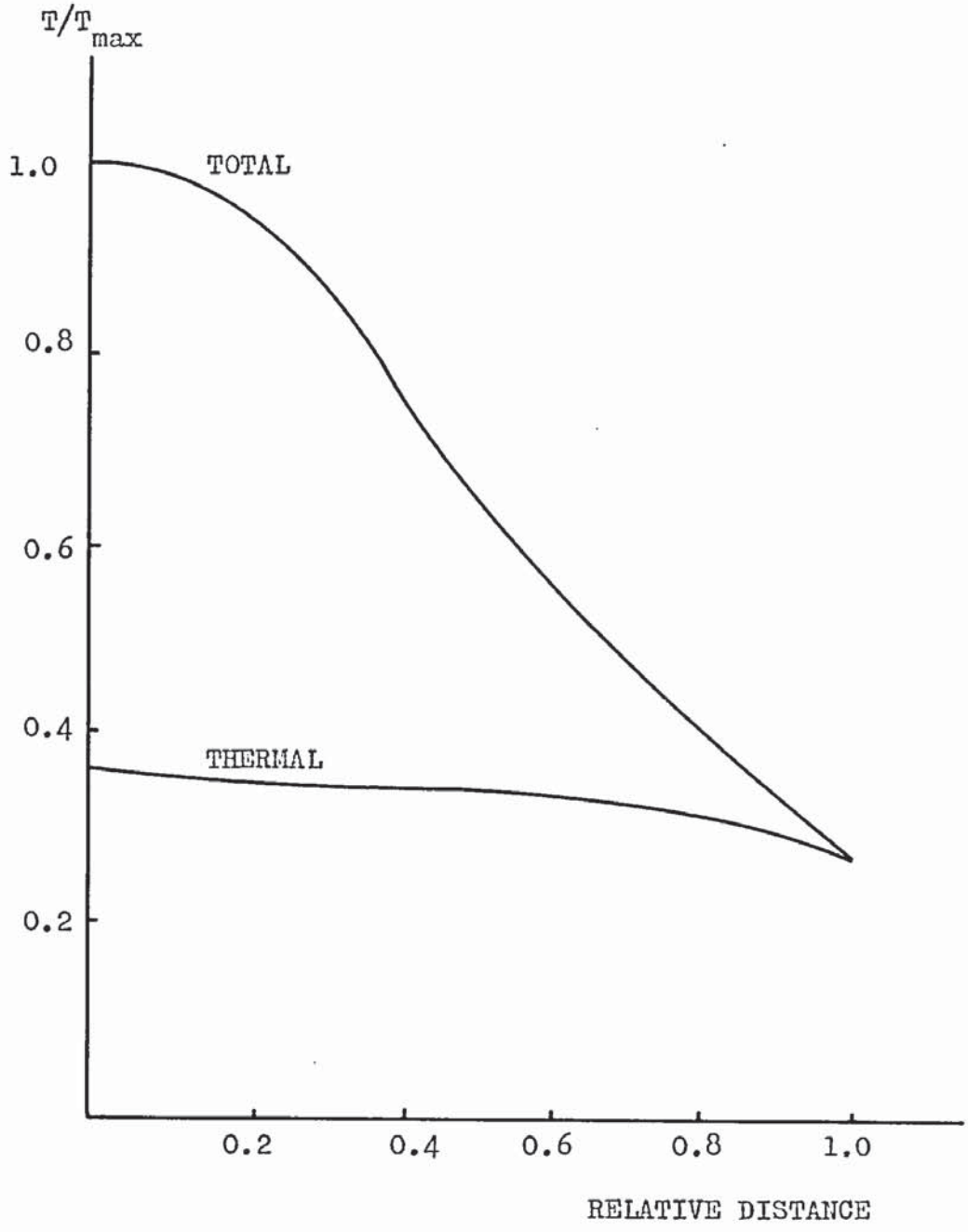

Fig. 4.4 Temperature Distribution in a Hot Spot (using Equations 3.4.6 and 3.4.8 at an Ambient Temperature of 77°K.)

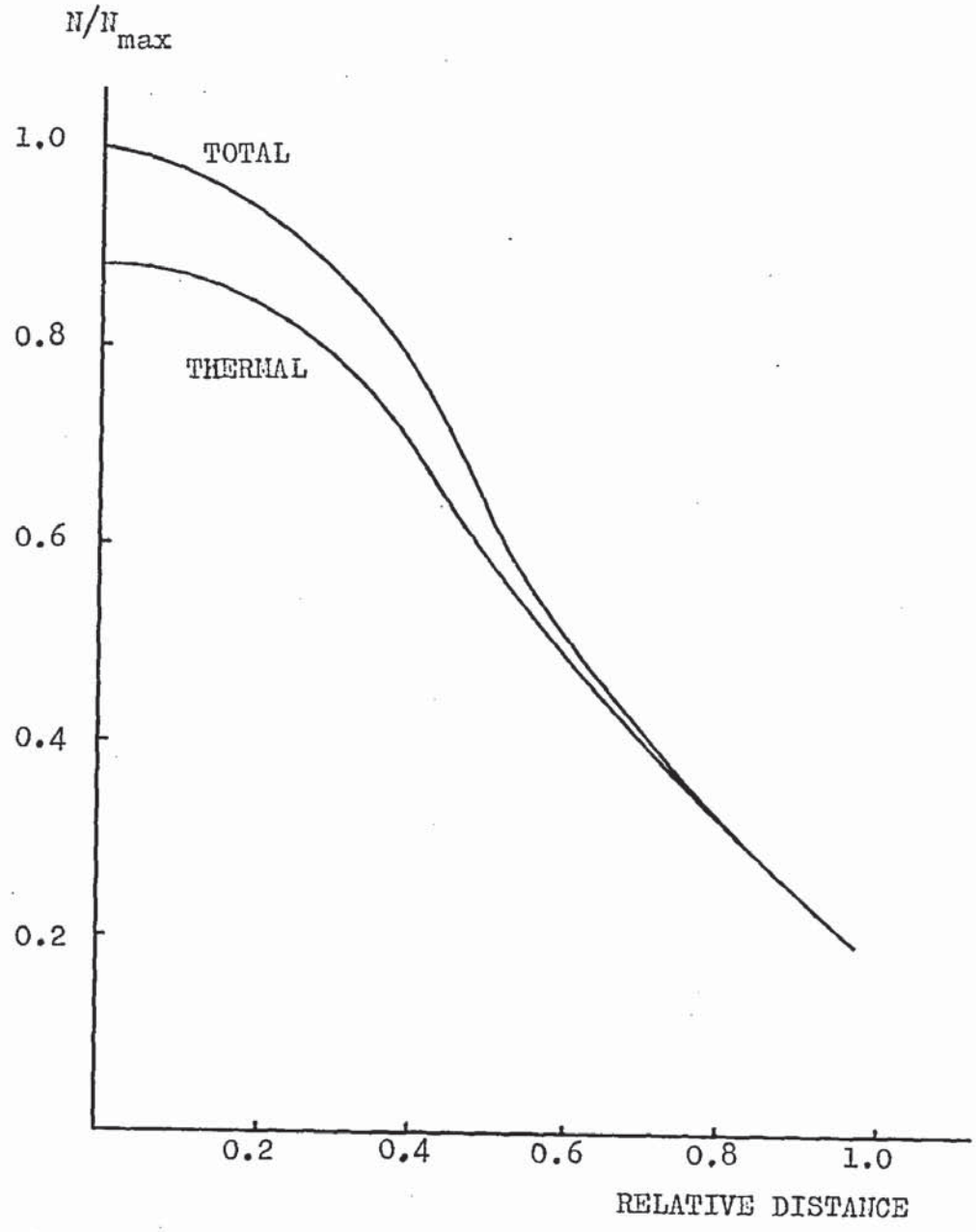

Fig. 4.5 Charge-Carrier Distribution in the Hot Spot (from Equation 3.3.27 and Fig. 4.3)

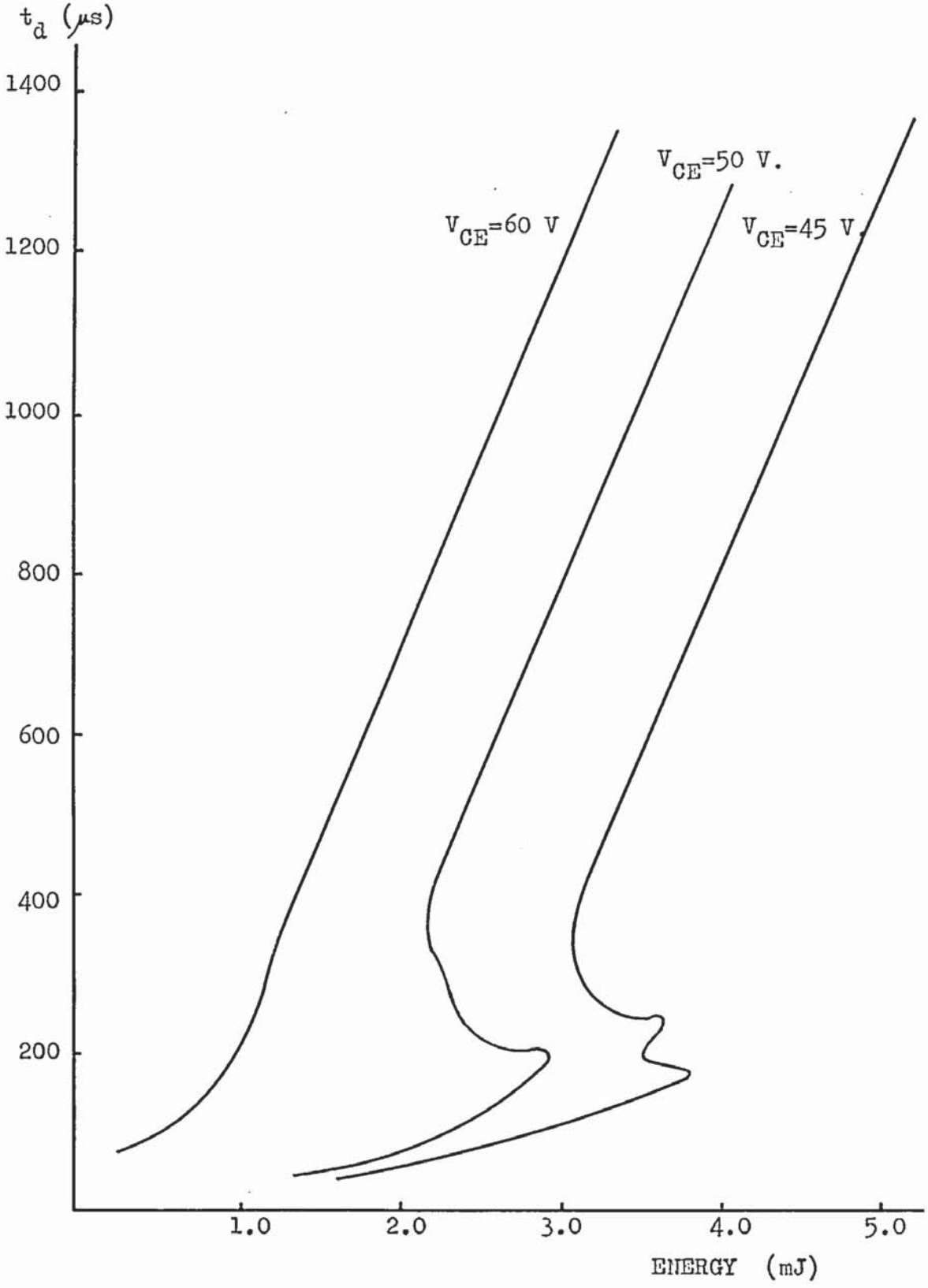

Fig. 4.6. (a) 2N 2218 Theoretical Delay Time – Breakdown Energy Characteristic (V_{CE} decreases by 1.0 V. for each 0.1 A. current increment)

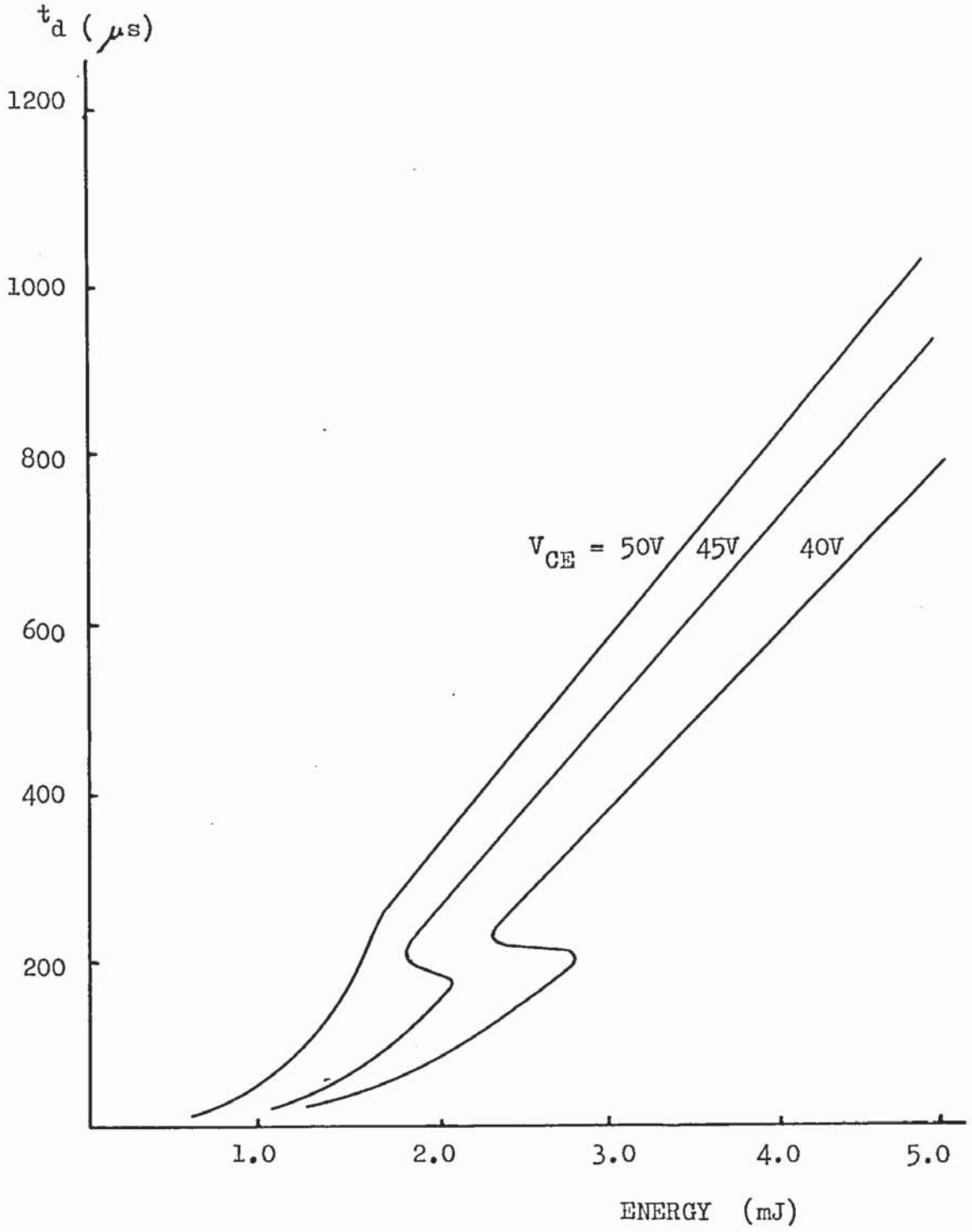

Fig. 4.6 (b) BFY 72 Theoretical Delay Time - Breakdown Energy Characteristic (Ambient Temperature 297°K)

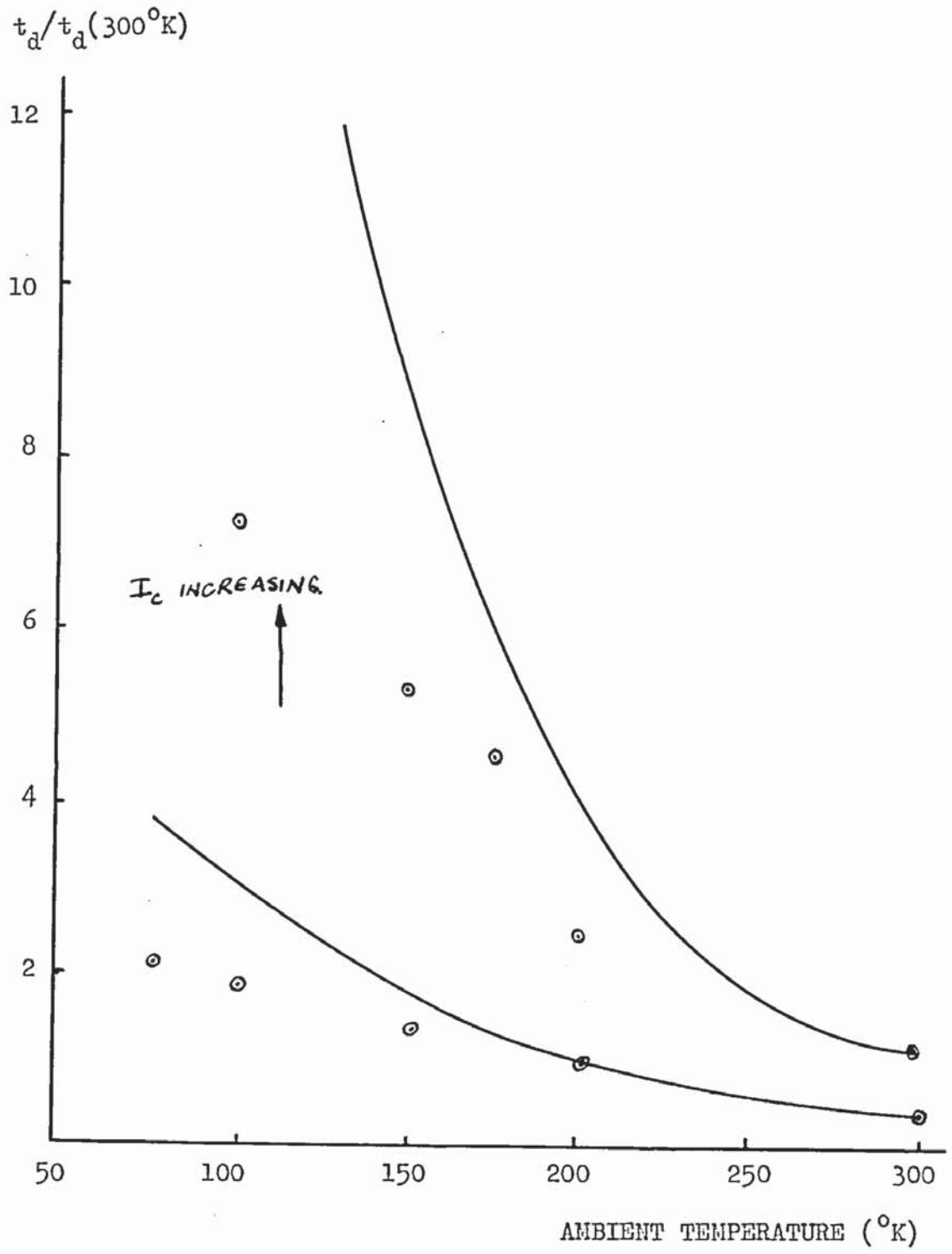

Fig. 4.7 Delay Time as a Function of Ambient Temperature for BFY 72 Operating with Forward Base-Bias and V_{CE} = 40V. Lines represent theoretical values (magnetic effects neglected) and points are experimental results) All values are normalised to the value of t_d at 300°K. Collector Current = 250 mA.

5. EXPERIMENTAL INVESTIGATION.

The devices used in the practical investigation of second breakdown were n - p - n Silicon epitaxial transistors. Samples were taken from commercially available devices having a representative range of emitter profiles. The selection of medium-power switching transistors was a compromise between the need for a large area and the complexity of transmitting clearly defined high-power pulses through long cables.

The experimental proceedure was divided into five sections. These were designed to justify the acceptance of the techniques, provide a basis for the theoretical work and, where possible, verify the theory. The outline of the investigation was as follows :

(i) Preliminary Investigation - determination of the limiting conditions under which second breakdown could be induced in each type of device.

(ii) Device Degradation - the effects of repetitive breakdown upon the transistor characteristics were examined.

(iii) Electrical Breakdown Characteristics - a detailed examination of the terminal characteristics of each type of device was made over a wide range of input power condition. This was performed in forward and open base modes.

(iv) The Temperature Distribution - infra-red radiation from the transistor surface was detected by means of an infra-red microscope. The radiation level was taken as an indication of the mean temperature of the small area under observation.

(v) The Critical Current - the collector current required to cause second breakdown under given conditions of supply voltage and ambient temperature was determined.

5.1 Preliminary Investigation.

During this stage of the experimental work, the time which the test transistor spent in the breakdown state was limited by an inhibiting circuit. This was discarded as soon as the operating range of the devices had been determined, since the load it presented to the test circuit affected the values of delay time and energy required to cause breakdown.

This investigation was used to verify the general findings of previously reported work, where appropriate.

(i) Reverse base-bias required higher voltages to cause breakdown than zero base-bias operation. The collector-emitter voltage after breakdown was found to be lower than for other modes of bias. Delay times were very short, generally less than 100 ns., and appeared almost independent of the collector current once the critical value was exceeded.

(ii) Forward base-bias produced second breakdown at the lowest supply voltages, avalanche breakdown not being required provided that the collector current was large enough. Delay times were an intimate function of collector current and were appreciably longer than for other modes of operation.

During these experiments it was noted that the devices with circular emitter configurations required much higher input power to cause breakdown in the forward bias mode, than for other emitter configurations. There appeared to be two distinct regions of

breakdown characteristics in the forward bias mode of operation.

5.2 Degradation Due to Second Breakdown.

A selection of each type of device was subjected to a series of repetitive breakdown tests to determine the effect of testing upon the transistor characteristics. The parameters selected for examination were, (a) current amplification factor (b) collector leakage current (c) delay time. These parameters were measured under carefully established operating conditions after each set of breakdown excursions. Measurements were taken before the first breakdown excursion to establish reference values for (a) and (b), the reference value for (c) was taken to be the value obtained from the first breakdown. Subsequent values were normalised to these reference values and a percentage deviation over 2.10^7 breakdown excursions obtained.

The initial tests were performed with a pulse width $1.1t_d$. Variations over the entire range were very small, the change being negligible after the first 100 breakdown excursions. The effect of a higher input energy was investigated by increasing the pulse width / delay time ratio to 2 : 1. The input power was ~~increased~~ decreased to prevent the mean device temperature rising significantly. A greater variation in the selected parameters was evident in this test, the leakage current showing a significant increase towards the end of the experiment. The results are shown graphically in Fig. 5.1.

It can be seen from the results obtained here that the values obtained from the subsequent series of tests can be accepted over a wide range of breakdown excursions. The pulse width to be used will

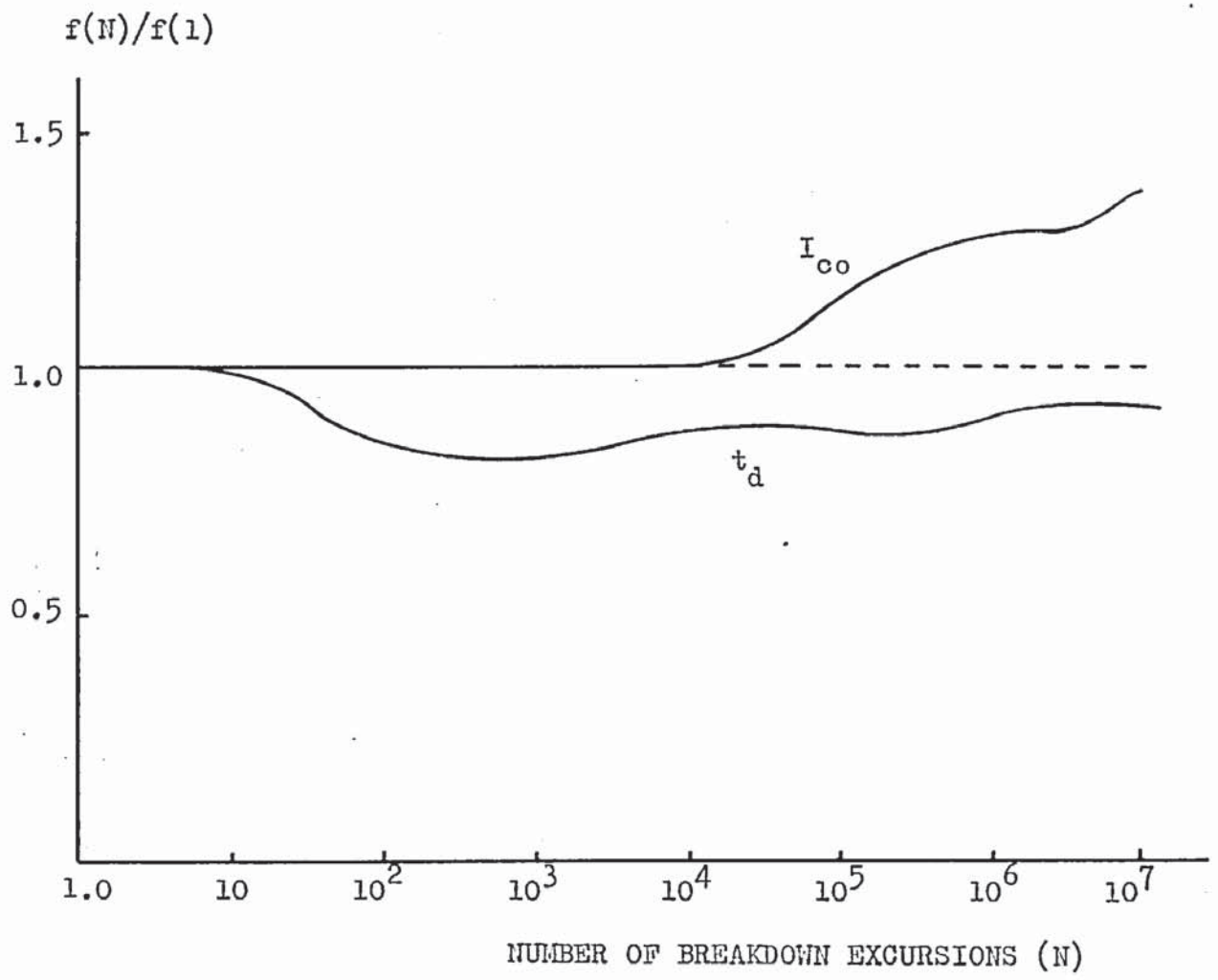

Fig. 5.1 The Effect of Second Breakdown on Transistor Performance.

Broken Line (1) V_{CE} = 40 V., I_c = 300 mA.,
t_d = 80μs., Pulse Width = 90μs.

Full Line (2) V_{CE} = 40 V., I_c = 500 mA.,
t_d = 30μs., Pulse Width = 60μs.

be restricted to times as close to t_d as stable breakdown conditions allow.

5.3 Breakdown Terminal Characteristics.

A minimum of twelve transistors of each type were subjected to a more detailed investigation of their electrical characteristics under breakdown conditions at room temperature. A number of these devices were examined at 273°K., and 195°K. Tests were performed in the forward and zero base-bias modes using a pulse separation of 40 ms., a collector-emitter voltage range up to 160 V., and a collector current pulse amplitude up to 1 A.

A detailed investigation was made of the relation between delay time and collector current, collector-emitter voltage and input energy to cause breakdown. The long term stability of ambient conditions in the laboratory allowed results to be obtained over a period of weeks, the consistency being maintained within 5%. Typical sets of results, together with a device outline diagram, are shown in Figs. 5.2 to 5.5.

It can be seen from the diagrams that, as the supply voltage approaches the avalanche breakdown voltage, the forward base-bias characteristics become similar to the open-base characteristic. At these high voltage levels the transition in the collector-emitter voltage changed from a single step to a double step as the current was increased. The biasing arrangement caused the emitter-base junction to be reverse biased by the initial voltage step. A small resistor placed in the base lead showed a reverse base current flow. It was found in subsequent investigations using an infra-red microscope that the breakdown site moved to the centre of the

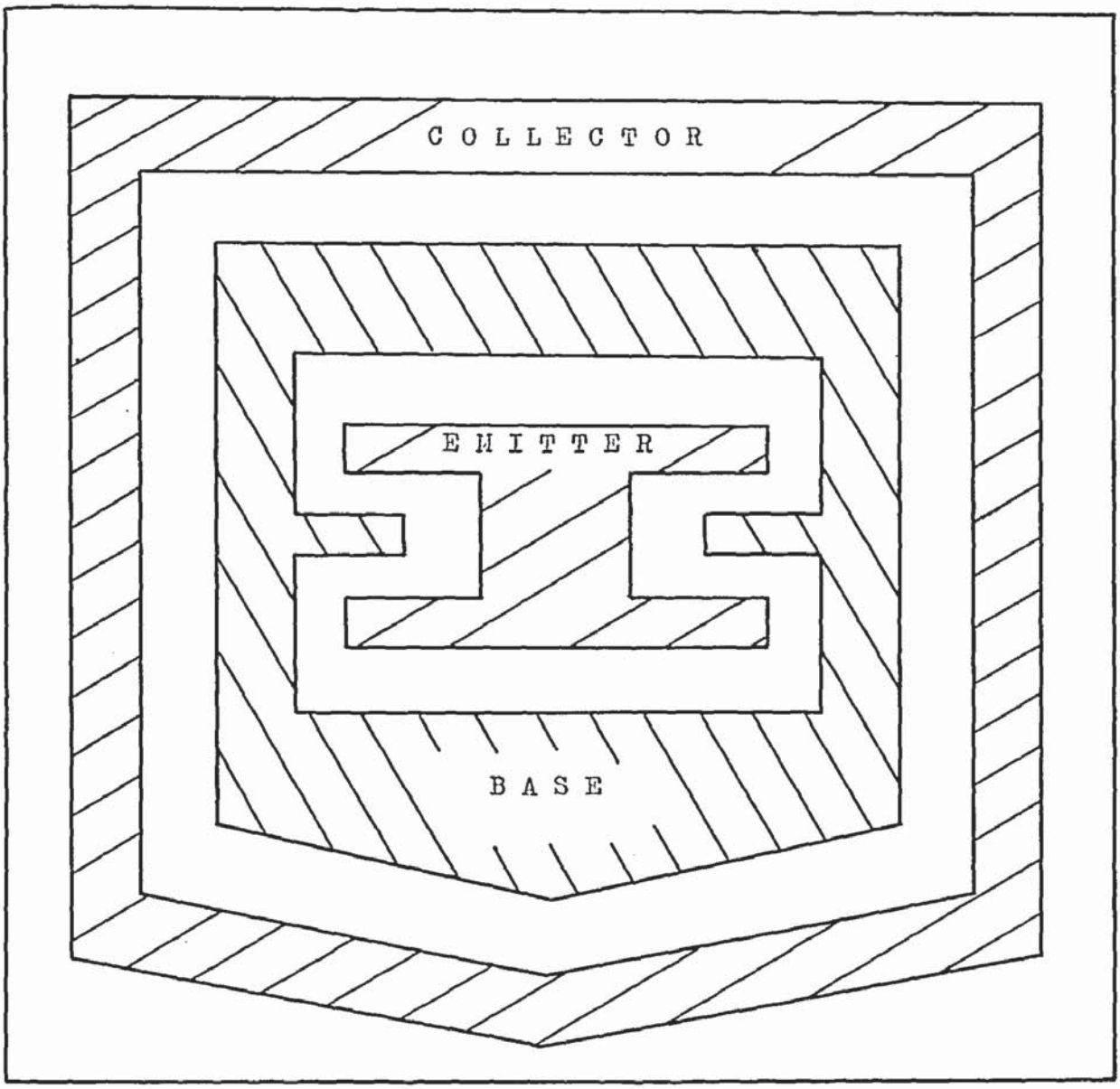

Fig. 5.2 (a) BFY 72 Contact Configuration.

Scale : 1" approx. 0.1 mm.

Fig. 5.2 (b) 2N 2218 Contact Configuration.

Scale : 1" approx. 0.1 mm.

Fig. 5.2 (c) 2N 2195 Contact Configuration.

Scale : 1" approx. 0.1 mm.

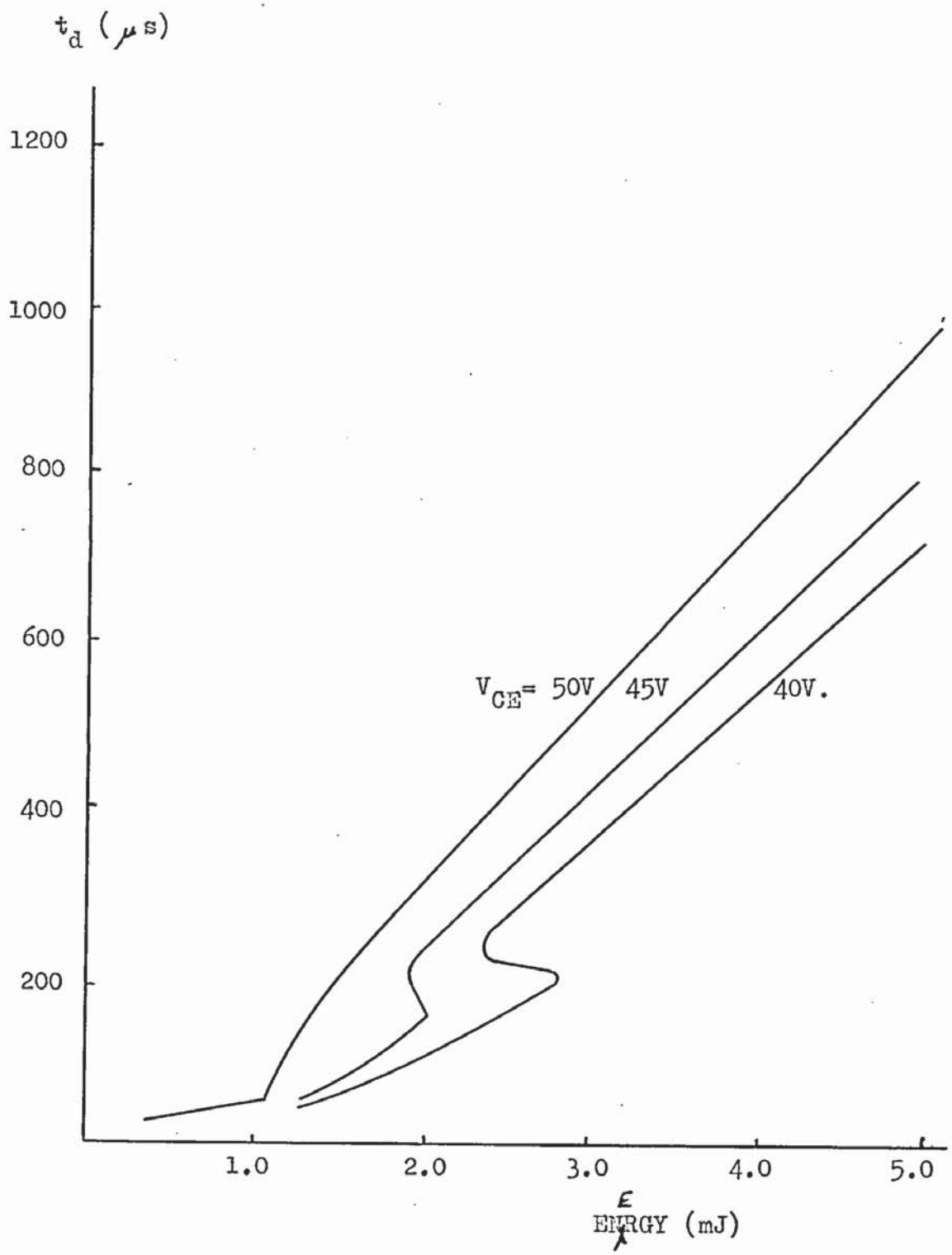

Fig. 5.3 (a) BFY 72 Delay Time - Breakdown Energy Characteristic at Ambient Temperature 297°K. (Forward base - bias)

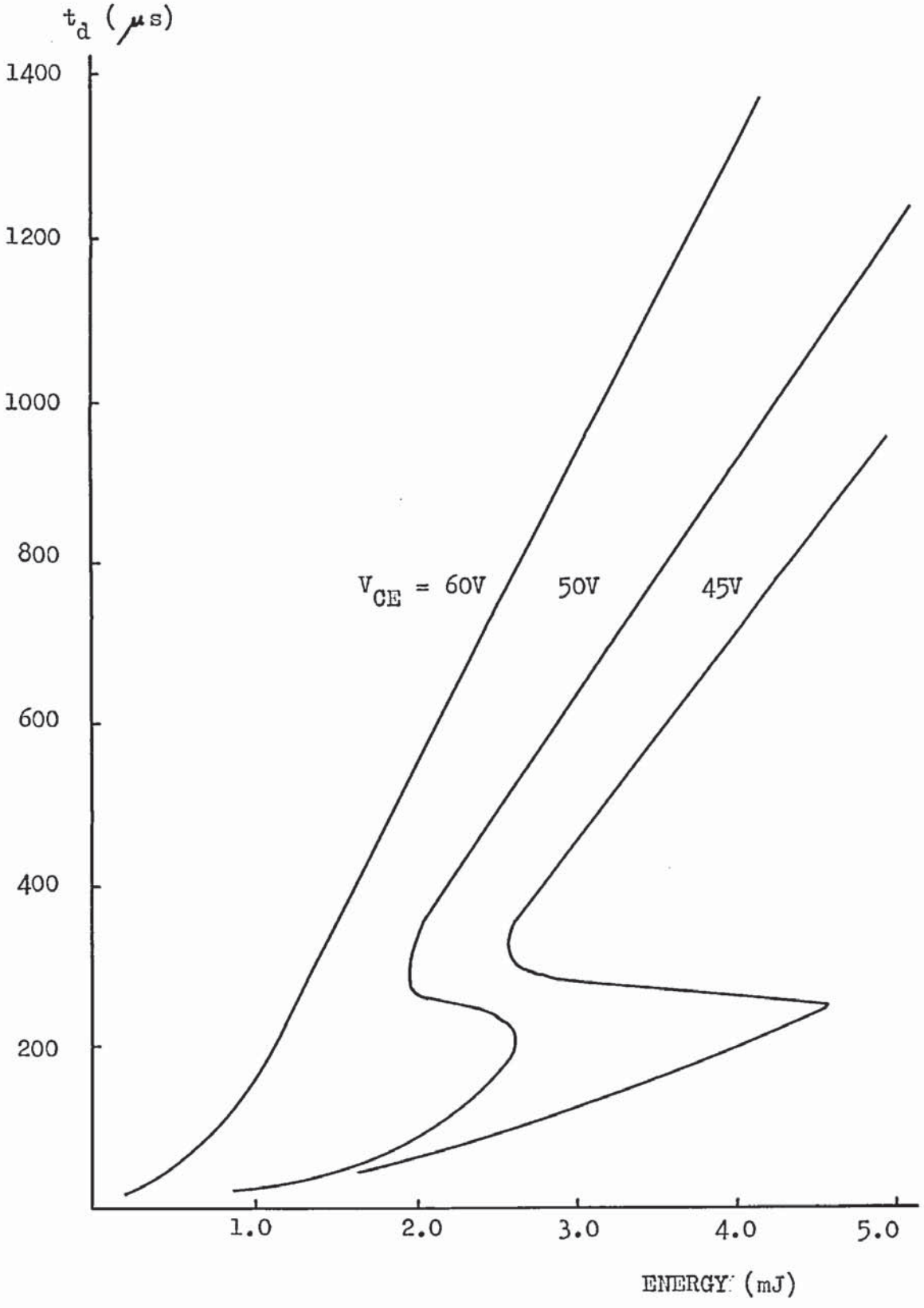

Fig. 5.3 (b) 2N 2218 Delay Time - Breakdown Energy Characteristic at Ambient Temperature 297°K. (Forward base-bias)

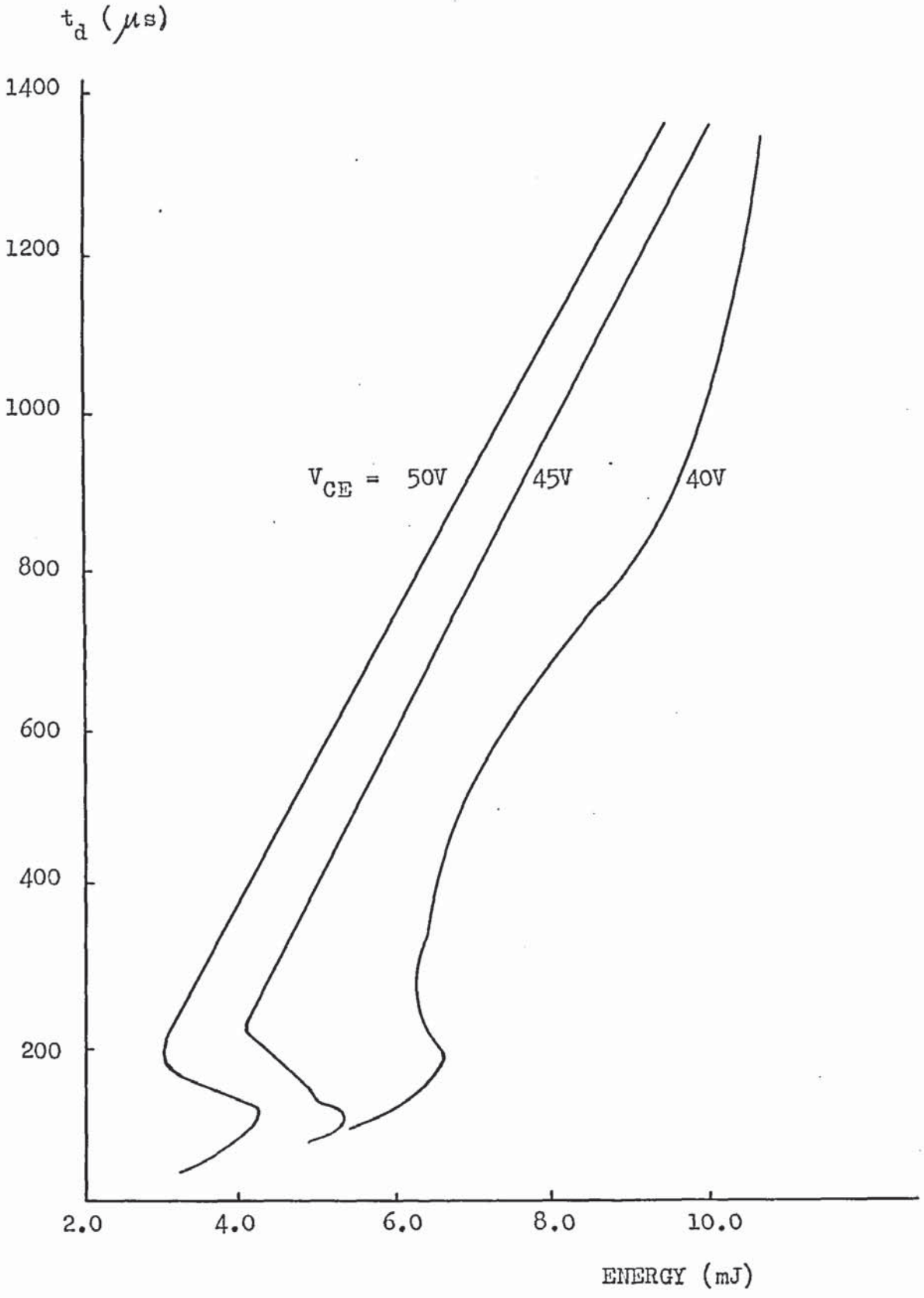

Fig. 5.3 (c) 2N 2195 Delay Time - Breakdown Energy Characteristic at Ambient Temperature 297°K. (Forward base-bias)

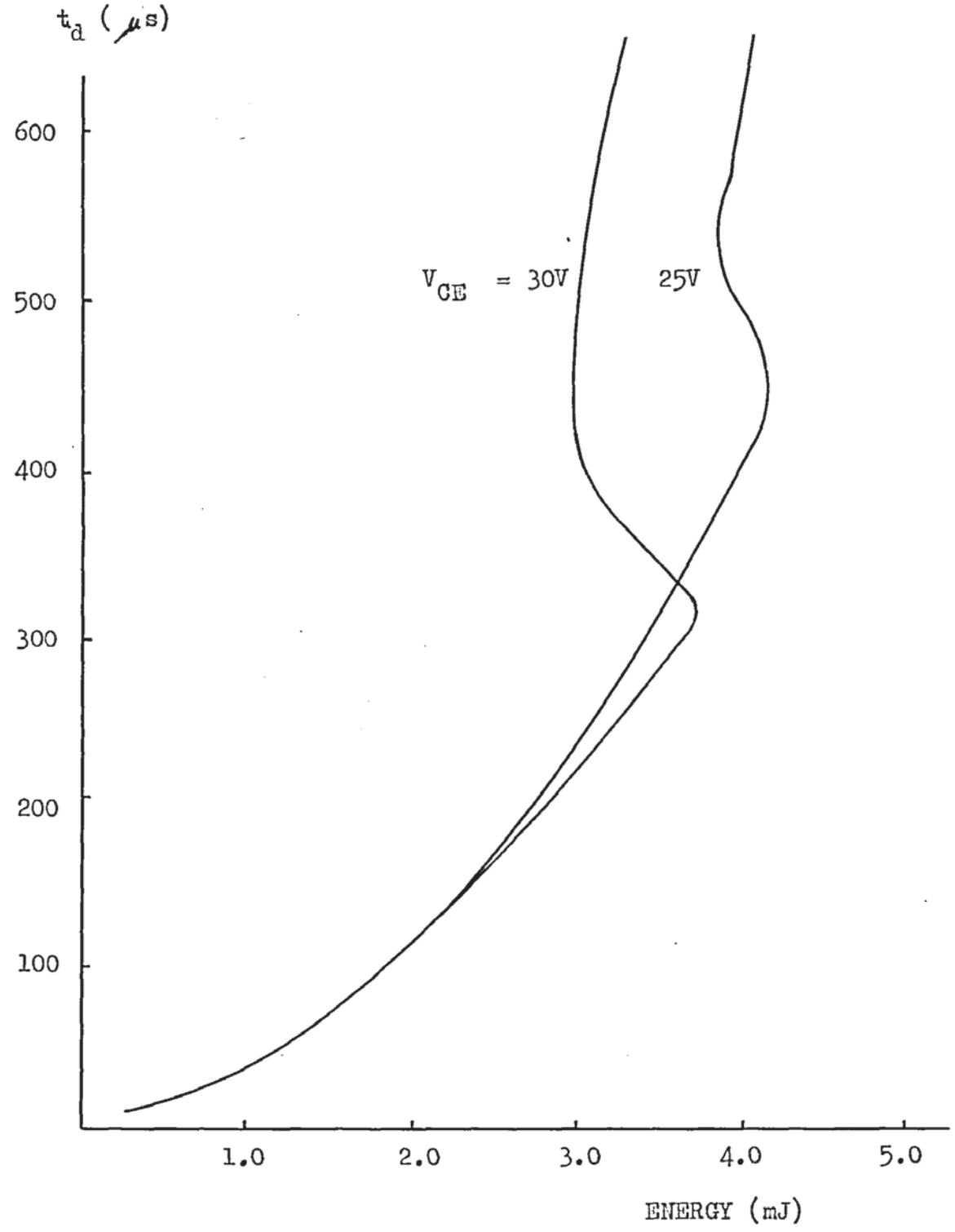

Fig. 5.3 (d) 2N 914 Delay Time - Breakdown Energy Characteristic at Ambient Temperature 297°K. (Forward base-bias)

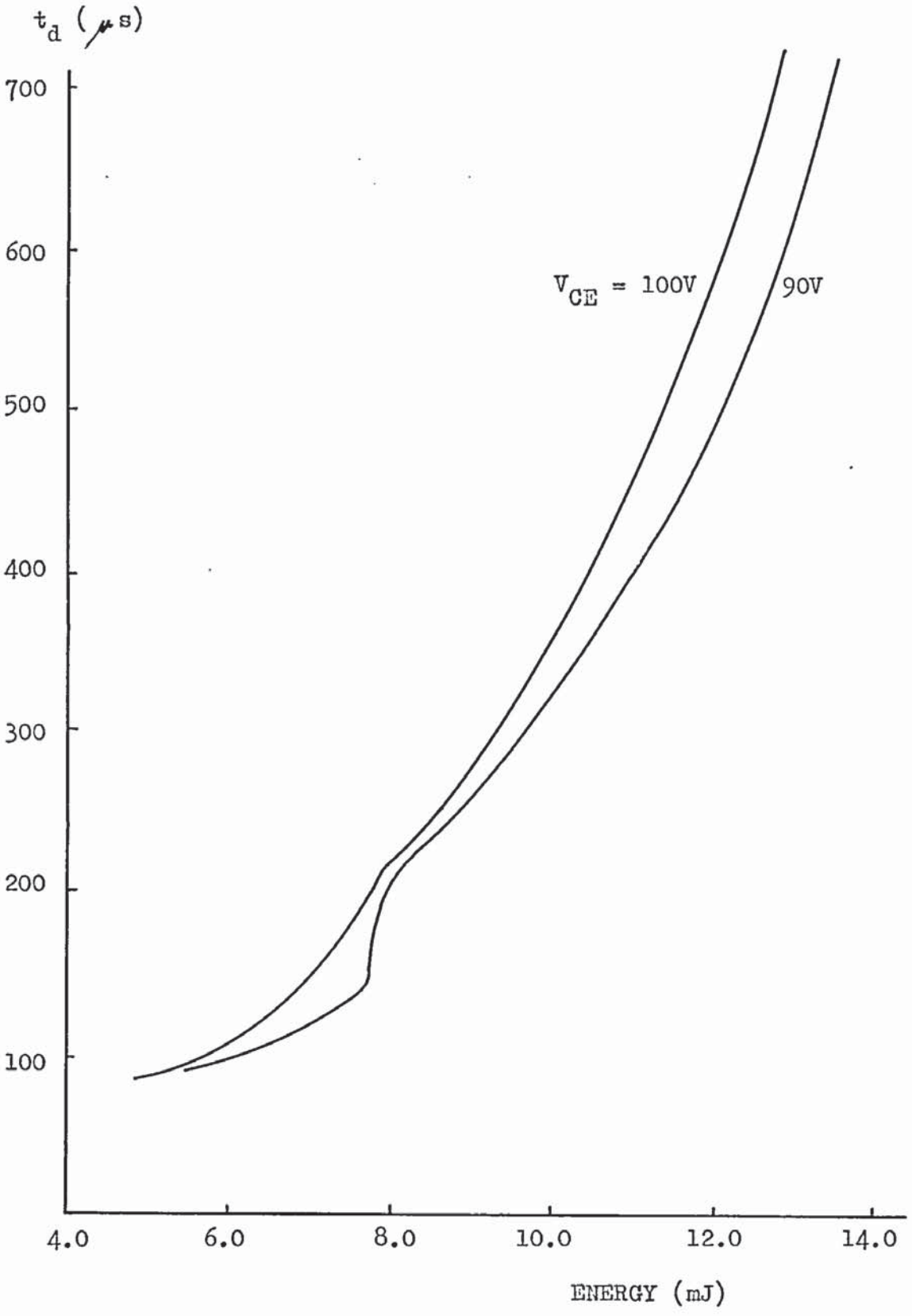

Fig. 5.3 (e) BFY 52 Delay Time - Breakdown Energy Characteristic at Ambient Temperature 297°K. (Forward base-bias)

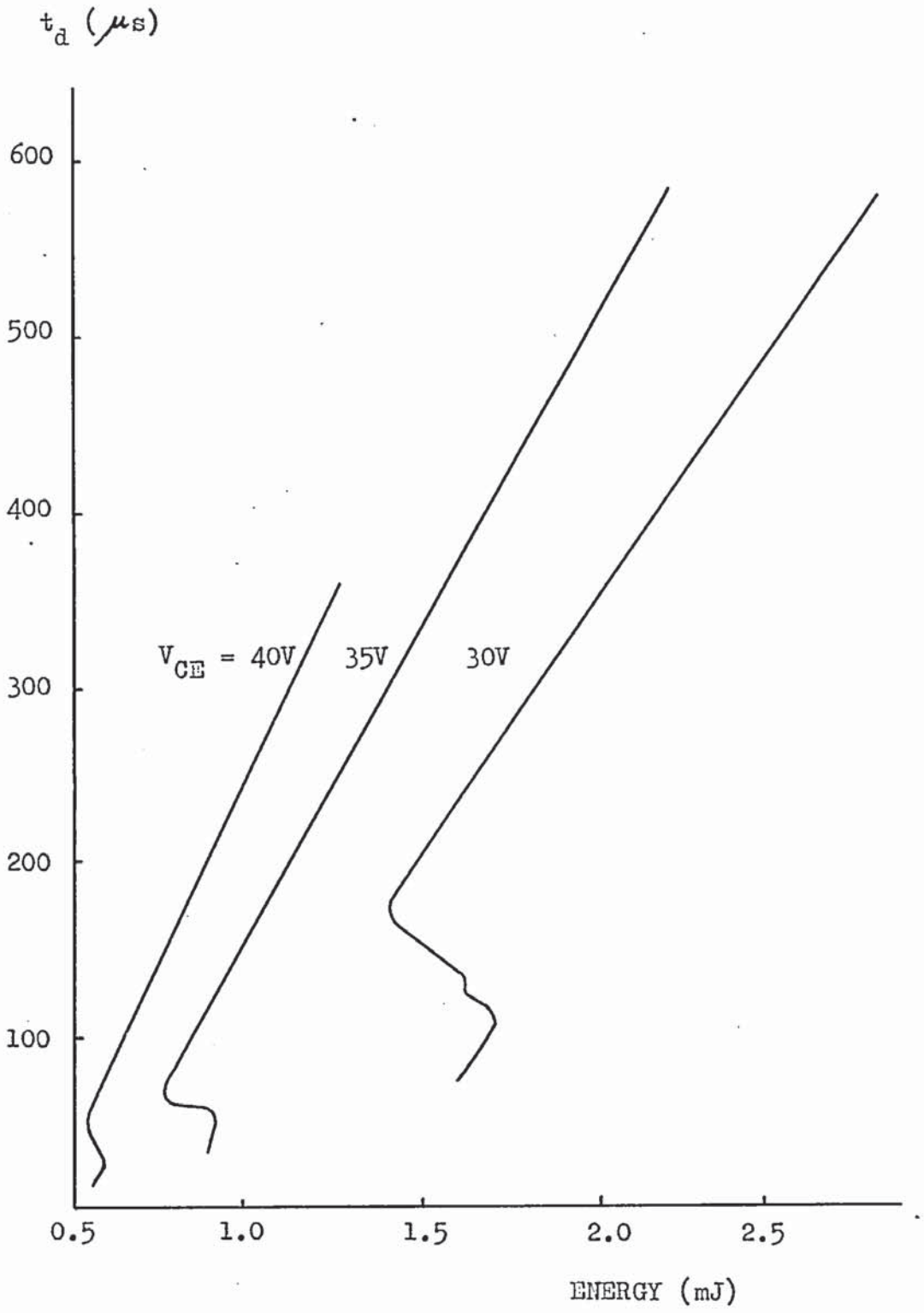

Fig. 5.3 (f) 2N 3734 Delay Time - Breakdown Energy Characteristic at Ambient Temperature 297°K. (Forward base-bias)

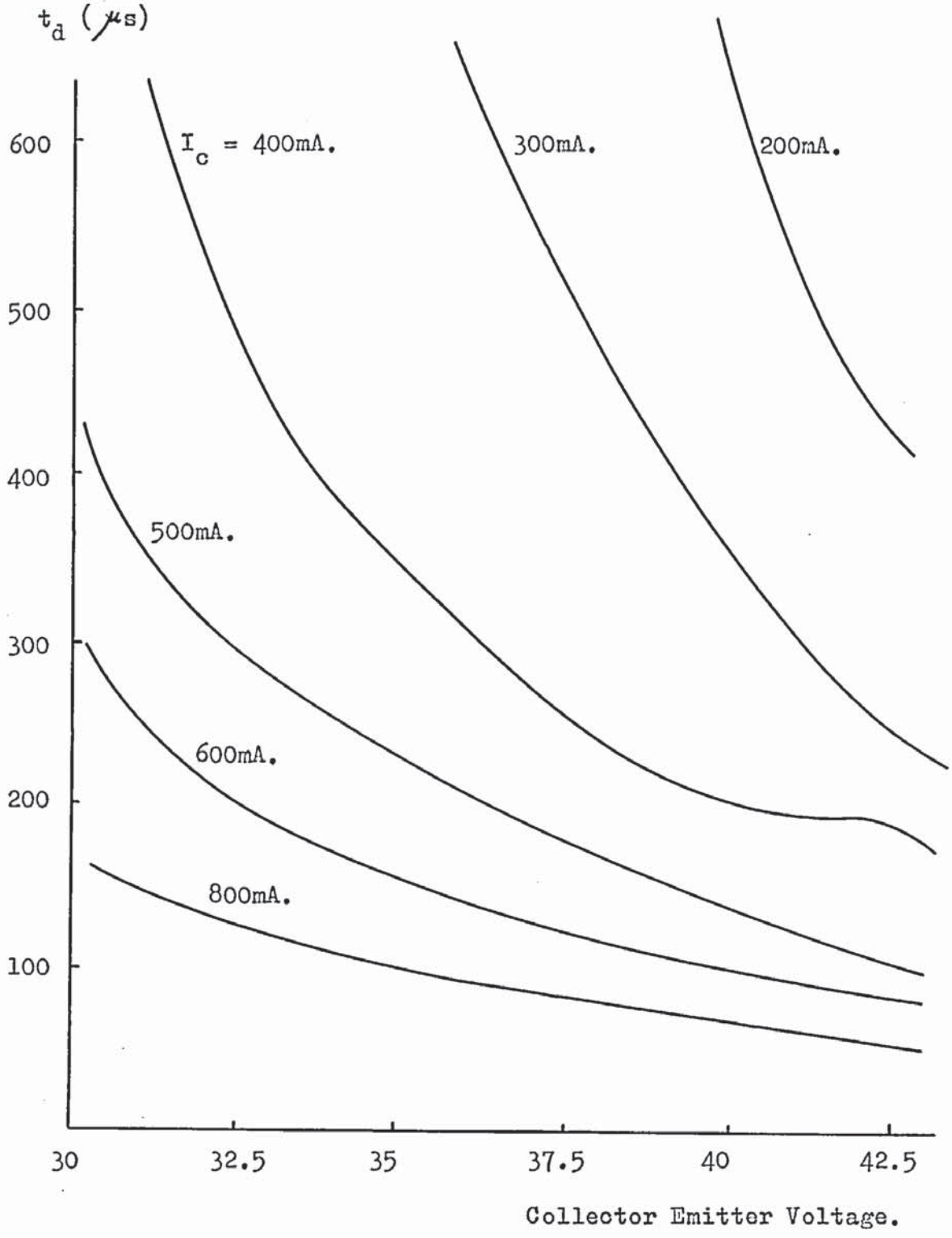

Fig. 5.4 (a) BFY 72 Delay Time as a Function of Collector-Emitter Voltage. Ambient Temperature 297°K. Forward base-bias operation. Collector Current as an independent variable.

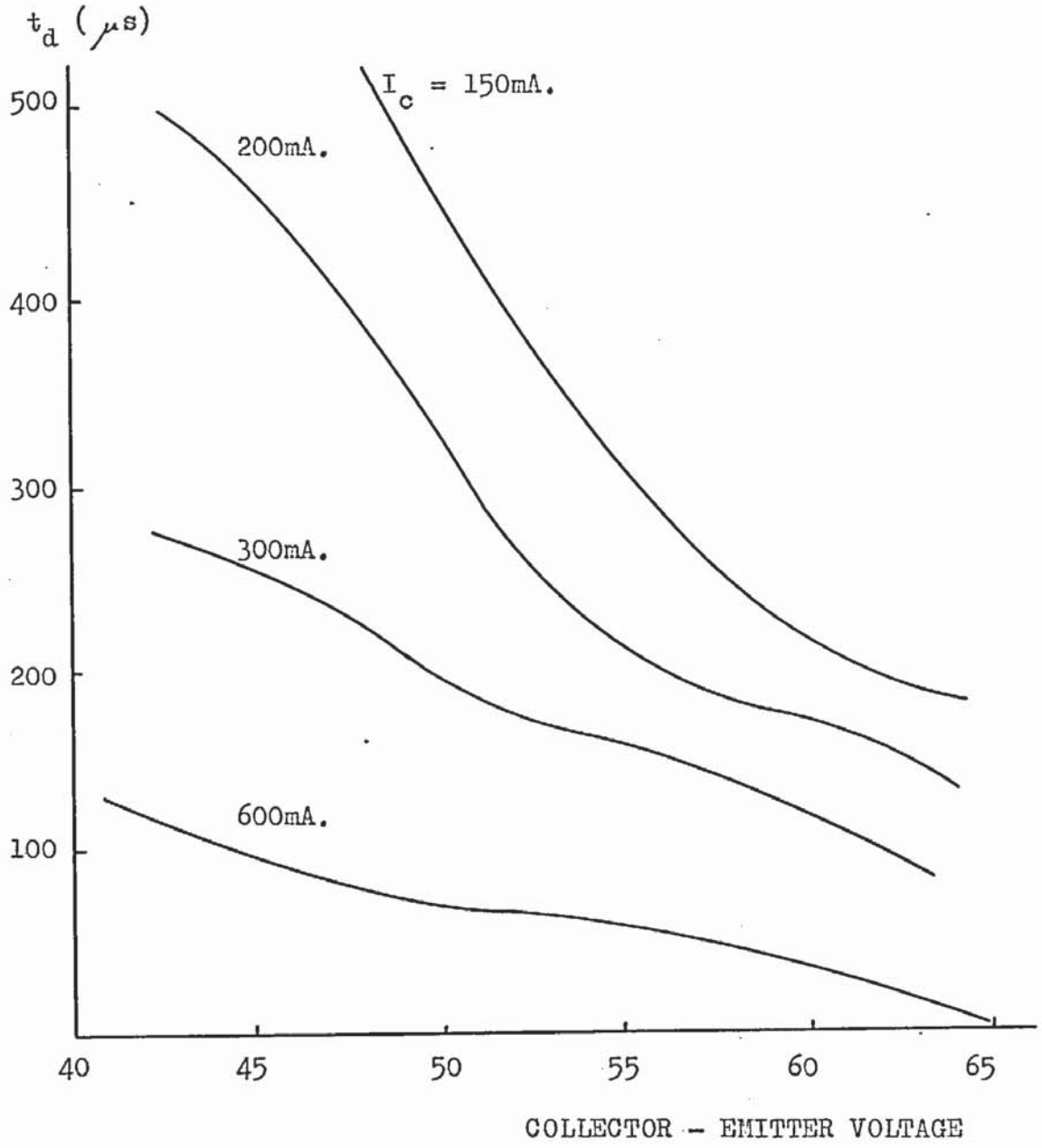

Fig. 5.4 (b) 2N 2218 Delay Time as a Function of Collector-Emitter Voltage. Ambient Temperature 297°K. Collector Current as an independent variable. Forward base-bias.

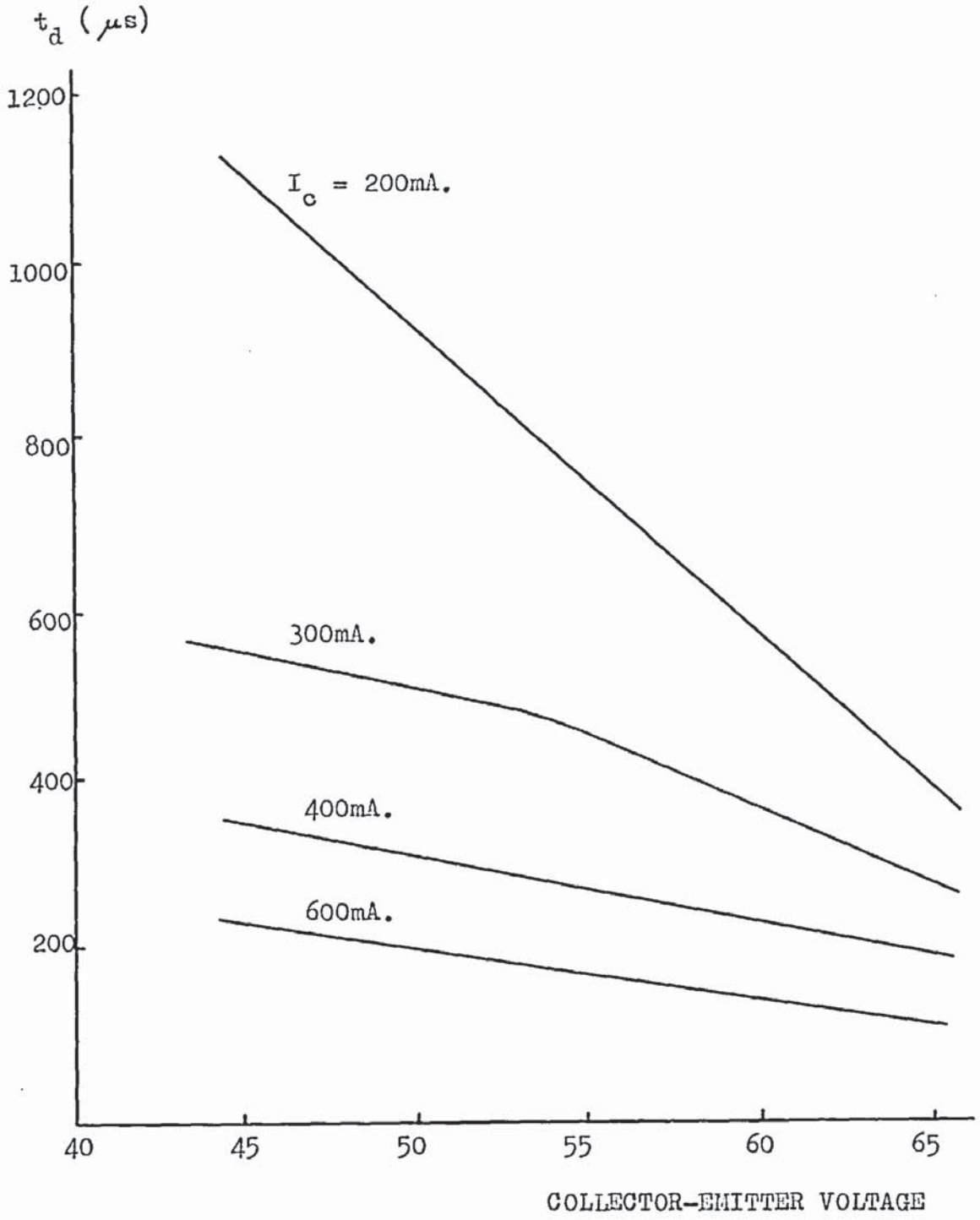

Fig. 5.4 (c) 2N 2195 Delay Time as a Function of Collector-Emitter Voltage. Ambient Temperature 297°K. Collector Current as an independent variable.

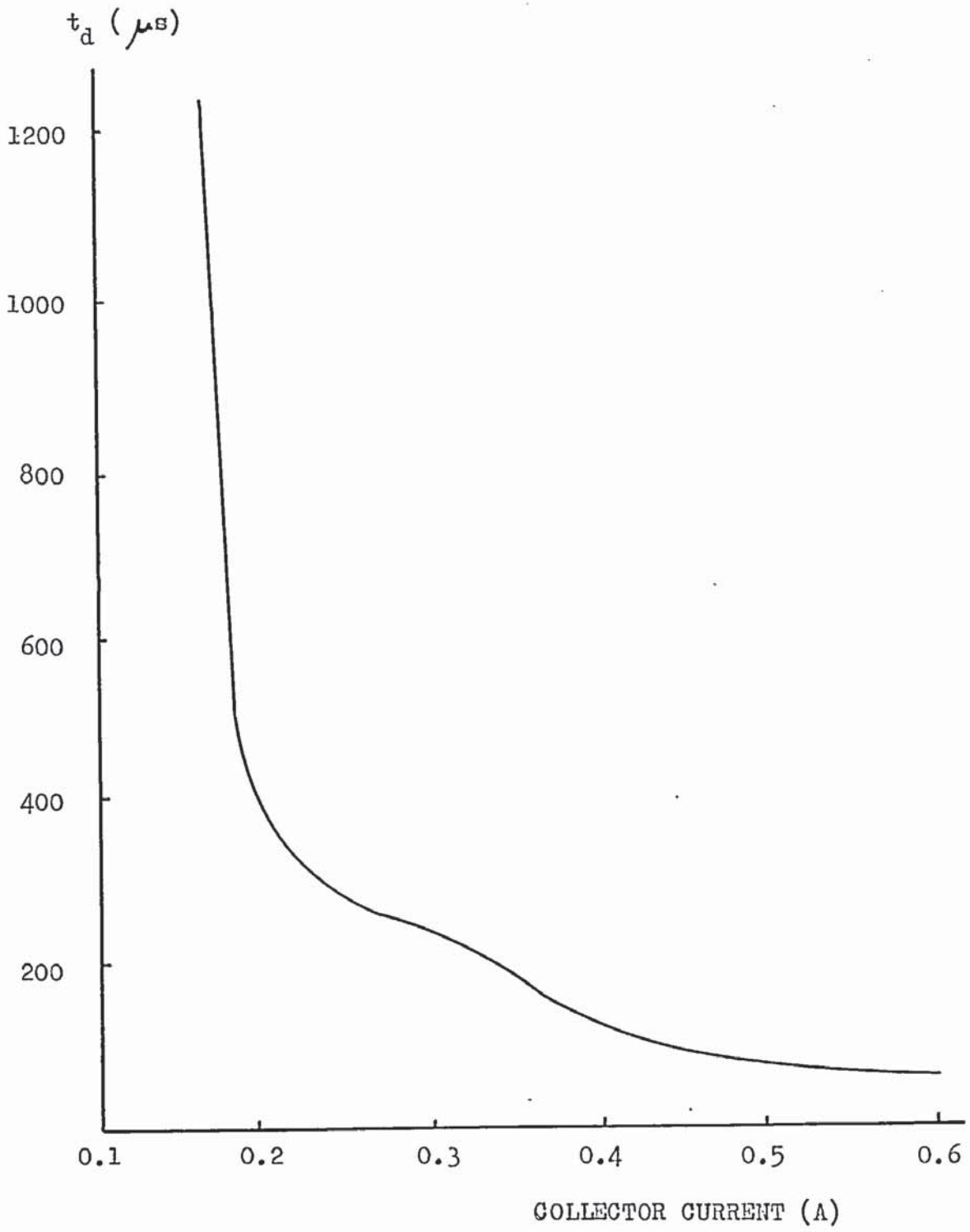

Fig. 5.5 (a) BFY 72 Delay Time as a Function of Collector Current. Collector-Emitter voltage = 40V. Ambient Temperature 297°K. (Forward base-bias)

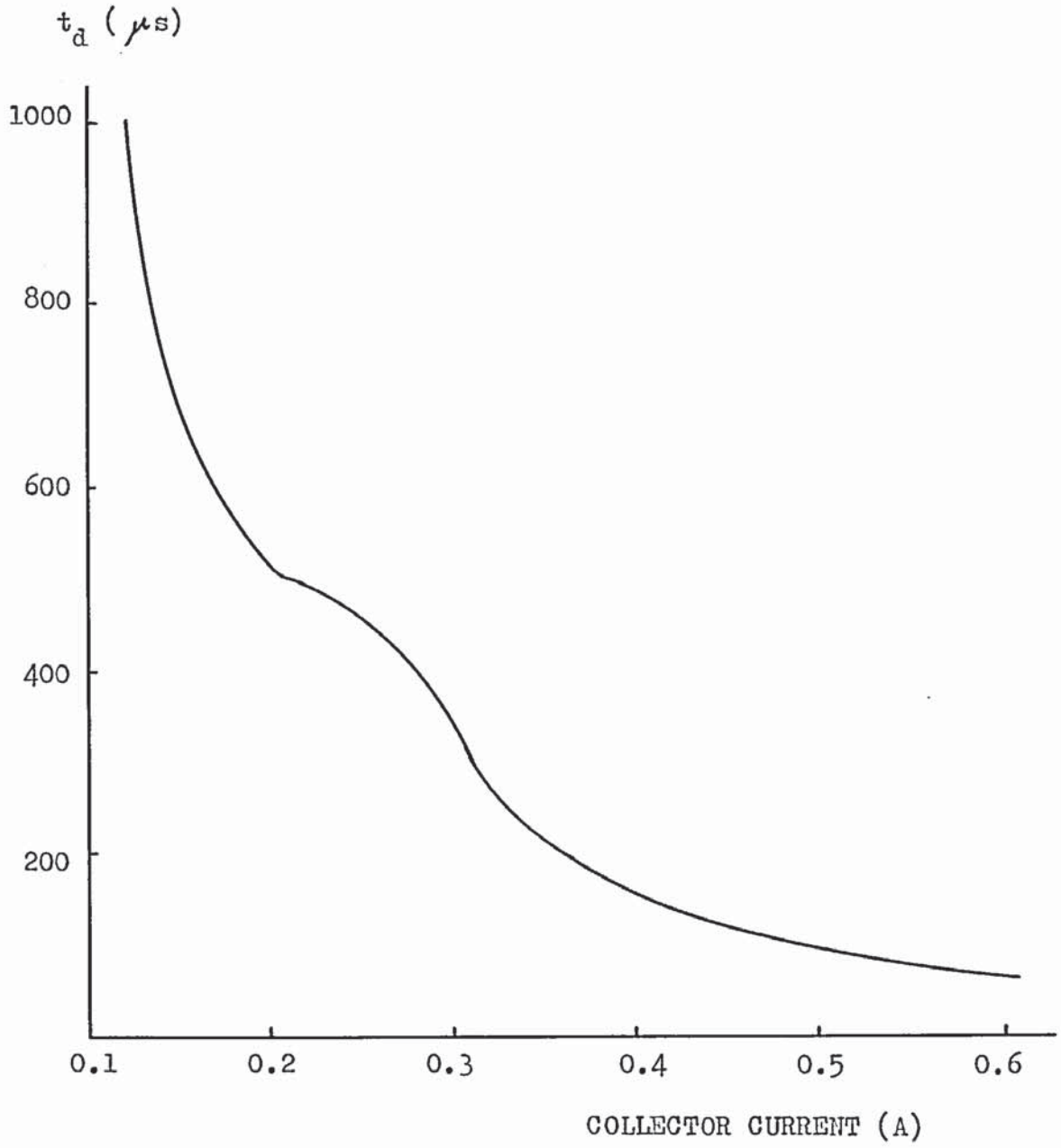

Fig. 5.5 (b) 2N 2218 Delay Time as a Function of Collector Current. Collector-Emitter voltage = 50V. Ambient Temperature 297°K. (Forward base-bias)

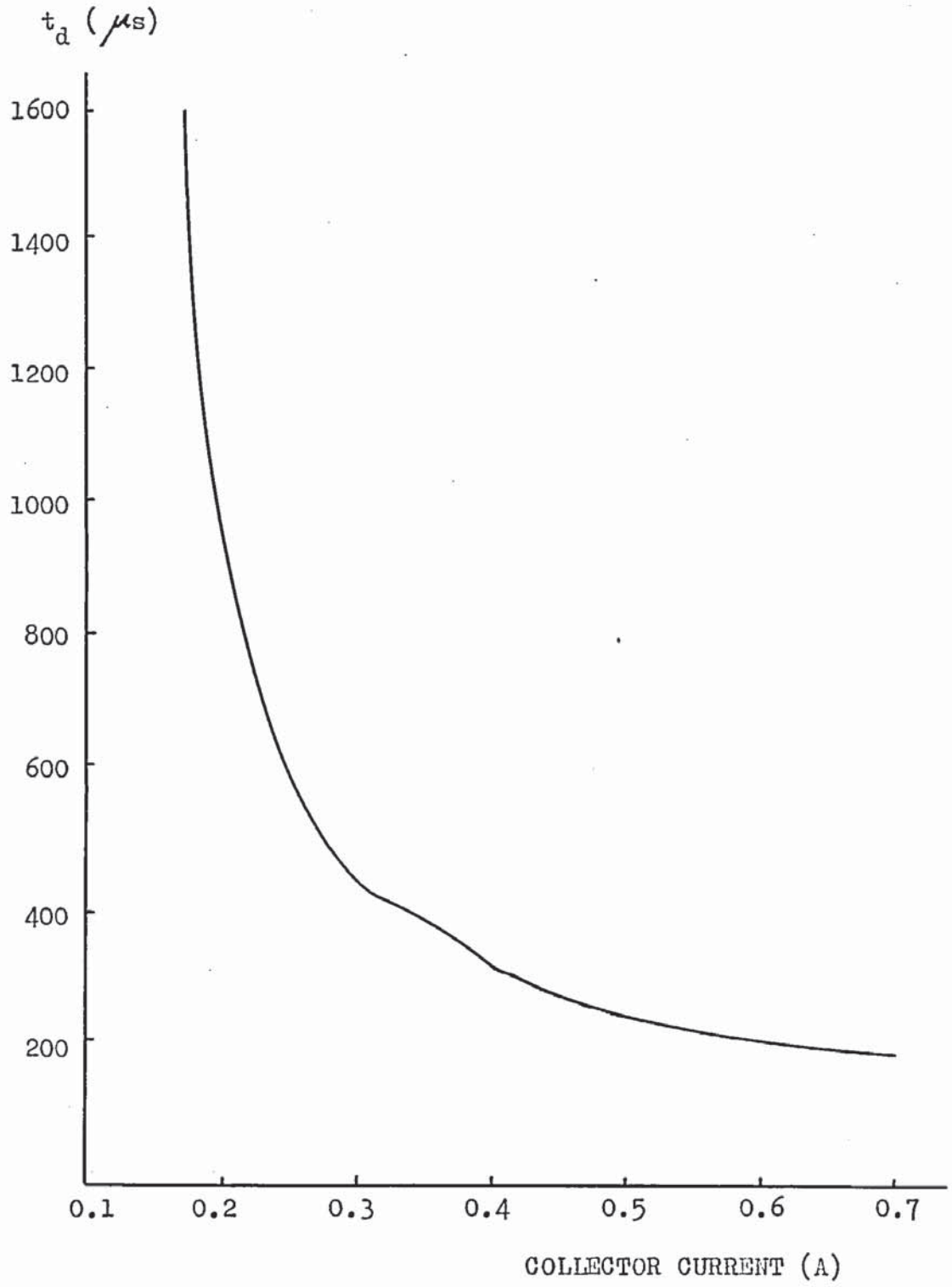

Fig. 5.5 (c) 2N 2195 Delay Time as a Function of Collector Current. Collector-Emitter voltage = 50V. Ambient Temperature 297°K. (Forward base-bias)

emitter under these conditions (the normal forward biased breakdown site is located at the edge of the emitter).

In the forward base-bias mode of operation samples of 2N2218 and 2N2195 transistors exhibited an unstable breakdown over a limited range of collector current and supply voltage. The instability was evident as an oscillation of the collector-emitter voltage between the supply voltage and the breakdown voltage. The instability was more readily obtained with the 2N2218 devices.

It can be seen from the t_d/I_c and $t_d/\mathcal{E}$ characteristics, in the forward base-bias mode, that there is a distinct difference between the low and high collector current relationships. The transition is not abrupt and repeatable breakdown conditions can be established in the intermediate region. This phenomenon is most evident in the $t_d/\mathcal{E}$ characteristic for non-circular emitter devices. At low supply voltages the transition showed a marked increase in the energy required to cause breakdown over the intermediate range of collector current levels. As the supply voltage increases the change in energy requirements is reduced. The unstable breakdown mentioned above occurs at supply voltages at which the $t_d/\mathcal{E}$ curve has a negligible distortion, but at a point which a distortion would be expected from the extrapolation of the low voltage results.

Multiple breakdown levels were observed at high power levels. The first step was similar to that already described above and caused the collector-emitter voltage to fall to a value approximately half the avalanche voltage. This voltage was found to be current dependent, the voltage rising slightly as the current increases. The first transition occurred almost instantaneously,

subsequent transitions being associated with a delay time, as shown in Fig. 5.6. The third and subsequent voltage steps were closely current dependent, the voltage reductions being of the order of 2 to 3 volts.

The deviation from a smooth curve for the $t_d/\mathcal{E}$ and t_d/I_c characteristics became more pronounced as the ambient temperature decreased. The energy input required to cause breakdown in the forward base-bias mode increased as the temperature fell.

A selection of 2N2218 devices with a spread of current amplification factor covering a range of 2 : 1 at a collector current of 300 mA. Devices having similar values of h_{fe} had similar values of delay time over the entire range of forward base-bias operation. At all current levels the delay time was seen to decrease as the current gain increased, see Fig. 5.7.

The results of an investigation of the effect of ambient temperature upon the delay time, for several values of collector current, are shown in Fig. 5.8. It can be seen that the temperature dependence is much stronger at low power levels. At large collector currents the delay time is almost independent of temperature. This indicates the increasing importance of non-thermal effects as the collector current rises.

It was found that results taken over a period of days showed a small deviation. Results obtained in the same series of readings performed in a single day were consistent. When taking low temperature readings therefore, the room temperature value was checked between each reading at reduced temperature and a complete series of results was obtained in one session.

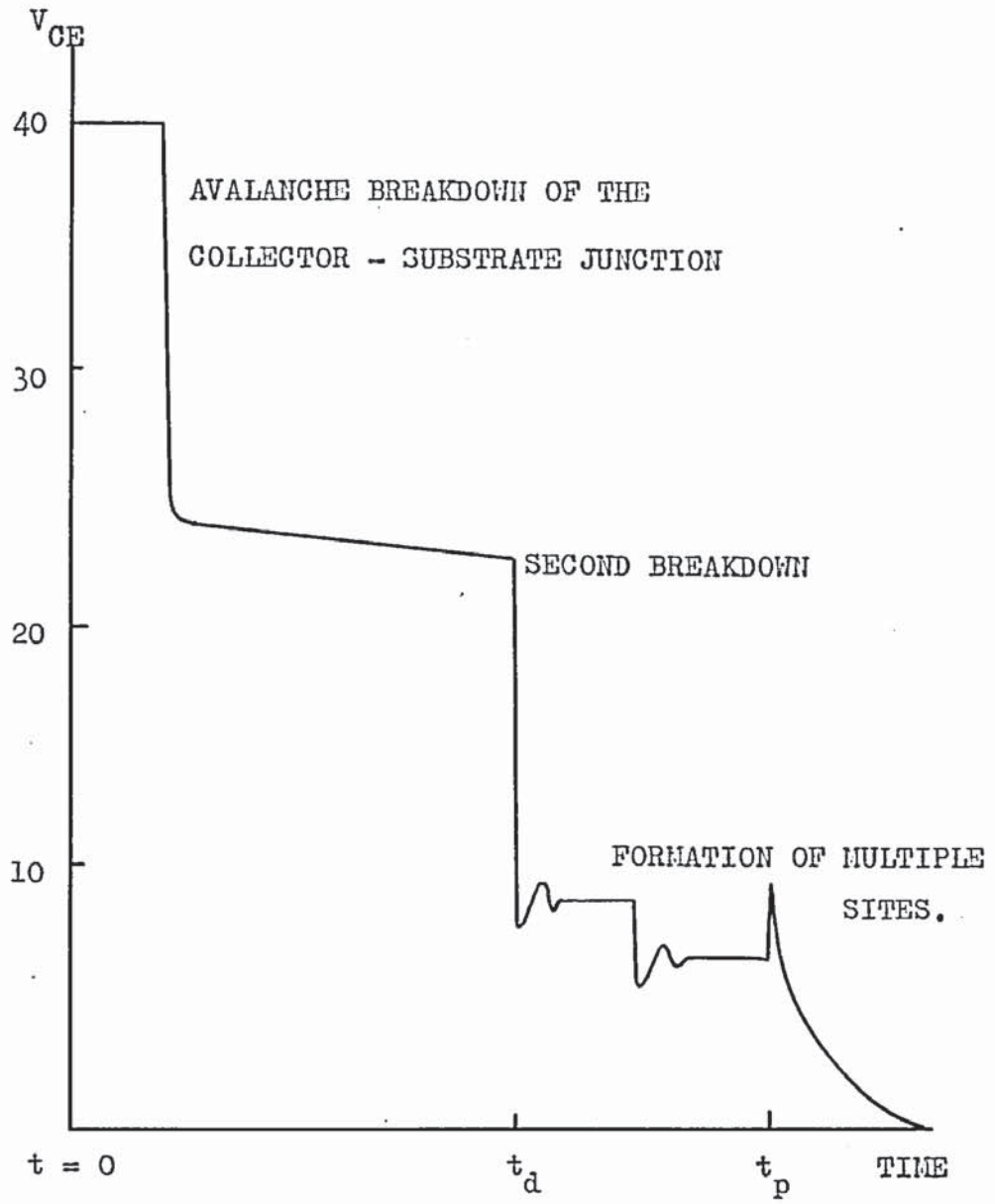

Fig. 5.6 Typical Collector-Emitter Voltage Changes for Forward Base-Bias Operation.

Collector-Substrate junction avalanches after the onset of current constriction. The resultant fall in V_{CE} reduces the local power dissipation and inhibits Second Breakdown.

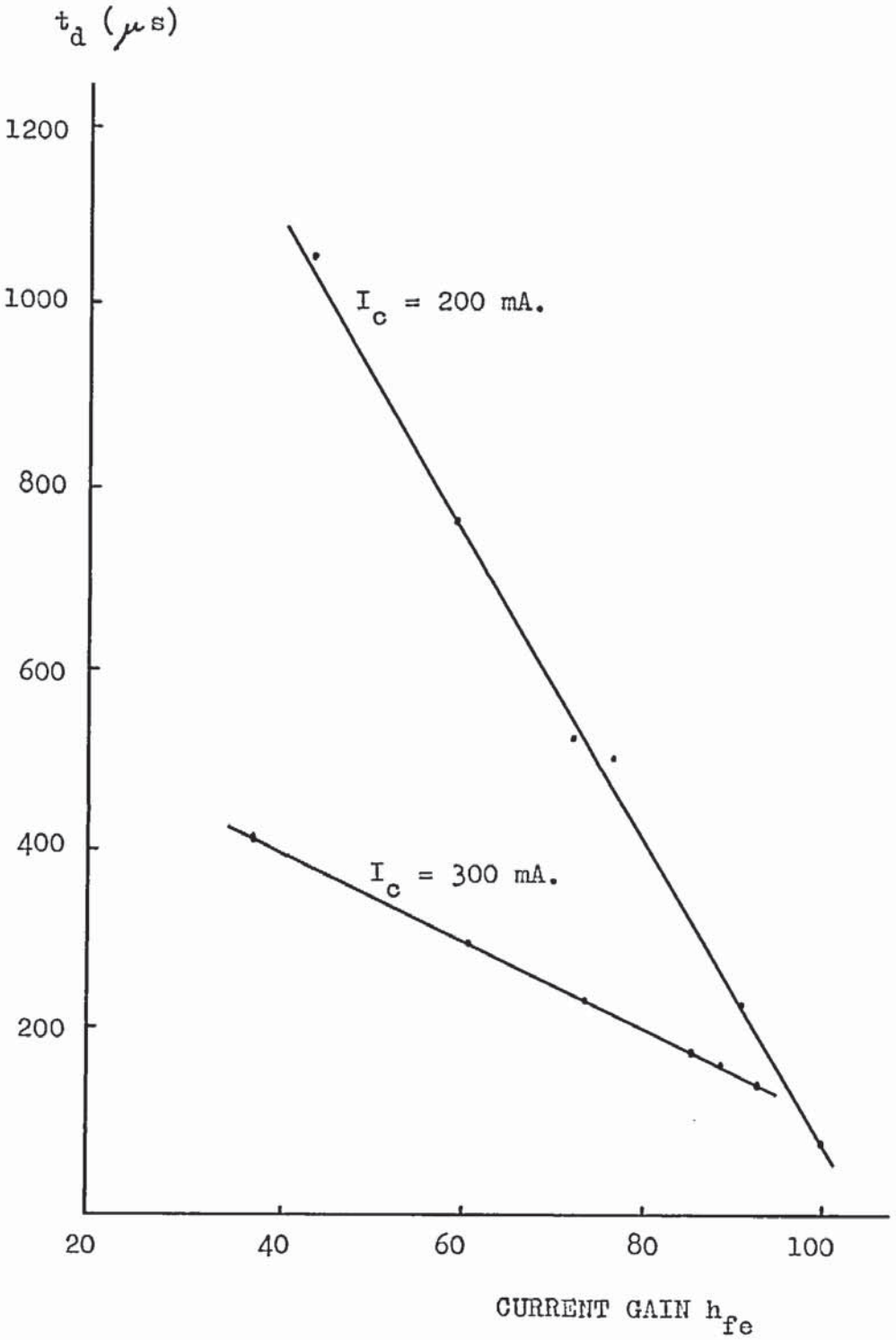

Fig. 5.7 The Effect of Current Gain Upon Delay Time for 2N 2218 Transistors. (Forward base-bias operation)

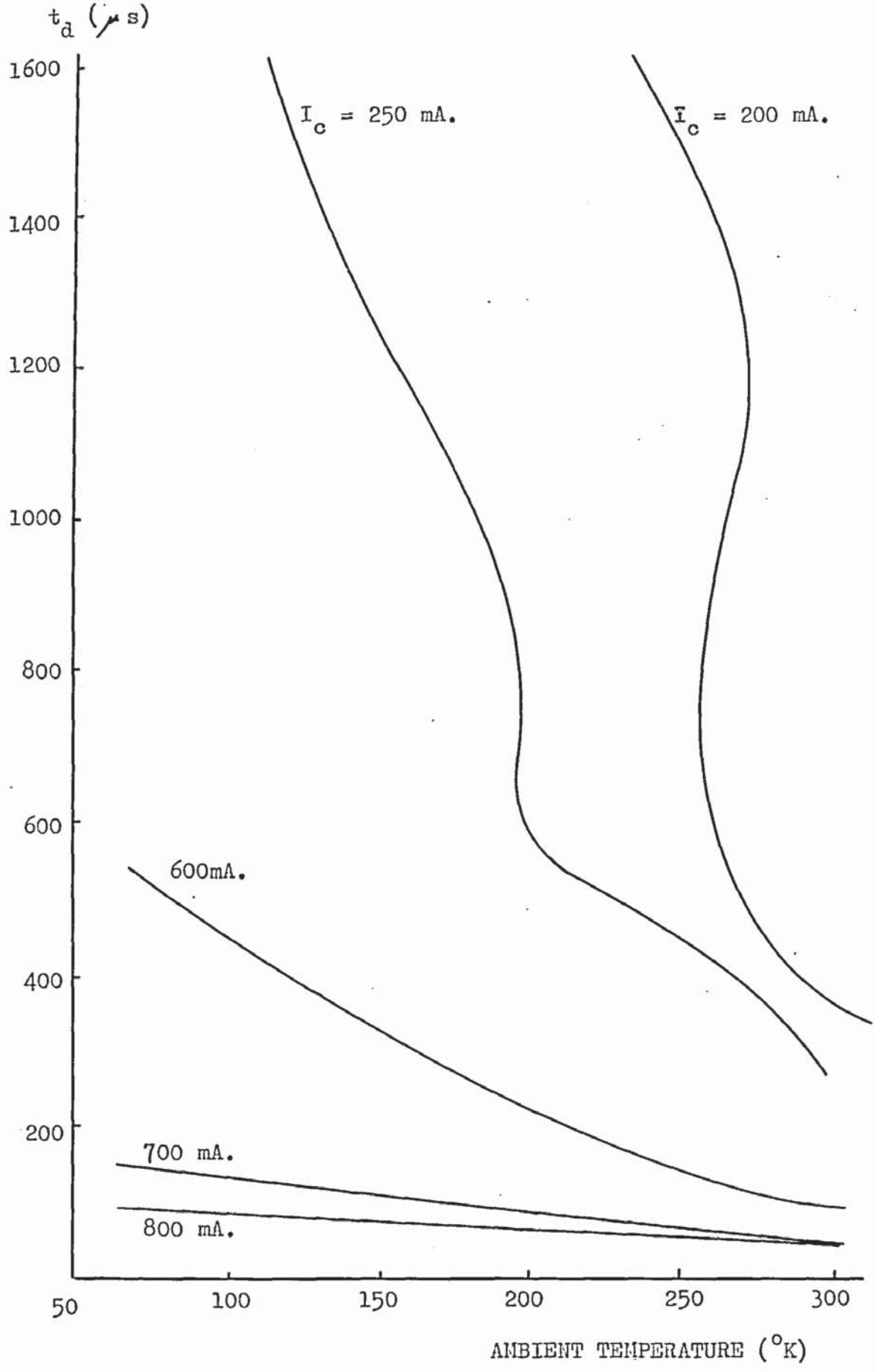

Fig. 5.8 (a) BFY 72 Delay Time as a Function of Ambient Temperature. V_{CE} = 40V. (Forward base-bias)

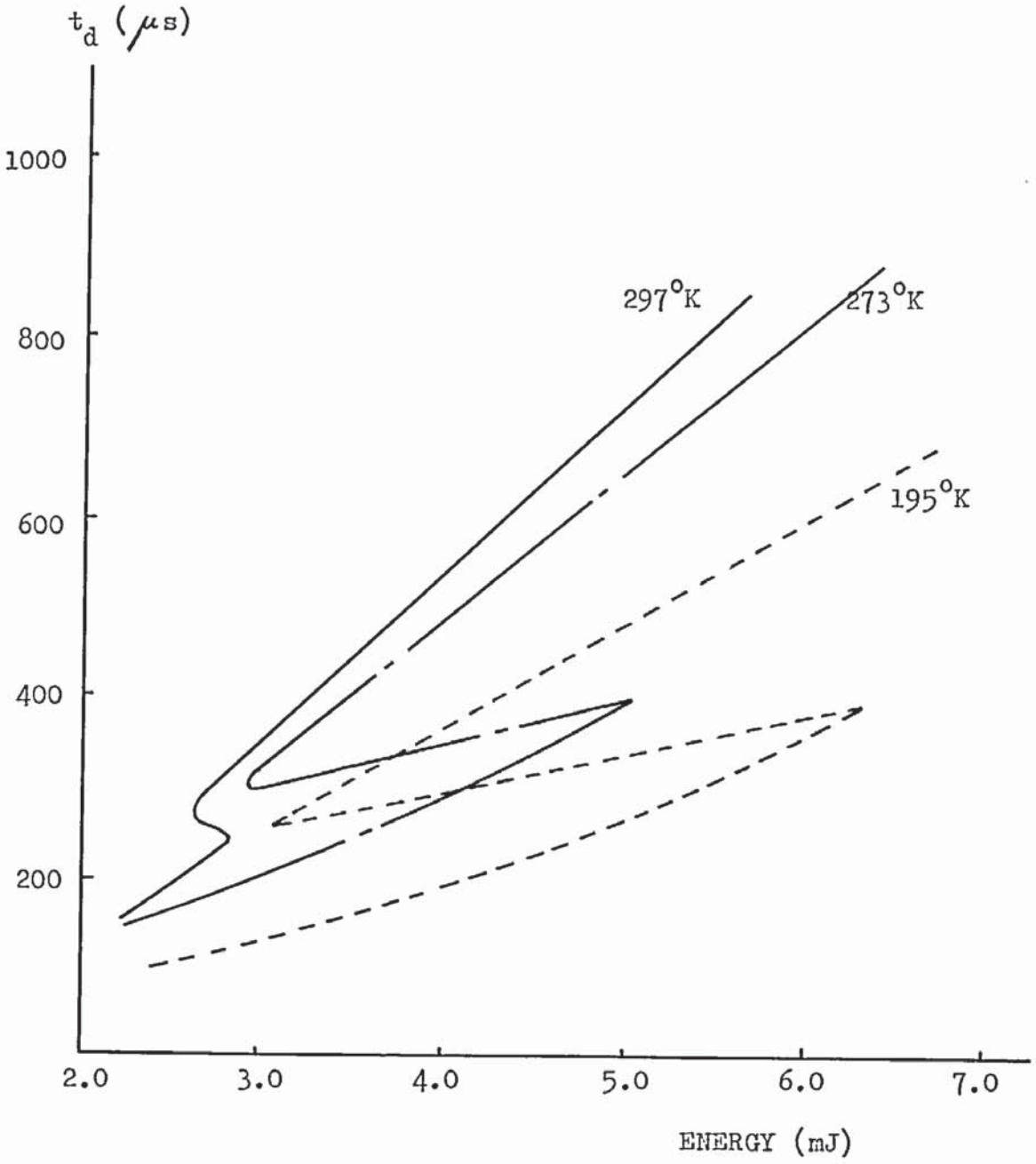

Fig. 5.8 (b) BFY 72 The Effect of Ambient Temperature Variation on the Delay Time - Breakdown Energy Characteristic. Forward base-bias operation.

V_{CE} = 40V.

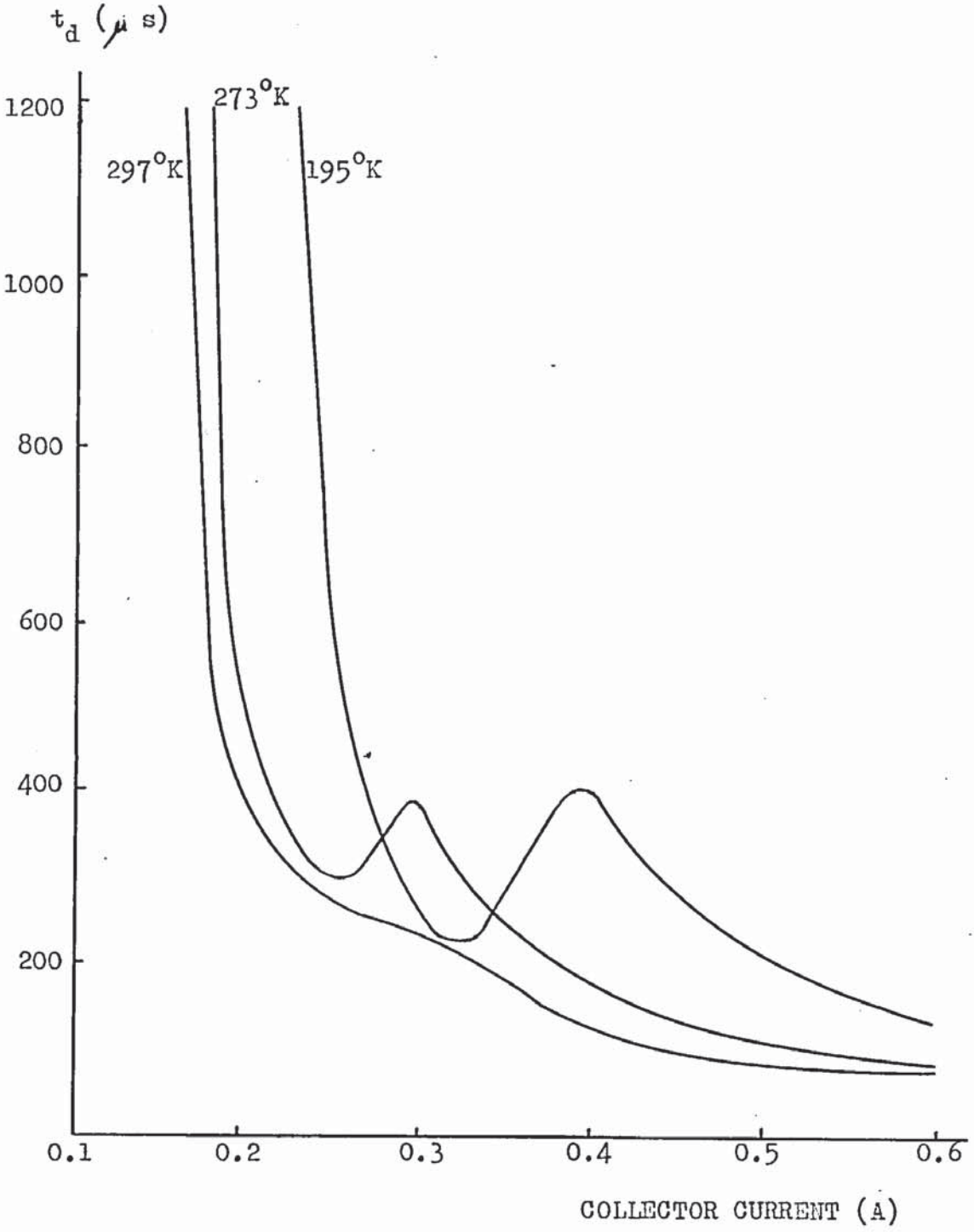

Fig. 5.8 (c) BFY 72 Delay Time as a Function of Collector Current Showing the Effect of Ambient Temperature Variation. Forward base-bias operation. V_{CE} = 40V.

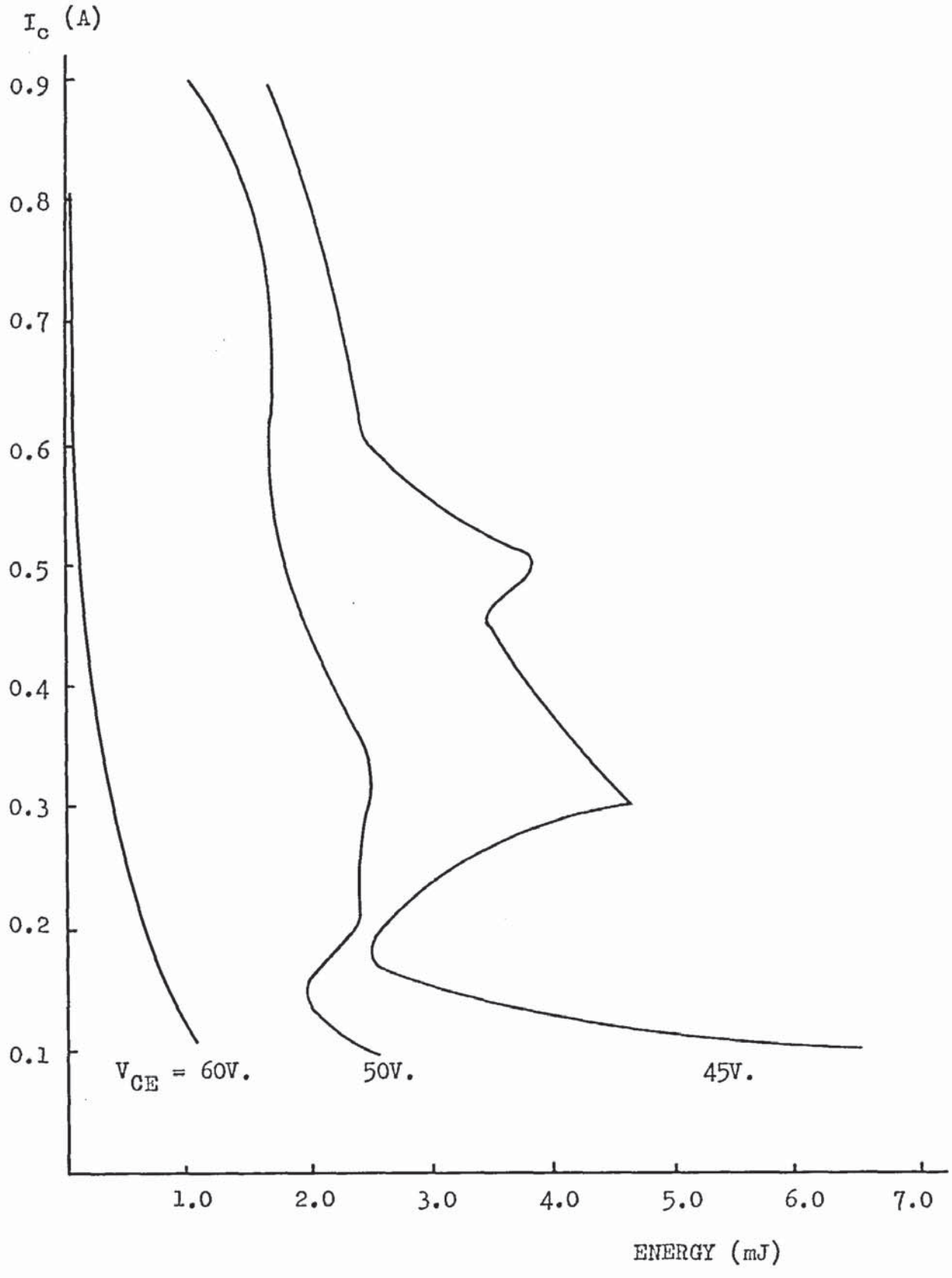

Fig. 5.9 (a) 2N 2218 Breakdown Energy as a Function of Collector Current. Forward base-bias operation. Ambient Temperature 297°K.

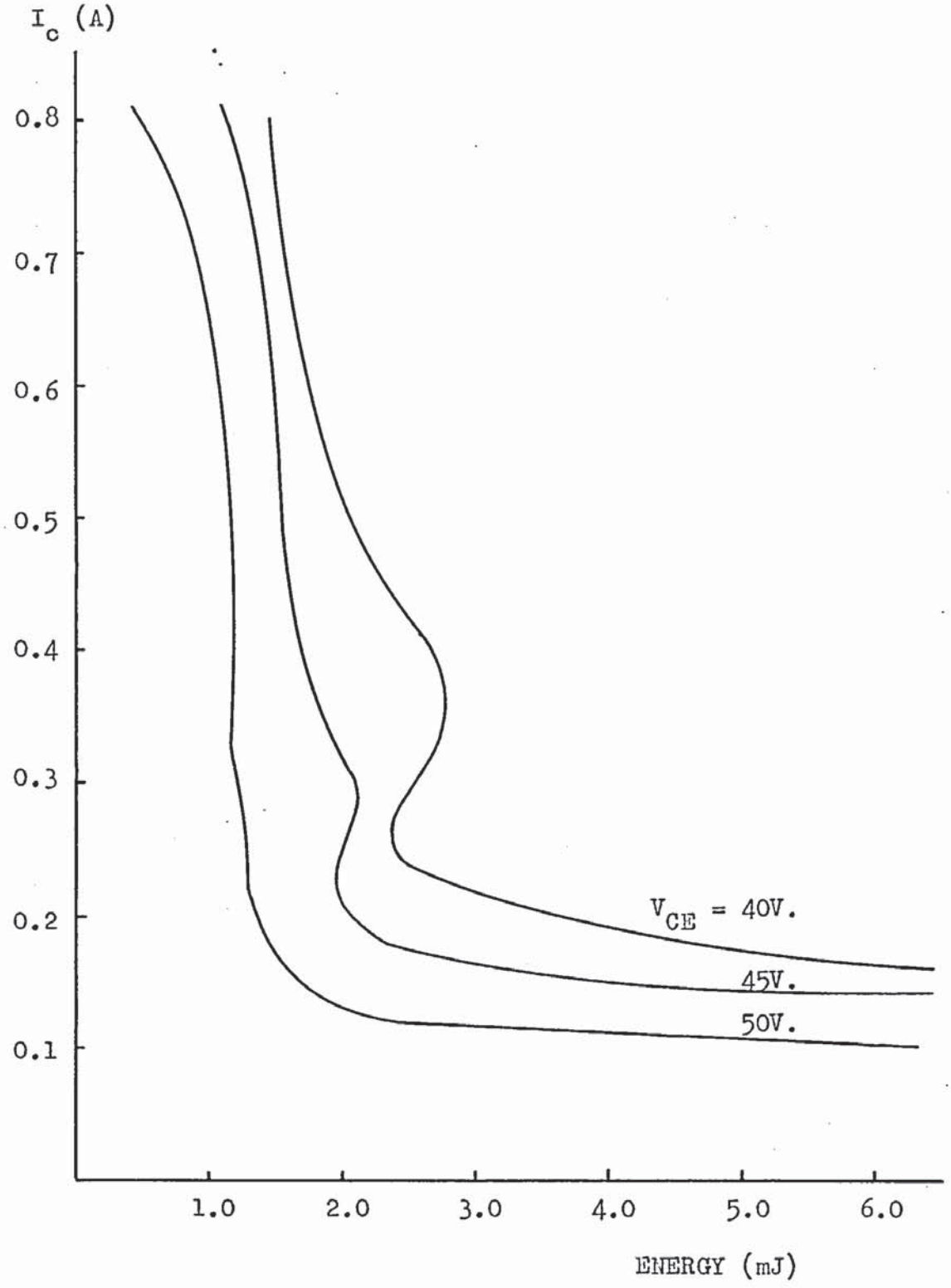

Fig. 5.9 (b) BFY 72 Breakdown Energy as a Function of Collector Current. Forward base-bias operation. Ambient Temperature 297°K.

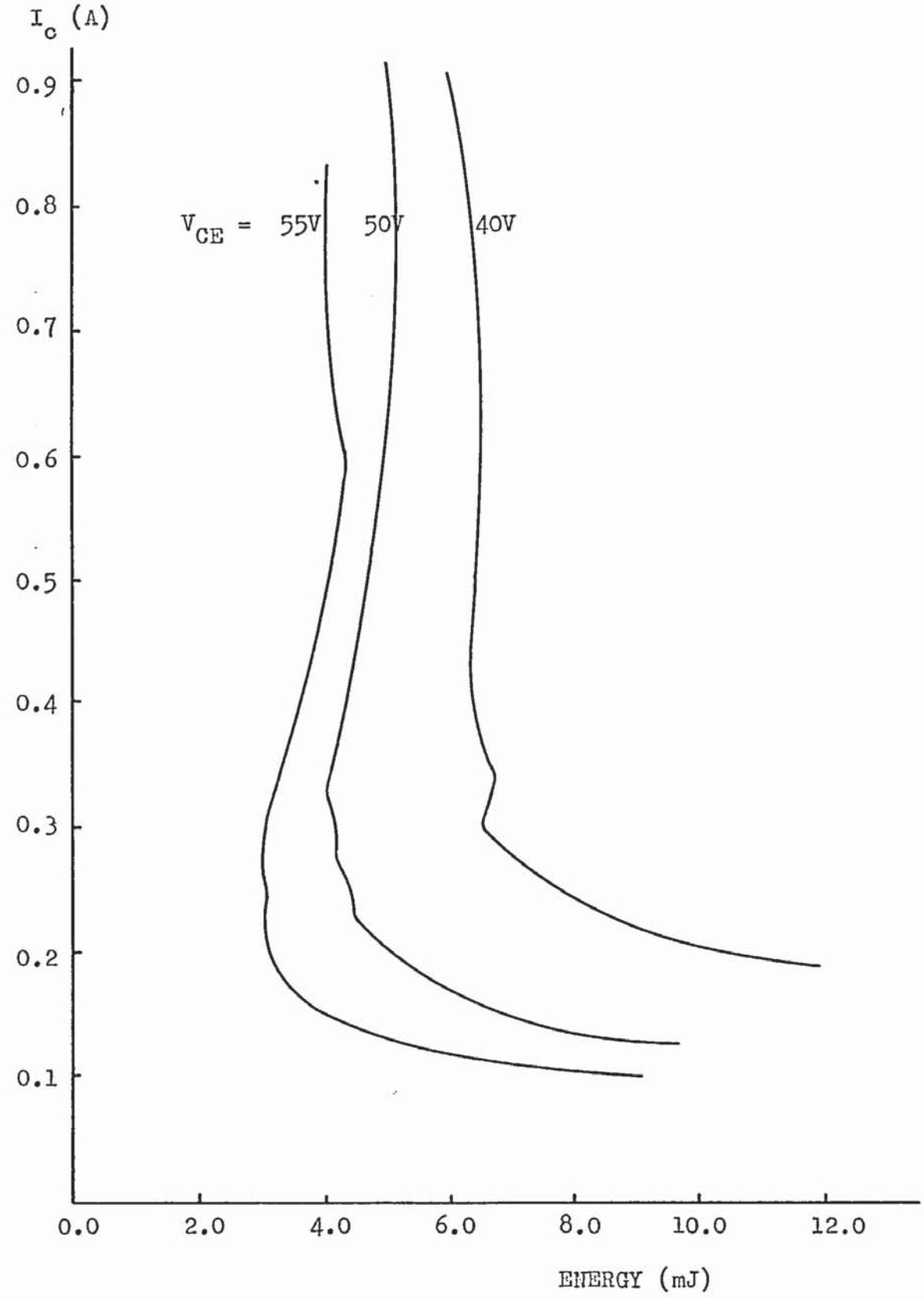

Fig. 5.9 (c) 2N 2195 Breakdown Energy as a Function of Collector Current. Forward base-bias operation. Ambient Temperature 297°K.

5.4 Surface Temperature Distribution.

Four transistors from each batch were selected for their close approximation to the mean breakdown electrical characteristics. The metal can was removed from the header to expose the semiconductor chip and the transistors were mounted on a vero-board block to facilitate testing while situated on the microscope platform. It was found that the long pillars carrying the base and emitter connections made accurate focusing of the microscope objective difficult with some devices.

The emissive properties of the transistor surface were examined by raising the device temperature by means of an external heat source. A scan of the entire surface was made, readings being taken at 10 μm. intervals. This investigation was carried out at 80°C., the assumption being made that the ratio of results obtained for the different regions would be maintained over the entire temperature range. The thin layer of Silicon Oxide ensured a small difference over the entire surface. The results obtained in this test were used to modify the readings taken with the transistors operating in second breakdown.

The temperature distribution during breakdown was obtained by scanning the device surface to locate the centre of the hot spot and taking readings at 5 μm. intervals in four directions from this point. Typical results are shown in Fig. 5.10 where the temperature is shown as a normalised value, taking the reading obtained at the centre point as the reference level. It was found that all devices had a similar temperature distribution, the heated region being approximately symmetrical in all directions. At low power levels with the transistor operating with forward base-bias some asymmetry

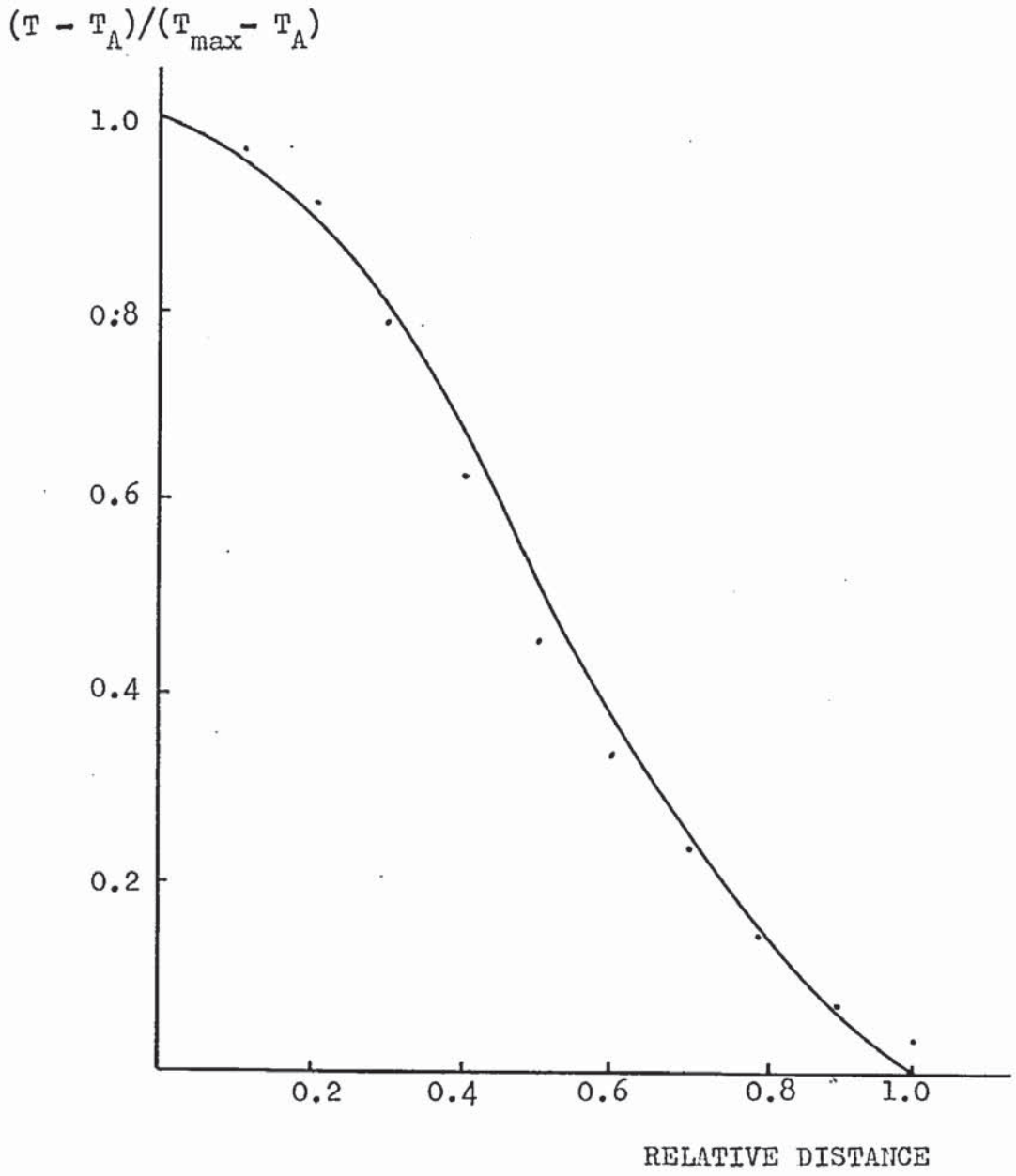

Fig. 5.10 Temperature Above Ambient in the Hot Spot. Curve derived from Equations 3.4.6 and 3.4.8 Points are experimental results (average of 4 transistors).

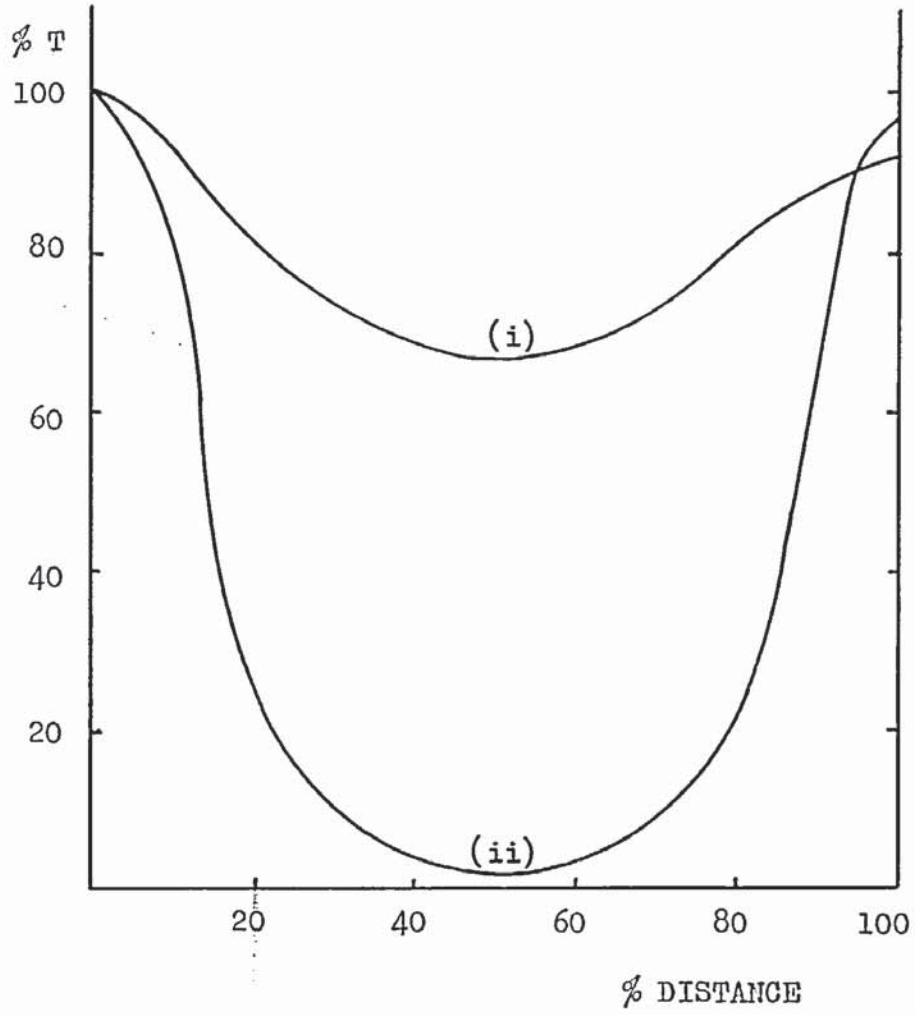

Fig. 5.10 (b) Distribution of Temperature with Two Hot Spots. (Forward base-bias)

(i) BFY 72, Hot Spots located at the extremities of one arm of the emitter. Plot taken over emitter metallisation. I_c = 600 mA., V_{CE} = 50V.

(ii) 2N 2218, Hot Spots located at the extremities of adjacent emitter segments. Plot taken over semiconductor regions. I_c = 200 mA. V_{CE} = 60 V. (Avalanche injection is high in this case)

Spot Separation : (i) 210 μm. (ii) 120 μm.

became evident. This is attributed to the rise in the bulk temperature of the chip with the larger pulse widths. With very long delay times the finite lateral dimensions of the chip become significant, particularly in the forward base bias mode.

Figure 5.10 (b) shows the temperature distribution for conditions producing two hot spots. The conditions for double breakdown site formation with the BFY 72 are restricted to high current levels, due to instability in the site location for high voltage - low current breakdown conditions. This instability was not as prevalent in the 2N2218 samples tested and may be characteristic of the paricular BFY 72 transistors used, since a limited supply was used for these tests.

The curves for the 2N2218 transistor follow the curve obtained with a single breakdown site near the breakdown centre. Deviation from the single curve at the edge of the hot spot is attributed to general device heating, due to the higher input power, and interaction of the two hot spots. The curve for the BFY 72 device differs greatly from the single hot spot curve. This is thought to be a result of the high mean power level required to form the double breakdown. The high thermal conductivity of the metal contact will tend to create an isothermal surface over the emitter. This effect was not significant at the low power levels used for the single site breakdown tests, the energy input and mean power levels being much lower. With the BFY 72 transistors the second breakdown site was obtained by establishing a single breakdown condition and reducing the pulse period until a second site formed. The closer thermal linking of the two sites with these transistors was probably significant in the formation of the second site.

Not all breakdown conditions produced symmetrical temperature distributions, such as those shown in Fig. 5.10 (b). The most stable twin breakdown conditions, however, were those in which the maximum temperatures differed by less than 30%. With sites having widely differing temperatures the position and existence of the second site (lowest temperature) was unstable.

5.5 Critical Current.

The minimum collector current at which second breakdown occurs with a given collector-emitter voltage, was obtained over the range of ambient temperature 333°K. to 77°K. The minimum current was determined by reducing the collector current pulse amplitude until breakdown no longer occurred in a 10 ms. time period. Several values were obtained using a 100 ms. time period, the resultant minimum collector current showed negligible difference from the values obtained with a 10 ms. period. The value of collector current obtained in this way was taken to be the critical breakdown current for the particular combination of transistor and supply voltage. Tests were performed with forward base terminal current and open base configurations.

Figures 5.11 and 5.12 show the results in graphical form, values plotted being the average of five randomly selected devices. The maximum deviation of any individual result from the mean was found to be less than $\pm$ 10%.

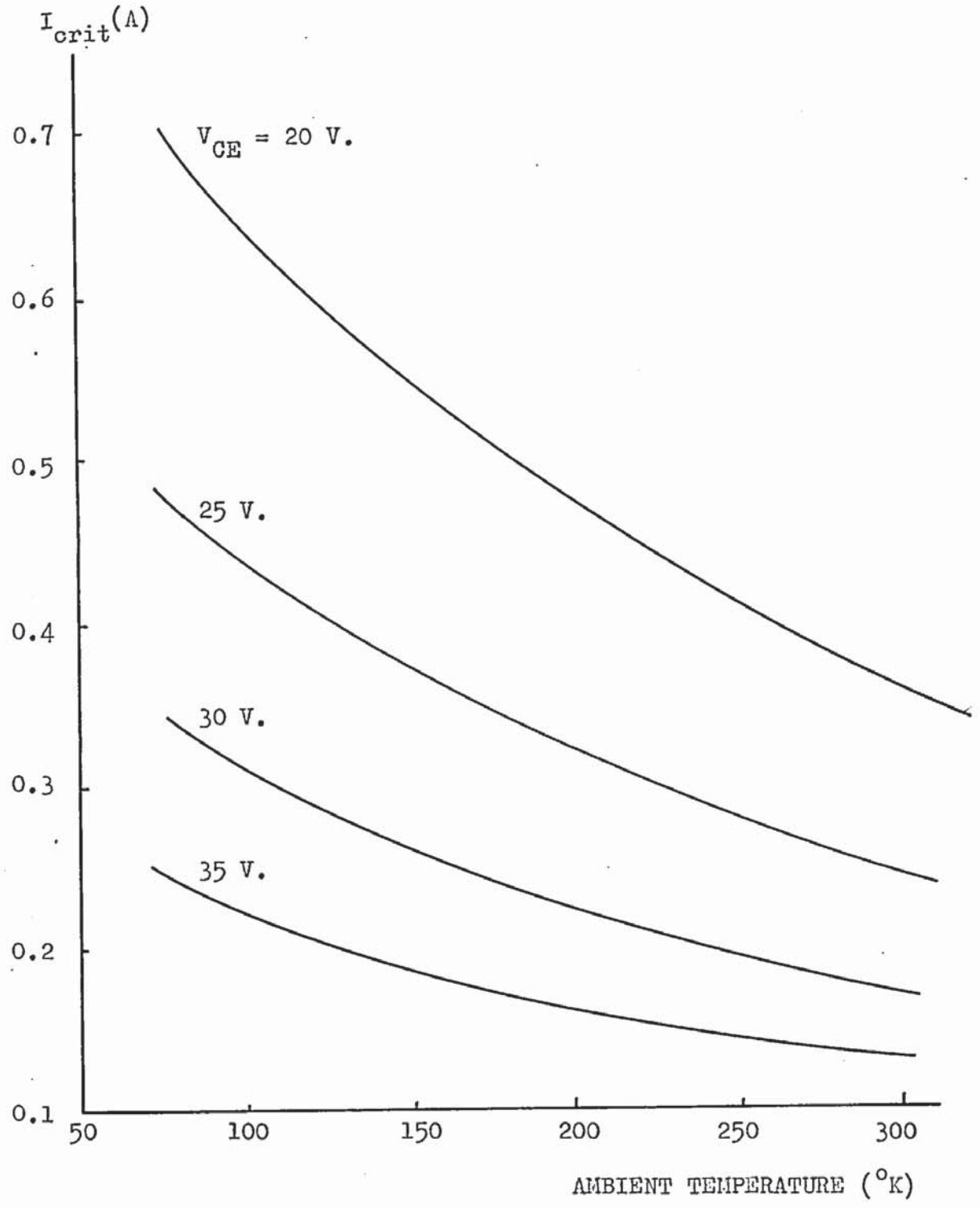

Fig. 5.11 (a) BFY 72 Critical Current as a Function of Ambient Temperature. (Forward base-bias) Experimental values averaged over 4 transistors.

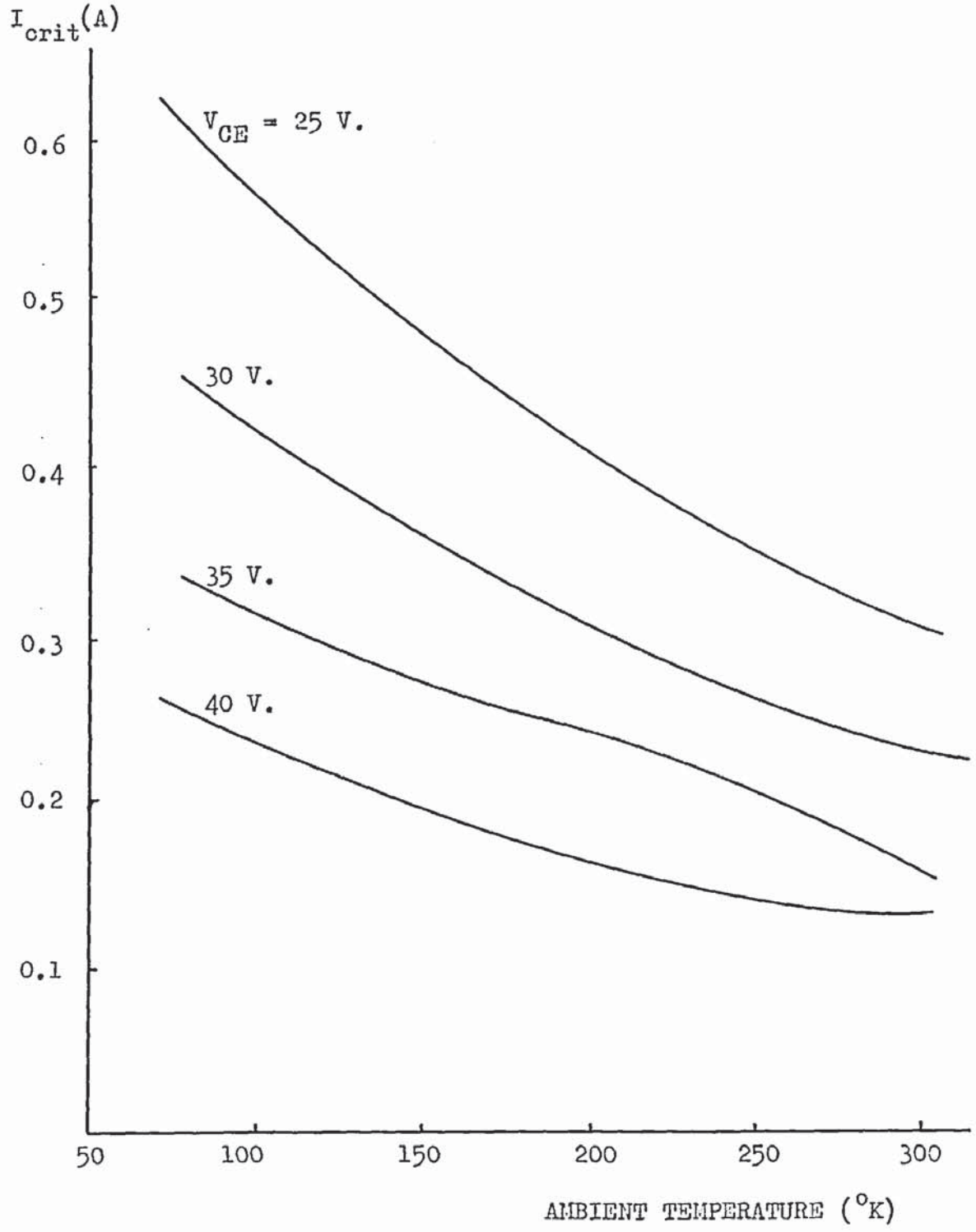

Fig. 5.11 (b) 2N 2218 Critical Collector Current Variation with Ambient Temperature. (Forward base-bias) Experimental results averaged from 4 transistors.

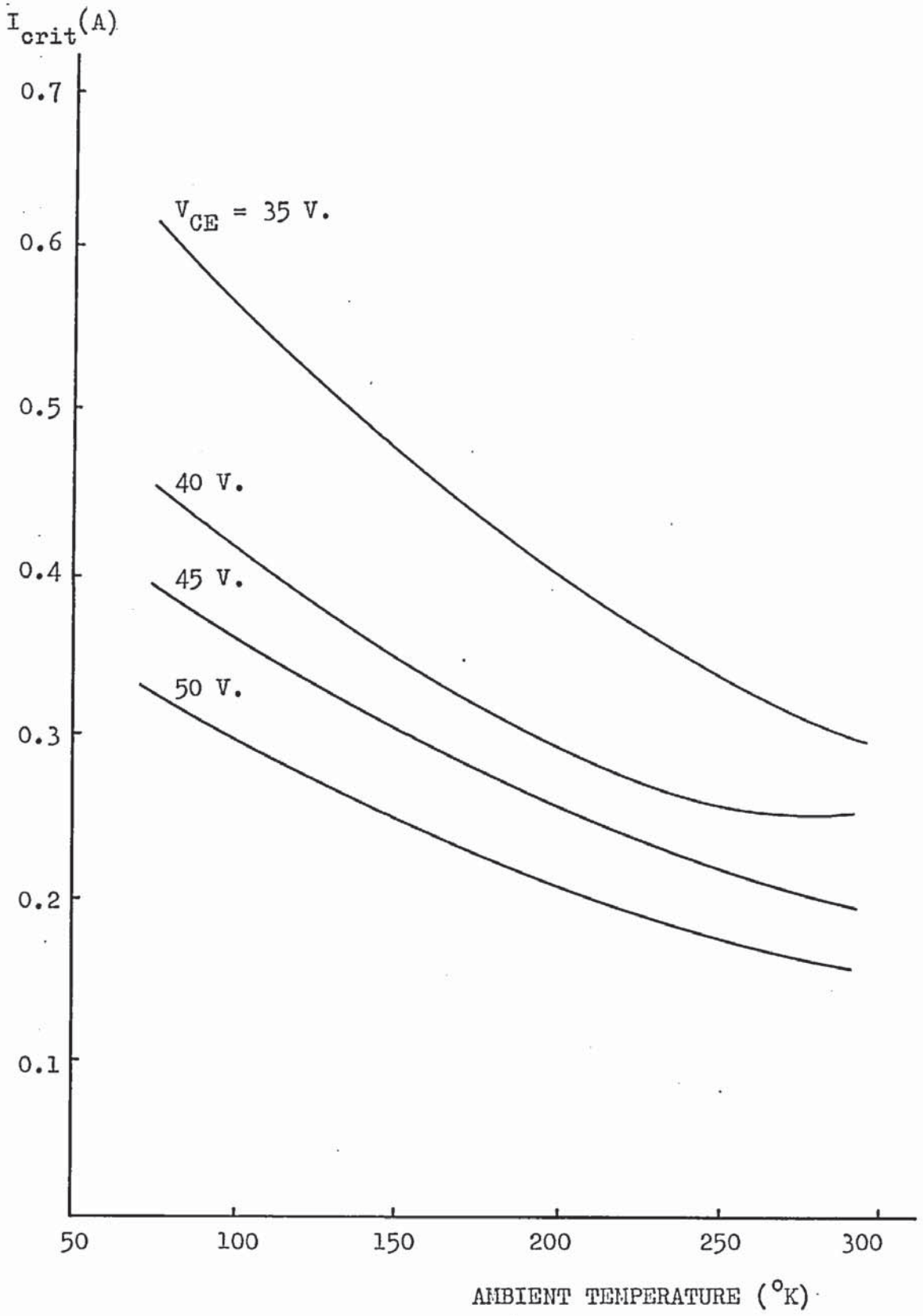

Fig. 5.11 (c) 2N 2195 Critical Collector Current as a Function of Ambient Temperature. (Forward base-bias). Experimental results averaged from 4 transistors.

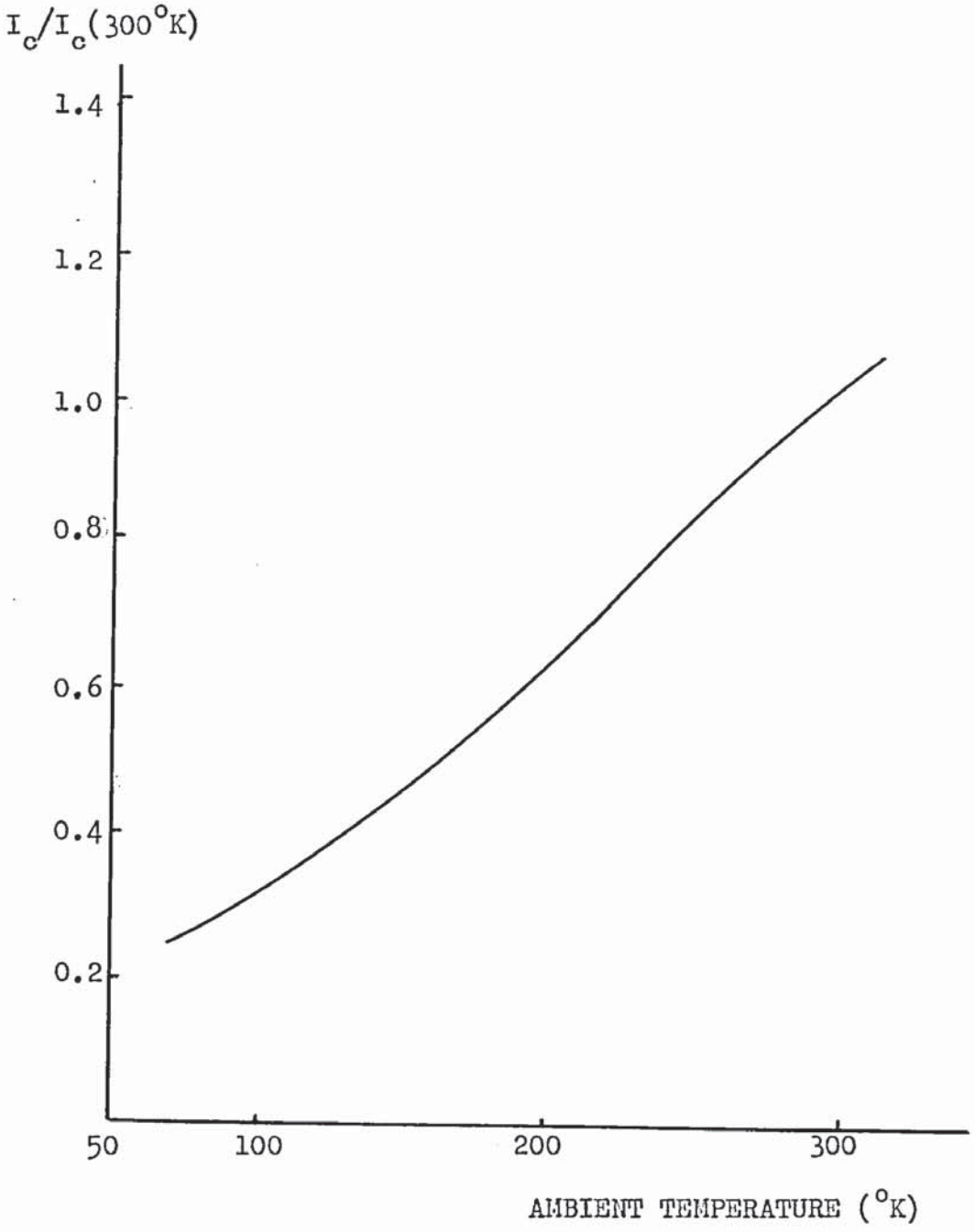

Fig. 5.12 Normalised Critical Collector Current as a Function of Ambient Temperature. Open base operation.

The normalised critical current values for all of the transistors tested lay close to this curve, irrespective of type.

6. DISCUSSION.

Direct verification of the theory of second breakdown requires detailed measurement of the transient charge-carrier distribution within the base and collector regions. Readily obtainable experimental results are confined to terminal relations and bulk, or mean, values. The theory has therefore been extended and tailored to produce expressions which relate to physically observable characteristics. Although not direct proof, the correspondence of experimental and theoretical characteristics covering a wide range can be taken as an indication of the validity of the premises upon which the theoretical expressions are based.

The complex structure of practical devices and the interdependence of the factors affecting charge-carrier transport and second breakdown result in a great number of approximations to make the expressions manageable. Great care must therefore be taken in the application of the equations describing detailed characteristics to other devices and to the devices considered under conditions differing from those specified. In particular the assumptions made about device geometry and recombination current flow in the base region can lead to significant errors if applied erroneously.

The proposal that second breakdown is dependent upon Energy Gap Modulation, Magnetic Constriction and Avalanche Multiplication is supported by several facts arising from the experimental results :

(i) The close fit between the theoretical and experimental values for critical collector current over the temperature range $77^{o}K.$ to $300^{o}K.$ Although the agreement is closer for the open-base condition

the basic temperature dependence is shown clearly for the forward bias mode of operation. The exact values obtained theoretically can be adjusted to give a better fit to the experimental results by modifying the approximate expressions for the current distribution. The agreement between these results indicates that, at low values of collector current, the thermal mechanism is dominant at room temperature and the magnetic mechanism becomes more significant as the ambient temperature falls (Fig. 4.2).

(ii) At low collector currents in the forward biased mode of operation the delay time is highly temperature dependent. As the collector current increases the temperature dependence is reduced, indicating the growing importance of a non-thermal breakdown mechanism. The correspondence between the theoretical and experimental delay time / Energy Characteristic supports the proposal that this mechanism is related to ionisation in the region of the collector-substrate junction. The wide spread in values obtained in the experiments prevents close comparison with calculated values, the nature of the characteristics preventing the use of mean values. It is clear from the graphs shown, however, that there is a good correspondence in the detailed form of the characteristic.

(iii) The agreement found between the calculated and measured temperature distribution in the hot spot supports the theory of Energy Gap Modulation as a principle cause of breakdown. These experiments were conducted at collector currents producing negligible ionisation at the collector-substrate junction. Some error is introduced through ignoring the surface layers above the hot spot, although normalisation of distance from the centre and temperature with respect to the maximum value minimises the discrepancy. The use of pulse widths very close to the delay time

and a large mark-space ratio reduces the influence of the emitter metallisation upon the formation of breakdown sites and the surface temperature distribution. With high input power the rapid time constant of the metal contacts, coupled with the power dissipation in the contact and metal-semiconductor junction, is expected to exert some influence over the location of the breakdown. The metal contact areas tend to produce a more uniform temperature distribution than is found in non-metallised regions. This is particularly noticeable at high power input and with multiple breakdown sites.

7. CONCLUSIONS.

The theoretical analysis of transistor operation in the region of second breakdown has resulted in equations demonstrating the effects upon second breakdown of

(i) Energy Gap temperature dependence

(ii) Avalanche multiplication

(iii) Magnetic constriction forces

(iv) Base width modulation

(v) Lateral injection

(vi) Ambient temperature

(vii) Device construction

(viii) Input power.

Although dealing specifically with triple-diffused epitaxial collector transistors, the principles and a large portion of the development, are applicable to most semiconductor junction devices subject to second breakdown.

Several points are demonstrated by the theoretical and experimental results :

(i) Reducing the ambient temperature reduces the critical collector current for open-base operation but, increases the critical current for forward base-terminal-current operation.

(ii) Circular single emitter transistors have a higher resistance to second breakdown than multi-emitter devices and those with a high horizontal aspect ratio.

(iii) In epitaxial collector transistors the transition to space-charge-limited current flow increases the energy required to initiate second breakdown for forward base bias operation.

(iv) Multiple breakdown collector voltage steps can be caused

by avalanche breakdown of the collector-substrate junction followed by true second breakdown. Further voltage reductions can be attributed to the formation of multiple hot spots and the penetration of the constricted column to the substrate layer, thus reducing the resistive potential difference across the device.

The theoretical analysis shows that even a perfect transistor will exhibit current constriction and second breakdown at some calculable collector current which is dependent upon the base bias and supply voltage. Defects in the base and collector regions can lead to second breakdown at much lower values of input power. These devices usually exhibit wide variations in other characteristics such as current gain, collector-base breakdown voltage and reverse base-emitter breakdown voltage.

8. SUGGESTIONS FOR FURTHER INVESTIGATION.

(a) Experimental.

The effect of ambient temperature upon the second breakdown characteristics requires a more detailed examination. The temperature distribution at low temperatures could be used to establish the significance of magnetic constriction of current in practical devices.

Transient temperature measurements would lead to a closer analysis of thermally controlled breakdown. This type of investigation would require specially constructed transistors which would provide a detectable surface temperature change having a very short delay time on the power pulse.

A detailed investigation of defects and composition of transistors and their relevance to the present theory is required. No attempt was made to establish the presence, or nature, of defects in this investigation. (The only precaution taken was to discard transistors exhibiting terminal characteristics which differed widely from the norm.)

Although moving breakdown sites have been mentioned briefly here, there are other effects associated with non-uniform transistor structure which have not been considered.

(b) Theoretical.

Theoretical analysis of second breakdown will be greatly improved by the development of a programme for the general equations derived here. This will provide an analysis of the transient behaviour during second breakdown and provide accurate current and

voltage time dependent profiles related to the properties of the semiconductor and to the structure.

The theoretical analysis requires extension to include the detailed effects of base terminal current and transistor geometry. An accurate analysis of second breakdown characteristics may then be possible for practical transistors under all operating conditions. The extension of the theory is needed to include transistors not having the epitaxial-collector structure and other semiconductor junction devices.

APPENDIX 1.

Examination of Space Charge Neutrality and Ambipolar Continuity Equations.

The derivation of the ambipolar continuity equations was based upon the assumption of space charge neutrality. This has been shown to be a good approximation for the low injection levels or heavily extrinsic semiconductors. Space charge neutrality is violated under conditions approaching the intrinsic state. The distribution of charge carrier is defined by ambipolar diffusion processes. (Refs.1,2).

Local electrical neutrality can be achieved by assuming either zero dielectric relaxation time or infinite coulomb forces. The presence of a space charge will, therefore, be more important in materials with a high resistivity and large relaxation times. An estimation of the tolerance of the space charge neutrality can be obtained by considering the general processes involved in the decay of an excess of charge carriers.

Consider an increase of space charge concentration in the x-direction. The continuity equation will be

$$\frac{\partial J}{\partial x} + \frac{\partial \rho}{\partial t} = 0$$

Poisson's equation becomes

$$\nabla^2 \phi = -\nabla.\bar{E} = -\frac{\rho}{\varepsilon}$$

$$= -\frac{dE}{dx}$$

Ohms Law states that $\bar{J} = \sigma \bar{E}$

Therefore combining the above gives

$$\frac{dJ}{dx} = \frac{\sigma}{\varepsilon}\rho = \frac{\partial \rho}{\partial t}$$

This leads to the time dependent relationship for charge density

$$\rho = \rho_0 \exp(-\sigma t/\varepsilon)$$

The time constant for a positive space charge concentration change in intrinsic silicon is approximately 0.2 μs. and for intrinsic germanium is 70 ps.

The preservation of space charge neutrality depends upon the impurity charge being compensated by the mobile charge (Ref.3). The charge carriers available for pinching processes are therefore obtained from two sources :

(a) An equal number of electrons and holes limited to the minority carrier concentration.

(b) Charge carriers injected by the emitter or by avalanche processes.

In heavily extrinsic semiconductors it is only the small number of charge carriers (a) that can be involved in a current constriction.

The assumption of space charge neutrality is not essential. The added complexity of the methods discussed in (Refs.4,5) are seldom justified in the light of other assumptions generally made.

APPENDIX 2.

Electron-Hole Pressure.

The velocity vector of charge carriers in a semiconductor can be separated into a drift component, $\bar{v}_d$, and a random velocity component, $\bar{v}_l$, (Ref.1). The charge carrier velocity is

$$\bar{v} = \bar{v}_d + \bar{v}_l$$

$$\langle v \rangle = v_d$$

$$\langle v_l \rangle = 0$$

Consider the Boltzman Transport Equation in the form

$$\frac{\partial f}{\partial t} + \bar{v} \nabla_r f + u \nabla_u f = \frac{\partial f}{\partial t}_{coll.}$$

where $$\nabla_r = \left(\frac{\partial}{\partial x} , \frac{\partial}{\partial y} , \frac{\partial}{\partial z} , \right)$$

and $$\nabla_u = \left(\frac{\partial}{\partial u_x} , \frac{\partial}{\partial u_y} , \frac{\partial}{\partial u_z} \right)$$

Continuity equations can be obtained by substituting appropriate expressions $\phi(r,u,t)$ for f and integrating over velocity space. To obtain momentum continuity $\phi = m^* v$ where m^* is the effective mass. Separating v into its component parts and assuming m^* and v are independent of t and r yields (Ref.1)

$$\frac{\partial n\bar{v}_d}{\partial t} + \frac{1}{m^*} \nabla_r.(m^* \langle n\bar{v}_l.\bar{v}_l \rangle) + \nabla_r.(\langle n\bar{v}_d.\bar{v}_d \rangle) - n\dot{u} = \nabla n \langle \phi \rangle$$

the term $m^* \langle n\bar{v}_l.\bar{v}_l \rangle$ is a pressure tensor (Ref.2).

The presence of a magnetic field does not affect the equilibrium condition of the charge carriers, so that a Maxwellian distribution can be maintained in spite of the curvature of their paths (Refs.3,4). Equipartition of energy applied to a Maxwellian velocity distribution yields

$$\frac{1}{2} m \langle v^2 \rangle = \frac{3}{2} kT$$

The pressure of a plasma having a carrier density n is

$$P = \frac{1}{3} m n \langle v^2 \rangle$$

This leads to the relationship

$$P = nkT$$

APPENDIX 3.

Fields Associated with Charged Particle Motion.

Consider a system in which charge carriers can be represented by point charges having a uniform velocity. The magnetic field, $\bar{B}$, is related to the electric field, $\bar{E}$, by an expression derived from Relativity Theory,

$$\bar{B} = \frac{1}{c^2} (\bar{u} \times \bar{E})$$

where c is the speed of light and $\bar{u}$ is the charge-carrier velocity. The force exerted on a hole having velocity, $\bar{v}$, by an electron having a velocity, $\bar{u}$, in direct opposition to $\bar{v}$ is (See Fig. A3)

$$\bar{F} = q (\bar{v} \times \bar{B})$$

$$= q (\bar{v} \times \frac{1}{c^2} (\bar{u} \times \bar{E}))$$

If the velocity, $\bar{u}$, makes an angle, θ , with the electric field then

$$\bar{u} \times \bar{E} = u E \sin\theta$$

and

$$\bar{v} \times (\bar{u} \times \bar{E}) = v u E \sin\theta$$

The magnitude of the term, $\bar{v} \times (\bar{u} \times \bar{E})$, in the direction of the electric field is therefore $v u E$. In an infinite system all forces of the $\cos\theta$ form sum to zero so that the force $\bar{F}$ can be written as

$$F = u v \bar{E} q / c^2$$

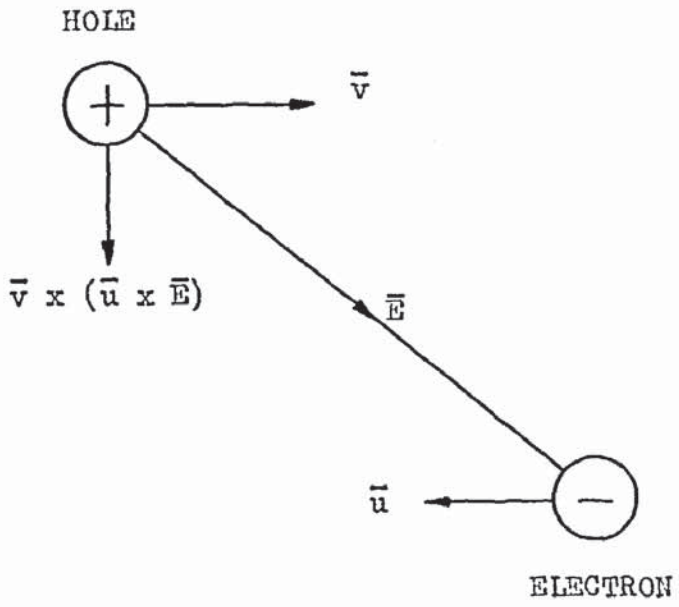

Fig. A.3 Forces on Charge Carriers.

The Lorentz equation gives the force exerted by an electron on a hole as

$$\bar{F}_{np} = q \left(\bar{E}_{np} + \bar{v} \times \bar{B} \right)$$

$$= q \bar{E}_{np} \left(1 + u v / c^2 \right)$$

Similarly

Force between two electrons

$$\bar{F}_{nn} = q \bar{E}_{nn} \left(1 - u^2 / c^2 \right)$$

Force between two holes

$$\bar{F}_{pp} = q \bar{E}_{pp} \left(1 - v^2 / c^2 \right)$$

In general, u,v are small compared with c , so that the magnetic effects are of minor importance. Under conditions of space-charge neutrality, however, the electric field forces sum to zero and the magnetic forces are then of significance.

Assuming electrons and holes to be moving in opposite directions, the magnetic forces are attractive in all cases. The injection of charge carriers into a space-charge neutral system (under conditions of high injection, holes and electrons are injected) results in a constricting force on the charge carrier flow.

APPENDIX 4.

Temperature Dependence of Mobility and Thermal Conductivity.

(a) Mobility.

Charge-carrier mobility is dependent upon scattering processes of two kinds ; thermal, or lattice, scattering giving μ_T , and ionisation impurity scattering giving μ_I . The total mobility can be approximated by (Ref.1)

$$\frac{1}{\mu} = \frac{1}{\mu_T} + \frac{1}{\mu_I}$$

Over a limited range of temperature the thermal mobility is the dominant term. Conwell (Ref.3) derived an empirical form for the temperature dependence

$$\mu = A_T T^{-a_T}$$

Values of constants, A_T and a_T, have been variously reported as

Reference	n		p	
	A_T	a_T	A_T	a_T
1	15.10^5	1.5	5.10^5	1.5
3	$2.1.10^9$	2.5	$2.3.10^9$	2.7
4	$5.5.10^6$	1.5	$2.4.10^8$	2.3
2		2.6		2.3

(b) Thermal Conductivity.

Two mechanisms play a major role in determining the thermal conductivity. These are associated with the electrons involved in

the electrical conduction and lattice scattering.

The term associated with the electrons can be expressed as (Ref.5)

$$K_e = \frac{8\, n\, k^2\, T\, L}{3(2\pi m^* kT)^{\frac{1}{2}}}$$

The lattice conductivity, K_l, due to phonon scattering processes has been shown to be almost inversely proportional to temperature. An approximate expression is given as

$$K_l = \frac{1}{3} C_v\, u\, L$$

where C_v is the specific heat

u is the velocity of sound

L is the mean free path of the phonons involved in the scattering.

Both K_e and K_l obey the Lorentz relation

$$K = TL_r\sigma$$

where σ = electrical conductivity

L_r = Lorentz Number

Glassbrenner and Slack (Ref.6) expressed the total conductivity in terms of temperature as

$$K^{-1} = \alpha T^2 + \beta T + \theta$$

where α, β and θ are constants.

In semiconductors the major contribution is given by the scattering term. The reduction of thermal conductivity with increasing impurity concentration indicates that the increase in

scattering due to the impurity is of greater importance than the availability of extra electrons.

The thermal conductivity over a wide range of temperatures of general interest can be approximated by (Ref.6)

$$K = B_T T^{-b_T}$$

where $B_T = 3.10^5$

$b_T = 1.33.$

APPENDIX 5.

Current Amplification Factor as a Function of Temperature.

The current gain of diffused epitaxial-collector transistors is generally found to be very temperature sensitive. Investigations by Buhannan (Ref.1) have shown that the current gain temperature coefficient is of an extremely complex nature and is linked to the impurity concentrations in the emitter and base regions.

The current amplification factor can be expressed as a function of emitter injection efficiency γ_e , base transport factor, β , and collector multiplication factor, M .

$$\alpha = \gamma_e \beta M$$

Expressing these in terms of device dimensions, material properties and supply voltage leads to an expression of the form (Refs.1,2)

$$\alpha = \frac{\operatorname{sech}(w/L_{nb})}{1 + (D_{pe}/D_{nb})(p_{ne}/n_{pb})(w/L_{pe})} \cdot \frac{1}{1 - f(V/V_B)^n}$$

where w = base width

L_{nb} = electron diffusion length in the base

L_{pe} = hole diffusion length in the emitter

D_{pe} = hole Diffusion Coefficient in the emitter

D_{nb} = electron Diffusion Coefficient in the base

p_{nb} = minority carrier concentration in the base

p_{ne} = minority carrier concentration in the emitter

V_B = Avalanche breakdown voltage

V = supply voltage

f and n are constants, dependent upon the type of material and charge carrier. (For Silicon $n \simeq 4$, $0.5 < f_n < 0.8$, $1.0 < f_p < 1.02$, (Ref.2))

The temperature dependence of the current amplification factor can be obtained by a detailed consideration of the above equation.

Diffusion Coefficient.

In most diffused transistor structures, the emitter has a high impurity concentration (greater than 10^{19} atoms/cm^3). This reduces the temperature dependence of the mobility in this region, owing to the predominance of scattering by impurity centres (Refs.1,3). The diffusion coefficient in the emitter, D_{pe}, is therefore directly proportional to temperature, through the Einstein Equation

$$D = \frac{\mu k T}{q}$$

The lower impurity concentration in the base region reduces the importance of impurity scattering and increases the dependence of mobility upon lattice scattering. This gives the temperature dependent mobility discussed in Appendix 4, which approaches

$$\mu = A_T T^{-a_T}$$

more nearly as the impurity concentration is reduced.

The temperature dependence of the base diffusion coefficient is therefore given by

$$D_{nb} = \frac{A_T k T^{(1 - a_T)}}{q}$$

which leads to the ratio

$$D_{pe} / D_{nb} = CT^{a_T}$$

Minority Carrier Path Length.

The minority carrier diffusion path length is dependent upon the carrier lifetime, and the diffusion coefficient

$$L = (D \tau)^{\frac{1}{2}}$$

The lifetime is a complex term which is dependent upon impurity concentration and recombination centre concentration (Ref.4). Terms involving the concentration of trapping and recombination centres are relatively insensitive to temperature changes. The temperature dependence of minority carrier lifetime is substantially that of n_i^2 (Ref.2)

$$\tau \propto n_i^2/qN_D$$

$$\propto T^3 \exp(-(\mathcal{E}_g - \Delta\mathcal{E})/kT)$$

The path length will therefore be temperature dependent in the following manner

$$L_{nb} \propto T^{(2 - \frac{1}{2}a_T)} \exp(-\mathcal{E}_g/2kT)$$

$$L_{pe} \propto T^2 \exp(-\mathcal{E}_g/2kT)$$

The base width is considered to be independent of temperature for all practical conditions. The change in base transport factor involving L_{nb} is compensated by the change in emitter efficiency

involving L_{pe}.

Minority Carrier Concentration.

Dislocation and deformations in the lattice structure of the emitter region, arising from the high impurity concentration are associated with a lowering of the energy band-gap (Ref.1). This results in a change in the temperature dependence of the charge-carrier concentration. The intrinsic charge-carrier concentration expression relating to the emitter region will differ from that relating to the base region according to

Emitter $$p_{ne} = n_{ie}^2/N_D = \frac{A\,T^3}{N_D} \exp(-(\mathcal{E}_g - \Delta\mathcal{E})/kT)$$

Base $$n_{pb} = n_{ib}^2/N_A = \frac{B\,T^3}{N_A} \exp(-\mathcal{E}_g/kT)$$

The ratio of the concentrations in the two regions will therefore be dependent upon temperature to an extent determined by this energy-gap change

$$p_{ne}/n_{pb} = K \exp(\Delta\mathcal{E}/kT)$$

where K is a constant for all but low temperatures at which all of the impurities cannot be considered to be ionised.

Collector Multiplication Factor.

Avalanche breakdown voltage has a temperature dependence which has been expressed as (Ref.5)

$$\frac{1}{V_b}\frac{dV_b}{dT} = \frac{h}{(p + 1/m + b/E_m)} \left\{ (p + b/E_m)\theta - \phi \right\}$$

where θ = $8.3.10^{-4}$ /°K.

ϕ = $12.1.10^{-4}$ /°K.

$b = {}_i/qL_r$

($\mathcal{E}_i$ = energy at threshold of ionisation

L_r = mean free path for optical phonon scattering.)

m and p are constants depending upon the nature of the junction.

	abrupt	linear
m	1	2
p	0.63	0.35

E_m = maximum electric field strength.

In general this temperature dependence will cause a variation in current amplification factor which is much smaller than the changes due to the other factors.

The temperature dependence of the current amplification obtained by combining the effects of the above considerations, neglecting the effect of breakdown voltage change, can be written as

$$\alpha = \frac{\operatorname{sech}(w/FT^{(2 - \frac{1}{2}a_T)}) \exp(-\mathcal{E}_g/2kT))}{1 + BwT^{(a_T - 2)} \exp((\mathcal{E}_g + 2\Delta\mathcal{E})/2kT)} \cdot \frac{1}{1 - f(V/V_b)^n}$$

where B and F are constants.

Under normal operating conditions, the controlling temperature dependent term will be the exponential function in the denominator.

APPENDIX 6.

Time Dependent Thermal Dissipation for a Circular Structure.

Analysis of a circular emitter structure can be simplified by assuming angular symmetry. Equation 3.6.1 can therefore be written as

$$\frac{1}{r}\frac{\partial}{\partial r}\left(r\frac{\partial T}{\partial r}\right) + \frac{\partial T}{\partial z^2} = \frac{1}{k_T}\frac{\partial T}{\partial t}$$

The temperature due to a point source can be expressed as

$$T = \frac{Q}{\rho C(\sqrt{\pi}\delta)^3}\exp(-m^2/\delta^2)$$

where the quantity of heat produced is $Q\rho C$.

$$\delta^2 = 4k_T(t - t_o)$$

$$m^2 = (r - r_o)^2 + (z - z_o)^2$$

Consider an elemental volume, $V = 2\pi r\, dr\, dz$, in which the power dissipation per unit volume can be expressed as $P(t)/V$. The temperature distribution for a cylindrical power source can be written as

$$T(r,z,t) =$$

$$\int_r \int_z \int_t \frac{P(t)}{\rho CV(\sqrt{\pi}\delta)^3}\exp(-m^2/\delta^2) \cdot 2\pi r\, dr.dz.dt$$

A step input of power produces the temperature distribution

$$T(r,z,t) = \frac{P}{4\rho CV\sqrt{\pi}} \int_{t_o}^{t} 1/\delta^3 \, dt. \int_0^r r \exp(-r^2/\delta^2) \, dr.$$

$$\left(\int_{H-w_b}^{-w_b} \exp\left(\frac{-(z - z_o)^2}{\delta^2} \right) dz + \int_{w_b}^{H+w_b} \exp\left(\frac{-(z - z_o)^2}{\delta^2} \right) dz \right)$$

which leads to

$$T(r,z,t) = \frac{P}{2\rho CV} \int_{t_o}^{t} \frac{1}{\delta^3} \left(2r \, \mathrm{erf}\left(\frac{r}{\delta}\right) + \frac{1}{\sqrt{\pi}} \left(\exp\left(\frac{-r^2}{\delta^2}\right) - 1 \right) \right)$$

$$\left(\mathrm{erf}\left(\frac{H + w_b + z}{\delta} \right) + \mathrm{erf}\left(\frac{- w_b - z}{\delta} \right) \right.$$

$$\left. + \mathrm{erf}\left(\frac{z - w_b}{\delta} \right) + \mathrm{erf}\left(\frac{w_b + H - z}{\delta} \right) \right) dt.$$

The natural time constant for the radial transient temperature change is $r_m^2/4k_T$, where r_m is the maximum radius considered. An input pulse duration which is short, compared with this time constant, leads to an approximate temperature distribution of the form (Ref.1)

$$T = 2 \left(\frac{k_T \, t}{\sqrt{\pi} K} \right)^{\frac{1}{2}} \cdot p_o$$

where p_o is the power density distribution at time $t = 0$.

APPENDIX 7.

Multiplication Factor at the Second Breakdown Threshold.

The following assumptions are made for the collector space-charge region : -

1. Recombination is negligibly small.
2. Thermal generation is negligibly small.
3. Electron and hole ionisation coefficients are equal.
4. Electron and hole drift velocities are equal to the saturation drift velocity.
5. The system can be represented by a one-dimensional approximation.

The electric field distribution on a cross-section of the transistor is shown in Fig. A.7 for high collector current density. The electric field strength is current dependent

$$E(z) = E(w_{cib}) + \frac{qz}{K_p \varepsilon_o} \left(\frac{J}{qv_1} - N_{DC} \right) \qquad (1)$$

In the region $z < z_1$ there is negligible ionisation and

$= 0$.

In the region $z_1 < z < w_{epi}$ the electric field is greater than the ionisation threshold value E_c and $\alpha > 0$

At $z = w_{cib}$ $J_n = J_p$

and $$J = J_n + J_p = qv_a (n + p) \qquad (2)$$

where v_a is the ambipolar saturated drift velocity.

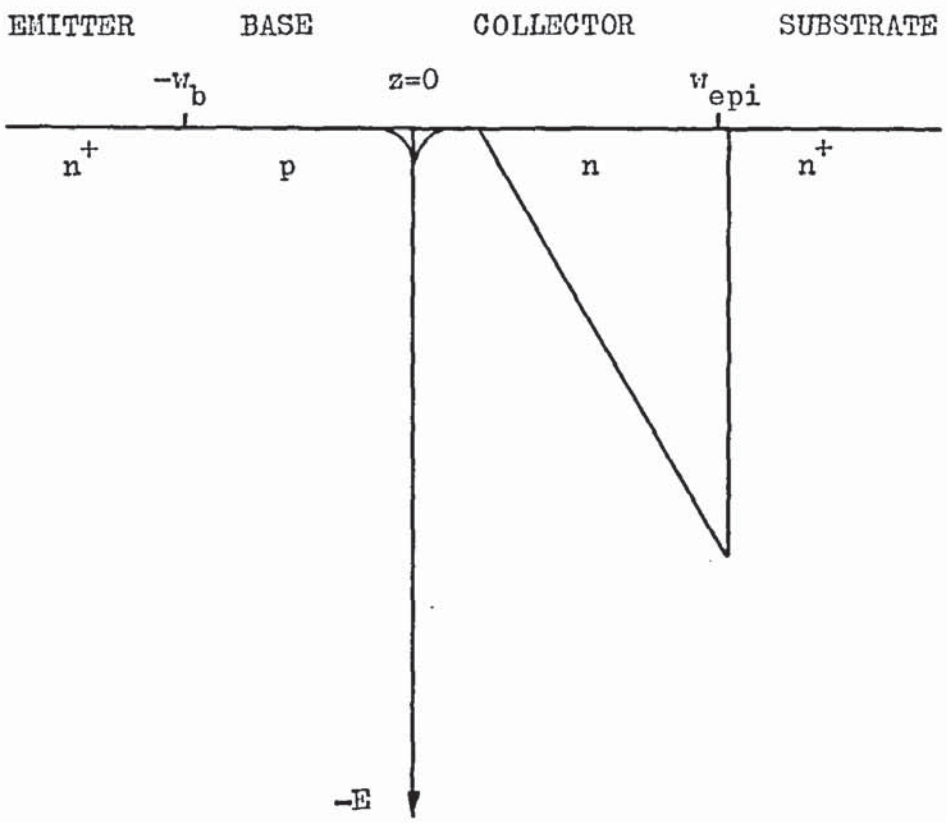

Fig. A.7 Eletric Field Distribution.

The charge continuity equations take the simplified form

$$\frac{dJ_n}{dz} = -\alpha J \tag{3}$$

$$\frac{dJ_p}{dz} = \alpha J \tag{4}$$

The multiplication factor, M, is the ratio of current leaving the region to current entering the region

$$M = \frac{J_n(W_{epi})}{J_n(z_1)} = \frac{J}{J_n(z_1)} \tag{5}$$

As a function of the electric field strength multiplication is given by

$$M = 1 / \left(1 - \int_{z_1}^{W_{epi}} \alpha\,(E)\, dz\right) \tag{6}$$

Combining Equations 2, 5 and 6 leads to

$$1 - \frac{J_n(z_1)}{J} = \int_{z_1}^{W_{epi}} \alpha\,(E)\, dz = \frac{J_p(z_1)}{J} \tag{7}$$

As the current density increases, z_1 approaches W_{epi}. In the limiting condition as n, p and J approach infinity, the difference p - n must remain finite and the condition

$$\frac{J_n(z_1)}{J} = \frac{J_p(z_1)}{J} = \frac{1}{2} \tag{8}$$

is approached.

Substitution of this condition into Equation 7 yields a limiting value of ionisation coefficient integral

$$\lim_{z_1 \to W_{epi}} \int_{z_1}^{W_{epi}} \alpha (E)\, dz = \frac{1}{2}$$

This gives a limiting value of multiplication factor,

$$M = 2.$$

1. References for Section 1.

1. C.G.Thornton and C.D.Simmons, "A New High Current Mode of Transistor Operation," IRE Trans. Electron Devices, vol. ED-15, p. 6-10, 1958.
2. Greenburg, "Extending Safe Areas for Fast Switching Pulses," Motorola Engineering Report No. 87.
3. Z.F.Chang and C.R.Turner, "Characterisation of Second Breakdown in Silicon Power Transistors," RCA Application Note SMA 21.
4. D.Stolnitz, "Experimental Demonstration and Theory of a Corrective To Second Breakdown in Si Power Transistors," IEEE Trans. Electron Devices, vol. ED-13, p. 643, 1966.
5. B.Reich, "New Aspects of Second Breakdown in Transistors," Solid State Design, p. 23, April 1964 and p. 24, May 1964.
6. H.A.Schafft and J.C.French, "Second Breakdown in Transistors," IRE Trans. Electron Devices, vol. ED-9, p. 129-136, 1962.
7. H.A.Schafft and J.C.French, "Second Breakdown ; Effects of Base Drive and Structural Defects," IEEE Electron Devices Meeting, Washington D.C., October 1963.
8. R.Morrisson and R.Billette, "Common Emitter Breakdown," IEEE Trans. Electron Devices, vol. ED-10, p. 351-356, 1963.
9. H.A.Schafft and J.C.French, "Second Breakdown and Current Distribution in Transistors," Solid State Electronics, vol. 9, p. 681-688, July 1966.
10. W.M.Portnoy and F.R.Gamble, "Fine Structure and Electromagnetic Radiation in Second Breakdown," IEEE Trans. Electron Devices, vol. ED-11, p. 470-478, 1964.

11. K.Takagi and K.Mano, "Transient Junction Temperature Rise and Second Breakdown in Transistors," IEEE Trans. Electron Devices, vol. ED-13, p. 759-763, 1966.

12. B.Reich and E.B.Hakim, "An Explanation of the Energy Dependence of Secondary Breakdown in Transistors," Proc. IEEE, vol. 53, p. 624-625, 1965.

13. J.Miller, "Sweep Test Picks Best Transistors to Bar Inductive Load Damage," Electronic Design, vol. 12, p. 44, October 24th 1964.

14. P.B.Balthasar, "Selecting Switching Circuit Transistors," Electrical Design News, vol. 10, p. 72, November 1965.

2. References for Section 2.

1. C.G.Thornton and C.D.Simmons, "A New High Current Mode of Transistor Operation," IRE Trans. Electron Devices, vol. ED-5, p. 6-10, January 1958.

2. H.A.Schafft and J.C.French, "Second Breakdown in Transistors," IRE Trans. vol. ED-9, p. 129-136, March 1962.

3. A.C.English and H.H.Power, "Mesoplasma Breakdown in Silicon Junctions," Proc. IEEE vol. 51, p. 500, March 1963.

4. A.C.English, "Mesoplasma and Second Breakdown in Silicon Junctions," Solid State Electronics, vol. 6, p. 511, September-October 1963.

5. T.Agatsuma, T.Kohisa and A.Sugyama, "Turnover Phenomena of $n^+ - n - n^+$ Plate Contact Silicon Devices and Second Breakdown in Transistors," Proc. IEEE vol. 53, p. 1372, December 1965.

6. H.A.Schafft and J.C.French, "Second Breakdown ; Effects of Base Drive and Structural Defects," IEEE Electron Devices Meeting, Washington D.C., October 1963.

7. A.C.English, "Physical Investigation of the Mesoplasma in Silicon," IEEE Trans. Electron Devices, vol. ED-13, p. 662-667, 1966.

8. F.Weitzsch, "A Discussion of Some Known Physical Models for Second Breakdown," IEEE Trans. Electron Devices, vol. ED-13, p. 731-734, November 1966.

9. R.Scarlett, W.Shockley and R.H.Haitz, "Thermal Instability and Hot-Spots in Junction Transistors," Physics of Failure in Electronics, Spartan Books, 1963.

10. F.Bergman and D.Gerstner, "Thermisch Bedingte Stromeinschnuring bei Hochfrequenz-Leistungstransistoren," Arch Elekt. Ubertragung, vol. 17, p. 467-475, October 1963.

11. G.H.Ford, "Collector to Emitter Breakdown Related to Thermal Runaway in Homogeneous Base Germanium Power Transistors," Solid State Design, vol. 4, p. 29-36, June 1963.

12. H.Melchior and H.J.O.Strutt, "Secondary Breakdown in Transistors," Proc. IEEE vol. 52, p. 439, April 1964.

13. D.K.Ferry and A.A.Dougal, "Input Power Induced Thermal Effects Related To Transition Times Between Avalanche and Second Breakdown in p - n Silicon Junctions," IEEE Trans. Electron Devices, vol. ED-13, p. 627, 1966.

14. B.Reich and E.B.Hakim, "An Explanation of the Energy Dependence of Secondary Breakdown in Transistors," Proc. IEEE vol. 53, p. 624, June 1965.

15. B.Reich and E.B.Hakim, "Secondary Breakdown Thermal Characterisation and Improvement of Semiconductor Devices," IEEE Trans. Electron Devices, vol. ED-13, p.734-737, November 1966.

16. B.Reich and E.B.Hakim, "Relations Between Hot Spot Formation and Second Breakdown in Transistors," Report ECOM 2944 (AD668902), February 1968.

17. H.C.Lin, A.R.Hlavacek and B.H.White, "Transient Operation of Transistors with Inductive Loads," IRE Trans. Electron Devices, vol. ED-7, p. 174-178, July 1960.

18. H.Egawa, "Avalanche Characteristics and Failure Mechanisms of High Voltage Diodes," IEEE Trans. Electron Devices, vol. ED-13, p. 662-667, 1966.

19. H.C.Josephs, "Analysis of Second Breakdown in Transistors Using a Simple Model," IEEE Trans. Electron Devices, vol. ED-13, p. 778-787, November 1966.

20. M.Kikuchi and K.Tachikawa, "Visible Light Emission and Microplasma Phenomena in Silicon p - n Junctions, I and II," Journal Phys. Soc. Japan, vol. 15, p. 835-848 and p. 1822-1831, 1960.

21. A.Goetzberger, B.McDonald, R.Haitz and R.M.Scarlett, "Avalanche Effects in Silicon p - n Junction ; II, Structurally Perfect Junctions," Journal Appl. Phys. vol. 34, p. 1591-1600, June 1963.

22. C.T.Kirk, IRE Trans. Electron Devices, vol. ED-9, p. 164, 1963.

23. H.B.Grutchfield and T.J.Moutoux, "Current Mode Second Breakdown in Epitaxial Planar Transistors," IEEE Trans. Electron Devices, vol. ED-13, p. 743, 1966.

24. G.Roman, "A Model for Computation of Second Breakdown in Transistors," Solid State Electronics, vol. 13, p. 961, 1970.

25. P.L.Hower and V.G.K.Reddi, "Avalanche Injection and Second Breakdown in Transistors," IEEE Trans. Electron Devices, vol. ED-17, n.4, p. 320, 1970.

26. S.M.Sze and G.Gibbons, "Effect of Junction Curvature on Breakdown Voltage in Semiconductors," Solid State Electronics, vol. 9, p. 837, September 1966.

27. D.V.Speency and G.P.Carey, "Experimental Study of the Effects of Junction Curvature on Breakdown Voltage in Si," Solid State Electronics, vol. 10, p. 177, March 1967.

28. J.Miller, "Sweep Test Picks Best Transistors to Bar Inductive Load Damage," Electronic Design, vol. 12, p. 44, 24th October 1964.

29. P.P.Balthasar, "Selecting Switching Circuit Transistors," Electrical Design News, vol. 10, p. 72, November 1965.

30. B.C.Banyard, "A Non-destructive Secondary Breakdown Tester," Electronic Components, p. 932, August 1969.

31. H.A.Schafft and J.C.French, "Second Breakdown and Current Distribution in Transistors," Solid State Electronics, vol. 9, p. 681-688, July 1966.

32. H.D.Frazier, "Temperature Dependent Fluorescent Paints a Graphic Display of Temperature Distribution," IEEE WESCON Conv. Record, pt. 3.1, vol. 7, p. 1-5, 1963.

33. T.Agatsuma, "Turnover Phenomena in n^+ -n Si Devices and Second Breakdown in Transistors," IEEE Trans. Electron Devices, vol. ED-13, p. 748-753, 1966.

34. T.Goskov, "The Measurement of Electrodynamic Characteristics by the Combined Probe Method," Soviet Phys. Journal, 1969.

35. R.M.Scarlett and W.Schroen, "Localised Thermal Effects in Silicon Power Transistors," Physics of Failure in Electronics, vol. 2, RADC Series in Reliability, Springfield Va., CFSTI, p. 285-303, 1964.

36. Mature and Lausko, "Scanning Electron Beam Display of Dislocation Space Charge," Appl. Phys. Lett., vol. 13, n.6, 15th September 1968.

37. Titchmarsh, Lapworth and Booker, "A New Method of Investigating the E. Field Regions of p - n Junctions," Phys. Stat. Solidi, vol. 34, n.2, p. K83, 1969.

38. K.A.Hughes and J.Coster, "Second Breakdown in Transistors," Contract No. B/SR/3051, Bangor University, Wales, 1970.

39. J.Beerman, "Pyroelectric Detector of Infra-red Radiation," IEEE Trans. Electron Devices, vol. ED-16, n.6, p. 554, 1969.

40. Yoder, "Temperature Measurement with an Infra-red Microscope," Appl. Optics (U.S.A.), vol. 7, p. 1791, September 1968.

41. Jarrat, "Infra-red Microscope for the Temperature Measurement of Small Areas," Mullard Tech. Comm., vol. 10, p. 101, May 1968.

42. Peterman, "Infra-red Radiometry of Semiconductor Devices," Microelectronics Reliability, vol. 6, p. 307, November 1967.

3. References for Section 3.

1. J.M.Ziman, "Electrons and Phonons," Oxford University Press, 1960.
2. A.C.Smith, J.F.Janak and R.B.Adler, "Electronic Conduction in Solids," McGraw-Hill, 1967.
3. E.H.Putley, "The Hall Effect and Semiconductor Physics," Dover Pub. Inc., New York, 1968.
4. S.Chapman and T.G.Cowling, "The Mathematical Theory of Non-Uniform Gases," Cambridge University Press, 1939.
5. J.S.Blakemore, "Solid State Physics," W.B.Saunders Co., 1970.
6. H.G.Reik and H.Risken, "Distribution Functions for Hot Electrons in Many-Valley Semiconductors," Phys. Rev. vol. 124, p. 777, 1961.
7. H.G.Reik and H.Risken, "Drift Velocity and Anisotropy of Hot Electrons in n Germanium," Phys. Rev. vol. 126. p. 1737, 1962.
8. J.S.Blakemore, "Semiconductor Statistics," Pergamon Press, 1962.
9. E.M.Conwell and M.O.Vassell, "High Field Distribution Function in GaAs," IEEE Trans. Electron Devices, vol. ED-13, p. 22, 1966.
10. C.Herring, "Transport Properties of a Many-Valley Semiconductor," Bell Syst. Tech. Journal, vol. 34, n.2, p. 237, March 1955.
11. C.Herring and E.Vogt, "Transport and Deformation Potential Theory for Many-Valley Semiconductors with Anisotropic Scattering," Phys. Rev. vol. 101, p. 944, 1956.

12. T.Misawa, "Negative Resistance in p - n Junctions Under Avalanche Breakdown Conditions," IEEE Trans. Electron Devices, vol. ED-13, p. 137, 1966.

13. Javid and Brown, "Field Analysis and Electromagnetics," McGraw-Hill, 1936.

14. W.Shockley, "Electrons and Holes in Semiconductors," Van Nostrand, 1966.

15. E.M.Conwell, "Properties of Silicon and Germanium II," Proc. IRE, vol. 46, p. 1281-1300, June 1958.

16. H.B.Prince, "Drift Mobilities in Semiconductors, II Silicon," Phys. Rev. vol. 39, p. 1204, March 1954.

17. Glassbrenner and Slack, "Thermal Conductivity of Silicon and Germanium from 3°K to the Melting Point," Phys. Rev. vol. 93, March 1954.

18. F.J.Morin and J.P.Maita, "Electrical Properties of Silicon Containing Arsenic and Boron," Phys. Rev. vol. 96, p. 28, October 1954.

19. J.B.Walsh, "Electromagnetic Theory and Engineering Applications," McGraw-Hill, 1963.

20. W.H.Bennett, "Magnetically Self-Focusing Streams," Phys. Rev. vol. 45, p. 890, 1934.

21. E.Condon, "Handbook of Physics," McGraw-Hill, 1967.

22. A.G.Chynoweth and A.A.Murray, "Pinch Effects in Indium Antimonide," Phys. Rev. vol. 123, p. 515, 1961.

23. K.G.McKay, "Avalanche Breakdown in Silicon," Phys. Rev. vol. 94, p. 877, 1954.

24. C.B.Norris and J.F.Gibbons, "Measurement of High-Field Carrier Drift Velocities in Silicon by a Time-of-Flight Technique," IEEE Trans. Electron Devices, vol. ED-14, p. 38, 1967.

25. V.Rodriguez, H.Ruegg and M.A.Nicolet, "Measurement of the Drift Velocities in Silicon at High-Field Strengths," IEEE Trans. Electron Devices, vol. ED-14, p. 44, 1967.

26. C.Y.Duh and J.L.Moll, "Electron Drift Velocity in Avalanching Silicon Diodes," IEEE Trans. Electron Devices, vol. ED-14, p. 46, 1967.

27. O.Jantsch and J.Feigt, "A Theory and Some Characteristics of Power Transistors at High Level Conditions," Proc. IEEE vol. 55, n.8, p. 1375, August 1967.

28. J.R.Hauser, "The Effects of Distributed Base Potential on I_c Injection Density and Effective Base Resistance for Stripe Transistor Geometries," IEEE Trans. Electron Devices, vol. ED-11, p. 238, 1964.

29. Ebner and Gray, "Static I - V Relationships in Transistors," IEEE Trans. Electron Devices, vol. ED-13, p. 699, 1966.

30. R.J.Whittier and D.A.Tremere, "Current Gain and Cut-Off Frequency Fall-Off at High Currents," IEEE Trans. Electron Devices, vol. ED-16, n.1, p. 39, 1969.

31. W.Van Roosbroeck, "The Transport of Added Current Carriers in a Homogeneous Semiconductor," Phys. Rev. vol. 91, p. 282-289, 1953.

32. W.Shockley and W.T.Read, "Statistics of the Recombination of Holes and Electrons," Phys. Rev. vol. 87, p. 835-842, 1952.

33. L.B.Valdes, "The Physical Theory of Transistors," McGraw-Hill, 1961.

34. H.Hartnagel, "Semiconductor Plasma Instabilities."

35. R.A.Smith, "Course 22, Semiconductors," Proc. International School of Physics, "Enrico Fermi", Varenna, Italy, (Academic Press, New York).

36. R.Hall, "Temperature Coefficient of the Breakdown Voltage of Silicon p - n Junctions," International Journal of Electronics, vol. 22, p. 513, 1967.

37. J.T.Wait and J.R.Hauser, "β Fall-Off in Transistors at High Collector Currents," Proc. IEEE vol. 56, p. 2087, 1968.

38. J.R.Hauser, "The Effects of Distributed Base Potential on Emitter Current Injection Density and Effective Base Resistance for Stripe Transistor Geometries," IEEE Trans. Electron Devices, vol. ED-11, p. 238, 1964.

39. Van der Ziel and Agouridis, "The Cut-Off Frequency Fall-Off in U.H.F. Transistors at High Currents," Proc. IEEE (Letters), vol. 56, n.12, p. 2176, December 1968.

40. T.Kirk, "A Theory of Transistor Cut-Off Frequency," IRE Trans. Electron Devices, vol. ED-9, p. 164-174, March 1962.

41. R.M.Scarlett and G.F.Hardy, "Second Breakdown in Silicon Power Transistors at High Collector Voltage," Symposium Physics of Failure in Electronics, Columbo, Ohio, November 1966.

42. Browne and Mars, "Avalanche Breakdown Characteristics of Bipolar Transistors," International Journal of Electronics, vol. 29, n.1, p. 73, 1968.

43. Ryghikov, "Carrier Injection into the Heavily Doped Regions of a $p^+ - n - n^+$ Diode," Radio Eng. and Electron Physics, p. 790, 1967.

44. P.L.Hower and V.G.K.Reddi, "Avalanche Injection and Second Breakdown in Transistors," IEEE Trans. Electron Devices, vol. ED-17, n.4, p. 320, 1970.

45. K.Papoular, "Electrical Phenomena in Gases," Illiffe Books, 1965.

46. L.B.Loeb, "Basic Processes of Gaseous Electronics," University of California, 1961.

47. A.K.Jonscher, "Principles of Semiconductor Device Operation," G.Bell & Son, 1960.

48. A.G.Chynoweth, "Uniform Silicon p - n Junctions II Ionisation Rates for Electrons," Journal Appl. Phys. vol. 31, n.7, p. 1161, 1960.

49. T.Ogawa, "Avalanche Breakdown and Multiplication in Silicon p - i - n Junctions," Japanese Journal of Appl. Phys. vol. 99, p. 1234, 1965.

50. P.D.Maycock, "Thermal Conductivity of Silicon, Germanium III - v Compounds and III - v Alloys," Solid State Electronics, vol. 10, p. 161-168, 1967.

51. G.Gibbons, "Transient Temperature Response of an Avalanche Diode," Solid State Electronics, vol. 13, p. 79, 1970.

52. G.Roman, "A Model for Computation of Second Breakdown in Transistors," Solid State Electronics, vol. 13, p. 961-980, 1970.

53. H.S.Carslaw and J.C.Jaeger, "Conduction of Heat in Solids," Oxford University Press, 1962.

54. S.S.Kutateladze and V.M.Borishanskiy, "Handbook of Heat Transfer - Section 4 - 11."

55. J.R.Hauser, "Boundary Conditions at a p - n Junction," Solid State Electronics, vol. 14, n.2, p. 133, 1971.

56. Jeffreys and Jeffreys, "Methods of Mathematical Physics," Cambridge University Press.

57. J.L.Moll, J.L.Su and A.C.Wang, "Multiplication in the Collector Junctions of Silicon n - p - n and p - n - p

Transistors," IEEE Trans. Electron Devices, vol. ED-17, n.5, p. 420, 1970.

58. R.H.F.Lloyd, "The Movement of Depletion Layer Boundaries at High Current Densities," IEEE Trans. Electron Devices, vol. ED-13, p. 991, 1966.

59. K.A.Hughes and J.Coster, "Second Breakdown in Transistors," Bangor University, 1970.

60. B.Reich and E.B.Hakim, "Second Breakdown Characterisation and Improvement of Semiconductor Devices," IEEE Trans. Electron Devices, vol. ED-13, p. 734-737, 1966.

61. K.Fujinuma, "Transistor Failure by Second Breakdown," IEEE Trans. Electron Devices, vol. ED-13, p. 651, 1966.

4. References for Appendix 1.

1. J.M.Ziman, "Electrons and Phonons," Oxford University Press, 1960.
2. J.Valdes, "The Physical Theory of Transistors," McGraw-Hill, 1961.
3. A.G.Chynoweth and A.A.Murray, "Pinch Effect in Indium Antimonide," Phys. Rev. vol. 123, p. 1542, 1961.
4. J.P.McKelvey, R.L.Longini and T.P.Brody, "Alternative Approach to the Solution of Added Carrier Transport Problems in Semiconductors," Phys. Rev. vol. 123, p. 51, 1961.
5. W.Van Roosbroeck, "Current-Carrier Transport with Space Charge in Semiconductors," Phys. Rev. vol. 123, p. 474, 1961.

5. References for Appendix 2.

1. H.Hartnagel, "Semiconductor Plasma Instabilities."
2. E.J.Hellund, "The Plasma State," Rumbold Pub. Co., 1961.
3. E.H.Kennard, "Kinetic Theory of Gases," McGraw-Hill, 1938.
4. W.Shockley, "Electrons and Holes in Semiconductors," Van Nostrand, 1966.

6. References for Appendix 4.

1. W.Shockley, "Electrons and Holes in Semiconductors," Van Nostrand, 1966.
2. F.J.Morin and J.P.Maita, "Electrical Properties of Silicon Containing Arsenic and Boron," Phys. Rev. vol. 96, p. 28, October 1954.
3. E.M.Conwell, Proc. IRE vol. 46, p. 1281-1300, June 1958.
4. H.B.Prince, "Drift Mobilities in Semiconductors II, Silicon," Phys. Rev. vol. 93, p. 1284, March 1954.
5. E.H.Putley, "The Hall Effect and Semiconductor Physics," Dover Pub. Inc., 1968.
6. Glassbrenner and Slack, "Thermal Conductivity of Silicon and Germanium from $3^{\circ}K$ to the Melting Point," Phys. Rev. vol. 93, p. 1204, March 1954.

7. References for Appendix 5.

1. Buhannan, "Current Gain and Temperature in Silicon Transistors," IEEE Trans. Electron Devices, vol. ED-16, n.1, p. 122, 1969.
2. J.L.Moll, J.L.Su and A.C.Wang, "Multiplication in the Collector Junctions of Silicon n - p - n and p - n - p Transistors," IEEE Trans. Electron Devices, vol. ED-17, n.5, p. 420, 1970.
3. W.Shockley, "Electrons and Holes in Semiconductors," Van Nostrand, 1950.
4. J.M.Ziman, "Electrons and Phonons," Oxford University Press, 1960.
5. R.Hall, "Temperature Coefficient of the Breakdown Voltage of Silicon p - n Junctions," International Journal of Electronics, vol. 22, p. 513, 1967.

8. References for Appendix 6.

1. G.Gibbons, "Transient Response of an Avalanche Diode," Solid State Electronics, vol. 13, p. 799, 1970.

LIST OF SYMBOLS.

A	Constant
A_c	Collection area
A_e	Emitter area
A_{eff}	Effective collection area (space-charge-limited operation)
A_T	Constant) associated with the temperature dependence of
a_T	Constant) charge carrier mobility
B	Constant
$\bar{B}$	Magnetic Field Vector
B_T	Constant) associated with the temperature dependence of
b_T	Constant) conductivity
b	Constant
C	Constant
C_b	Bulk heat capacity
C_s	Local heat capacity
C_T	Specific heat
D	Constant
D_a	Ambipolar Diffusion Coefficient
D_e	Electron Diffusion Coefficient
D_p	Hole Diffusion Coefficient
E	Electric field strength
E_m	Maximum electric field strength
	Energy

$\mathcal{E}_c$ Conduction band-edge energy

$\mathcal{E}_F$ Fermi energy

$\mathcal{E}_g$ Band-edge energy gap

$\mathcal{E}_g(0)$ Band-edge energy gap at $0^\circ K$.

$\mathcal{E}_v$ Valence band-edge energy

$\bar{F}$ Force vector

F_A Thermal resistance correction factor for changes in horizontal aspect ratio of the heat source

F_h Thermal resistance correction factor for changes in the thickness of the heat source

F_w Thermal resistance correction factor for changes in the depth of the heat source below the adiabatic surface

f Function

f_o Equilibrium function

G Rate of charge generation

g Charge-carrier generation rate

g_o Generation rate of charge carrier due to thermal processes

h Thickness of the collector space-charge region

h Plank's Constant

I Current

I_c Collector current

I_{crit} Critical collector current

J	Current density
J_n	Electron current density
J_o	Limiting value of current density for normal unipolar conduction
J_p	Hole current density
J_T	Current density at the threshold of space-charge-limited operation
K	Thermal Conductivity
k	Boltzman's Constant
K_p	Relative Permittivity
k_T	Thermal Diffusivity
L	Emitter length
L_c	Collection region length
M	Avalanche multiplication factor
m	Charge carrier mass
m^*	Effective mass of charge-carrier
m_l	Distance from a reference point
N	Charge-carrier concentration
n	Electron concentration
N_A	Acceptor concentration
N_c	Effective density of states in the conduction band
N_D	Donor concentration
N_i	Impurity concentration
N_v	Effective density of states in the valence band

n_{cc} Charge-carrier concentration at the threshold of space-charge-limited operation

$\bar{n}$ Mean charge-carrier concentration

P Power

p Hole concentration

P_n Electron pressure

P_p Hole pressure

p_w Power density

Q Constant associated with ionisation integral approximation

q Charge on an electron

r Radius

$\bar{r}$ Position vector

r_m Maximum constriction radius

$\bar{s}$ Line vector

T_A Ambient Temperature

T_{cc} Temperature at space-charge-limited conduction threshold

T_n Local electron temperature

T_o Reference temperature

T_p Local hole temperature

t_d Second breakdown delay time

t_o Reference time (start of a specified time period)

t_{tr} Transit time (diffusion in the base region)

t time.

u	Constant (ionisation integral approximation)
$\bar{u}$	Local velocity vector
V	Volume
V_{CB}	Collector-Base Voltage
V_{CE}	Collector-Emitter Voltage
V_s	Supply Voltage
$\bar{v}$	Velocity vector
v_l	Saturated drift velocity
v_o	Saturated drift velocity at $0^{\circ}K$.
W_c	Width of collector space-charge region
w_b	Base region thickness
w_{be}	Effective base region thickness
w_{cib}	Current induced base region thickness
w_{epi}	Width of epitaxial layer
w_{eff}	Function associated with the solution of $\int (E)\, dz$
x	Co-ordinate direction
y	Co-ordinate direction
z	Co-ordinate direction
α	Current amplification factor
α_i	Ionisation coefficient for electrons
α_∞	Asymptotic value for the ionisation coefficient

β_i Ionisation coefficient for holes

γ Coefficient of Energy Gap Modulation by Temperature

δ $(4k_T(t - t_o))^{\frac{1}{2}}$

ε_o Permittivity of free space

θ_B Bulk thermal resistance

θ_o Thermal resistance under reference conditions

θ_s Local thermal resistance

ϕ Potential

φ Potential

ψ_c Energy (N k T)

ρ Charge density

ρ_D Density of medium

λ^2 $= \frac{2\mu kT\gamma}{q}$

μ Mobility

μ_a Ambipolar mobility

μ_n Mobility of electrons

μ_o Permeability

μ_p Mobility of holes

$\mathcal{J}$ Number of emitter sections

σ Electrical conductivity

τ Relaxation time constant (scattering approximation)

τ_b Thermal time constant associated with bulk effects

τ_s Thermal time constant associated with local effects

Subscripts.

a	Ambipolar
b,B	Base
c,C	Collector
crit	Conditions at breakdown threshold
e,E	Emitter
f	Field
n	Electron
p	Hole
r	Radial
pr	Pressure
s	Local
T	Thermal process.

INDEX.

Appendices.

1. Examination of Space-Charge Neutrality and Ambipolar Continuity Equations
2. Electron-Hole Pressure
3. Fields Associated with Charged Particle Motion
4. Temperature Dependence of Mobility and Thermal Conductivity
5. Current Amplification Factor as a Function of Temperature
6. Time Dependent Thermal Dissipation for a Circular Structure
7. Multiplication Factor at the Second Breakdown Threshold.

DIAGRAM INDEX.